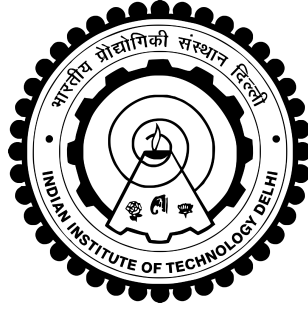


NEIGHBORHOOD DENSITY ESTIMATION USING
SPACE-PARTITIONING BASED HASHING SCHEMES

AASHI JINDAL



DEPARTMENT OF ELECTRICAL ENGINEERING
INDIAN INSTITUTE OF TECHNOLOGY DELHI

June 2023

NEIGHBORHOOD DENSITY ESTIMATION USING
SPACE-PARTITIONING BASED HASHING SCHEMES

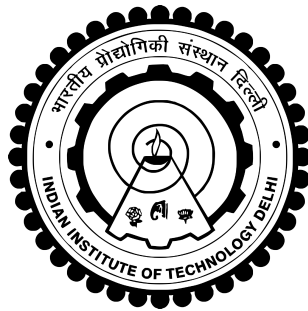
by

AASHI JINDAL

DEPARTMENT OF ELECTRICAL ENGINEERING

Submitted

*in fulfillment of the requirements of the degree of Doctor of Philosophy
to the*



INDIAN INSTITUTE OF TECHNOLOGY DELHI

June 2023

Certificate

This is to certify that the thesis entitled “**Neighborhood Density Estimation Using Space-Partitioning Based Hashing Schemes**”, being submitted by **Aashi Jindal** for the award of the degree of **Doctor of Philosophy** to the Department of Electrical Engineering, Indian Institute of Technology Delhi, is a record of bonafide work done by her under my supervision and guidance. The matter embodied in this thesis has not been submitted to any other University or Institute for the award of any other degree or diploma.

Dr. Jayadeva

Professor

Department of Electrical Engineering,
Indian Institute of Technology Delhi,
Hauz Khas, New Delhi - 110016,
INDIA.

Dr. Shyam Prabhakar

Associate Director

Laboratory of Systems Biology and Data Analytics,
Genome Institute of Singapore,
SINGAPORE

Dr. Debarka Sengupta

Associate Professor

Department of Computer Science & Engineering,
Department of Computational Biology,
Centre for Artificial Intelligence,
Indraprastha Institute of Information Technology,
Okhla Phase III, Delhi - 110020, India
(Adj.) Associate Professor
Institute of Health & Biomedical Innovation,
QUT, AUSTRALIA

Acknowledgements

I sincerely thank my supervisors Dr. Jayadeva, Dr. Debarka Sengupta and Dr. Shyam Prabhakar for their valuable feedback. I also thank other SRC members Dr. I.N. Kar, Dr. Shouri Chatterjee, and Dr. Vivekanandan Perumal. I thank Prof. Suresh Chandra for his encouragement. I thank my colleagues Dr. Sumit Soman and Dr. Udit Kumar for their moral support. I thank department staff members Rakesh, Yatindra, Satish, and Mukesh for always helping with the department work.

I thank my parents, Rakesh Jindal and Meena Jindal, for always believing in me and supporting me in my decisions. I thank my parents-in-law, Sanjiv Kumar Gupta and Snehlata Gupta for being always understanding. I thank my husband Prashant Gupta for always being there whenever I needed him. He supported me both professionally and personally. My brother, Sahil Jindal always holds a special place in my life. My core family members, Shruti Singla, Praveen Singla, Shaffi Bindal, Mohit Bindal, Khushboo Mehrotra, Yuvan Singla, Tejas Bindal, and Vanya Bindal are an important part of my life.

I also thank my current employers, Ashok Juneja and Shweta Singla for giving me the time to complete my pending research work when needed. I am thankful to my company, Applied Solar Technologies India Pvt. Ltd. and my colleagues, Subhdip Rakshit, Amod Kumar, Shubham Sinha, Pulkit Tyagi, Bikas Gupta, Sukrit Singh Negi, Abhishek Chaudhary and Anil Hansda.

The following have been the three main philosophies of my life, "There is an almighty somewhere looking after us and guiding us to the correct path." "Behind every successful woman is her parents, husband, and family that supported her in her unconventional choices." Last, but not the least, "...all's well, that ends well."

(Aashi Jindal)

Abstract

Single cell messenger RNA sequencing (scRNA-seq) offers a view into transcriptional landscapes in complex tissues. Recent developments in droplet based transcriptomics platforms have made it possible to simultaneously screen hundreds of thousands of cells. It is advantageous to use large-scale single cell transcriptomics since it could lead to the discovery of a number of rare cell sub-populations. When the sample size reaches the order of hundreds of thousands, existing techniques to discover rare cells either scale unbearably slow or terminate altogether. We suggest the Finder of Rare Entities (FiRE), an algorithm that quickly assigns a rareness score to every individual expression profile under consideration. We show how FiRE scores can assist bioinformaticians in limiting the downstream analyses to only on a subset of expression profiles within ultra-large scRNA-seq data.

Anomaly detection methods differ in their time complexity, sensitivity to data dimensions, and their ability to detect local/global outliers. The proposed algorithm FiRE is a 'sketching' based linear-time algorithm for identifying global outliers. FiRE.1, an extended implementation of FiRE fares well on local outliers as well. We provide an extensive comparison with 18 state-of-the-art anomaly detection algorithms on a diverse collection of 1000 annotated datasets. Five different evaluation metrics have been employed. FiRE.1's performance was particularly remarkable on datasets featuring a large number of local outliers. In the sequel, we propose a new "outlierness" criterion to infer the local or global identity of outliers.

We propose Enhash, a fast ensemble learner that detects *concept drift* in a data stream. A stream may consist of abrupt, gradual, virtual, or recurring events, or a mixture of various types of drift. Enhash employs projection hash to insert an incoming sample. We show empirically that the proposed method has competitive performance to existing ensemble learners in much lesser time. Also, Enhash has moderate resource requirements. Experiments relevant to performance comparison were performed on 6 artificial and 4 real datasets consisting of various types of drifts.

एकक कोशिका दूत-RNA (scRNA-seq) अनुक्रमण जटिल ऊतकों के लिप्यंतरण का एक दृश्य प्रस्तुत करता है। छोटी बूंदों पर आधारित अत्याधुनिक प्रतिलेख यंत्रों के माध्यम से लाखों एकक कोशिकाओं को एक साथ परखना संभव हो गया है। बड़े पैमाने पर एकक कोशिकाओं के प्रतिलेखों का उपयोग दुर्लभ कोशिकाओं को खोजने में किया जा सकता है। जब एकक कोशिकाओं के प्रतिदर्शों का आकड़ा लाखों में पहुँचता है तो उपलब्ध कलन विधिओं असहनीय रूप से शिथिल हो जाती हैं तथा इनका उपयोग करके दुर्लभ कोशिकाओं की खोज करना लगभग असंभव हो जाता है। इस शोध प्रबंध में दुर्लभता के अंकमान की गड़ना के लिए एक कलन विधि, दुर्लभ इकाईओं का खोजक (FiRE) को प्रस्तुत किया गया है। यह कलन विधि तीव्र गति से प्रत्येक कोशिकाओं के प्रतिलेख को एक दुर्लभता का अंकमान प्रदान करती है। हम यह भी दिखाते हैं FiRE अंकमान जैव सूचना वैज्ञानिकों को अत्यधिक विशाल scRNA-seq आंकड़ाकोशों में से केवल कुछ महत्वपूर्ण एकक कोशिकाओं के विश्लेषण करने में सहायता करता है।

विसंगति का पता लगाने के तरीके उनकी समय जटिलता, विवरण आयामों, तथा स्थानीय/वैश्विक रूप से विचित्र प्रतिदृश्यों की खोज करने की छमता में भिन्न होते हैं। प्रस्तावित कलन विधि FiRE वैश्विक रूप से विचित्र प्रतिदृश्यों को रेखीय अवधि में अवगत कराती है तथा इसके लिए स्केचिंग, एक हैशिंग पे आधारिक कलन विधि का उपयोग करती है। FiRE का विस्तारित कार्यान्वयन FiRE.1 स्थानीय रूप से विचित्र प्रतिदृश्यों की खोज करने में सक्षम है। इस शोध प्रबंध में हम १००० मापदंड आंकड़ा संचयों के विविध संग्रह पे १८ अत्याधुनिक विसंगति का पता लगाने वाली कलन विधिओं की व्यापक तुलना प्रदान करते हैं। इस तुलना के लिए ५ भिन्न प्रकार की तुलना विधिओं को नियोजित किया गया है। बड़ी संख्या में स्थानीय रूप से विचित्र प्रतिदृश्यों से परिपूर्ण आंकड़ा संकलनो पर FiRE.1 का प्रदर्शन उल्लेखनीय है। अगली कड़ी में हम स्थानीय और वैश्विक रूप से विचित्र प्रतिदृश्यों का अनुमान लगाने के लिए एक "बाह्यता" मानदंड प्रस्तावित करते हैं।

इस शोध प्रबंध के अंतिम भाग में हम एक तीव्र समवेत कलन विधि, Enhash, को प्रस्तुत करते हैं जो आंकड़ों की धारा में से अवधारणा के बहाव का पता लगाने में सक्षम है। एक आंकड़ों की धारा में आकस्मिक, क्रमिक, आभासी, या आवर्ती घटनाये, या इनके मिश्रण उपास्थिक हो सकते हैं। Enhash आने वाले प्रतिदर्शियों को सम्मिलित करने के लिए प्रक्षेप हैश का उपयोग करता है। हम अनुभवजन्य रूप से दिखाते हैं की प्रस्तावित कलन विधि का प्रदर्शन उपलब्ध समवेत आधारित कलन विधिओं की अपेक्षा प्रतिस्पर्धी है तथा प्रस्तावित कलन विधि यह प्रदर्शन अन्य विधिओं की तुलना में कम समय तथा मध्यम संसाधनों का उपयोग करके प्राप्त करती है। प्रस्तावित कलन विधि के प्रदर्शन की तुलना ६ कृत्रिम तथा ४ वास्तविक आंकड़ा संचयों पर की गई है। यह आंकड़ा संचय विभिन्न प्रकार के अवधारणाओं के मिश्रण से बने हैं।

Contents

Certificate	i
Acknowledgements	iii
Abstract	v
Hindi Abstract	vii
List of Figures	xiii
List of Tables	xix
List of Abbreviations	xxi
1 Introduction	1
1.1 Scope and objectives	1
1.2 Locality Sensitive Hashing	2
1.2.1 Sketching	3
1.2.2 Binary hash	3
1.2.3 Projection hash	3
1.3 Outlier detection	4
1.3.1 Outlier detection: Definition	4
1.3.2 Outlier detection: Use cases	4
1.3.3 Outlier detection: Existing techniques	4
1.3.4 Outlier detection: Motivation	9
1.3.5 Outlier detection: Proposed technique	10

1.4	Concept drift detection	11
1.4.1	Concept drift detection: Definition and use cases	11
1.4.2	Concept drift detection: Existing techniques	11
1.4.3	Concept drift detection: Motivation and proposed technique . . .	12
1.5	Organization of the thesis	13
2	Identification of Rare Events*	15
2.1	Introduction	15
2.2	Overview of FiRE	17
2.2.1	Steps involved in FiRE	19
2.3	Results	20
2.3.1	Experimental setup	20
2.3.2	FiRE discovers cells with varying degrees of rareness	25
2.3.3	FiRE detects artificially planted rare cells with high accuracy . .	26
2.3.4	FiRE is sensitive to cell type identity	27
2.3.5	FiRE is scalable and fast	29
2.3.6	FiRE resolves heterogeneity among dendritic cells	33
2.4	Conclusions	35
3	Linear Time Identification of Local and Global Outliers[†]	37
3.1	Introduction	37
3.2	FiRE.1: FiRE for local outliers	38
3.3	Outlier score on unseen data	41
3.3.1	Local vs Global outliers	42
3.4	Run time complexity	42
3.5	Experimental setup	44
3.5.1	Description of datasets	44
3.5.2	Metrics for comparing outlier detection methods	44
3.6	Performance comparison of methods on a repository of almost 1000 datasets	46
3.6.1	Tuning of hyperparameters	46

*The work presented in this chapter has been published as a research paper titled “*Discovery of rare cells from voluminous single cell expression data*” in Nature Communications (2018).

[†]The work presented in this chapter has been published as a research paper titled “*Linear time identification of local and global outliers*” in Neurocomputing (2021).

3.6.2	Comparison of methods using Friedman ranking	47
3.6.3	Comparison of linear complexity methods from the perspective of outlierness type	49
3.6.4	Performance comparison of linear-time methods on large datasets	51
3.7	Conclusions	53
4	Enhash: A Fast Streaming Algorithm for Concept Drift Detection[‡]	55
4.1	Introduction	55
4.2	The proposed method: Enhash	56
4.2.1	Implementation details	59
4.2.2	Time complexity analysis	61
4.3	Experimental Setup	64
4.3.1	Evaluation metrics for performance comparison	64
4.3.2	Description of datasets	64
4.3.3	System details	65
4.4	Tuning of parameters for Enhash	65
4.4.1	Constraints to tune L	66
4.4.2	Constraints to tune <i>bin-width</i>	66
4.5	Experimental Results	67
4.6	Ablation study	71
4.7	Conclusions	72
5	Conclusions and Future Work	73
5.1	Conclusions	73
5.2	Future Work	75
5.2.1	Identification of anomalies in time-series data	75
	List of Publications	91
	Brief Biodata of Author	93

[‡]The work presented in this chapter has been published as a research paper titled “*Enhash: A fast streaming algorithm for concept drift detection*” in ESANN proceedings (2021).

List of Figures

1.1	Overall categorization of well-known unsupervised anomaly detection algorithms. The three broad categories are statistical, sub-space based, and nearest-neighbor based.	9
2.1	Overview of FiRE. The first step is to assign each cell to a hash-code. As numerous similar cells can share the same hash-code, it is possible to think of a hash-code as an imagined bucket. The phase of creating the hash-code is repeated L times to test the reliability of rarity estimates. The chance that any point will fall into the bucket of a given cell i and estimator l is calculated as p_{il} . These probabilities are combined in the algorithm's second phase to get an estimate of how rare each cell is. . .	18
2.2	Stability of FiRE. (a),(c) RMS (Root Mean Square) difference in values of FiRE-score of every cell between two successive estimators. For calculation of RMS, FiRE-score is averaged across multiple seeds and normalized by the value of L . (b),(d) RMS difference in values of FiRE-score between two successive values of M . For calculation of RMS, FiRE-score is averaged across multiple seeds and normalized by the value of M . (a)-(b) RMS has been shown on a simulated dataset consisting of a mixture of Jurkat and 293T cells [148]. (c)-(d) RMS has been shown on $\sim 68k$ Peripheral Blood Mononuclear Cells (PBMCs) [148].	24

2.3	Performance evaluation of FiRE on Peripheral Blood Mononuclear Cells (PBMCs). (a) t-SNE based 2D embedding of the data with color coded cluster identities as reported by Zheng and colleagues [148]. (b) Rare population identified by FiRE using IQR-thresholding-criteria. (c) Heat map of FiRE scores for the individual PBMCs. The cluster of megakaryocytes (0.3%), the rarest of all the cell types are assigned the highest FiRE scores.	25
2.4	In the $\sim 68k$ PBMC data [148], the appearance of minor cell populations with varying degrees of rarity is accompanied by a rise in the number of chosen rare cells. Figures (a)-(c) demonstrate, respectively, the top 0.25%, 2%, and 5% cells chosen based on FiRE scores.	26
2.5	Minor cell types' detectability in a simulated dataset with a mixture of Jurkat and 293T cells (known annotations) [148]. (a) F_1 scores were determined relative to the rare (Jurkat) population, while bioinformatically altering the percentage of artificially planted rare cells. It is noteworthy that both FiRE and LOF [13] use a threshold to their continuous scores for zeroing on the rare cells. On the other hand, GiniClust [63] and RaceID [51] offer binary annotations for cell-rarity. (b) t-SNE based 2D embedding of the cells with color-coded identities. (c) FiRE-score intensities were displayed on the t-SNE based 2D map. Figures (d)-(g) demonstrate the rare cells detected by various algorithms. (h) Congruence of methods with known annotations. Note: Results shown in Figures (b)-(h) correspond to a rare cell concentration of 2.5%.	28
2.6	Congruence of methods with known annotations and congruence between pairs of methods on a simulated, scRNA-seq data consisting of 293T and Jurkat cells mixed <i>in vitro</i> in equal proportion [148].	29

2.7	Congruence of methods using Venn diagrams. (a),(b) Performance comparison of FiRE, GiniClust [63], RaceID [51] and LOF [13] as per the rare cells identified by them. (a) Performance comparison of methods above on Embryonic Stem Cells (ESCs) data [70]. FiRE could easily identify the Zscan-4 enriched, 2C-like cell cluster as reported by Jiang <i>et al.</i> [63]. Also, the FiRE predicted rare cells had the least overlap with the ones predicted by RaceID, which could not identify those 2C-like cells. (b) Performance on mouse small intestine cells [51]. FiRE could identify the rare cell types in the secretory lineage, which consisted of goblet, enteroendocrine, paneth and tuft cells (as discussed in Grun <i>et al.</i> [51]).	30
2.8	Sensitivity of FiRE to cell type. As soon as there are enough differentially expressed genes to create a small cluster that represents the minor cell subpopulation, fire begins properly identifying the minor cell type on scRNA-seq data generated using the R tool splatter [143]. The succeeding ROC-AUC plots use the figure in the upper-left corner as their legend. Each t-SNE and ROC figure pair represents one of the 1000 times the experiment was run with respect to a particular set of differentially expressed genes. Cell-group annotations were used in the ROC-AUC study, and individual cells were given FiRE ratings.	31
2.9	FiRE is fast. Execution time collected for the four methods with cell counts varying from 1k to ~68k.	32
2.10	FiRE-defined dendritic cell heterogeneity in human blood. (a) t-SNE based 2D plot of rare cells detected by FiRE. Cells are color coded based on their cluster identity as determined by dropClust. (b) Dendritic cells, annotated by the authors, are highlighted in the 2D map adopted from Zheng <i>et al</i> [148]. (c) Dendritic cell sub-types detected from FiRE-reported rare cells are color-coded as per Figure (a). (d) Characterization of dendritic cell sub-types using markers reported by Villani and colleagues [124].	34
2.11	2D embedding of rare cells detected by FiRE on ~68k PBMCs. Cells are color coded based on the cell type annotations reported by Zheng [148].	35

3.1	Performance of FiRE and FiRE.1 on a simulated dataset with local and global outliers (the illustration is inspired by [79]). (a) A 2-dimensional simulated dataset containing both local and global outliers. (b) Distribution of <i>FiRE-score</i> when $M = 2$. Global outliers are well captured and have high values of <i>FiRE-score</i> . On the other hand, local outliers deviating marginally from a local population are not captured. (c) Distribution of <i>FiRE-score</i> when $M > d$ ($M = 100$). In addition to global outliers, local ones are also identified since sufficient hash indexes account for minor differences between local outliers and their local population. (d) FiRE.1 identifies both local and global outliers. (e) Variation of outlieriness criterion <i>o-score</i> on different types of outliers. For global outliers, the values are high and vice-versa.	39
3.2	An overview of FiRE.1 on a simulated dataset. The heatmap depicts FiRE.1 approximated regional densities.	40
3.3	Performance comparison of 18 outlier detection methods on ~ 1000 datasets. The performance of all methods was evaluated on 5 evaluation metrics. Friedman ranking determined for every method for each metric. The method with the smallest Friedman rank performs the best on a given measure. The color intensity in a heatmap depicts the inverse of the Friedman ranking.	48
3.4	Performance comparison of linear time complexity outlier detection methods - FiRE.1, FiRE, and HBOS based on <i>o-score</i> . The datasets are grouped into 5 different clusters using hierarchical clustering. Cluster#1 consists of 127 (11.2% of the entire collection of datasets), cluster#2 has 667 (59.1%), cluster#3 has 31 (2.7%), cluster#4 has 113 (10%), and cluster#5 has 191 (16.9%) datasets. Every row in the heatmap represents a dataset. The <i>o-score</i> of a given dataset is distributed in 20 bins of a histogram. The bin edges are arranged in columns along the corresponding row of the dataset. The distribution of <i>o-score</i> varies across clusters.	50

3.5	Density plot and heatmap illustrating the distribution of <i>o-score</i> for 4 different large size datasets. The density plot shows the frequency distribution of <i>o-score</i> for outliers. Every row in the heatmap represents a dataset. The <i>o-score</i> of a given dataset is distributed in 20 bins of a histogram. The bin edges are arranged in columns along the corresponding row of the dataset.	52
4.1	Enhash accommodates both virtual and real drift.	58
4.2	Tuning of <i>L</i> . For both synthetic and real datasets, we show a trend in performance metrics, Error (%), and Time(hrs) for an increase in values of <i>L</i> . The value of <i>L</i> varies from [2, 14]. For a given value of <i>L</i> , the running time is measured across all the samples for all the estimators in a configuration. The value of error is evaluated across all the samples for a given value of <i>L</i>	66
4.3	Tuning of <i>bin-width</i> . For both synthetic and real datasets, we show a trend in performance metrics, Error (%), and Ram-hours for different values of <i>bin-width</i> . The value of <i>bin-width</i> varies in [0.0001, 0.0005, 0.001, 0.005, 0.01, 0.05, 0.1, 0.5]. a) The value of error is evaluated across all the samples for a given value of <i>bin-width</i> . The values of <i>bin-width</i> on x-axis are on logarithmic scale. b) Ram-hours are calculated across all the samples for all the estimators for a given configuration. The values of <i>bin-width</i> on x-axis and Ram-hours on y-axis, both are on log scale. .	67
5.1	The data stream is periodic, has no fluctuation in observed values across different time periods and there is no anomaly.	76
5.2	A periodic data stream with minor fluctuations and no anomaly.	76
5.3	A periodic time-series with an anomaly.	76
5.4	The presence of an anomaly in an aperiodic time-series.	77
5.5	A data stream with a concept drift.	77

List of Tables

2.1	Run-time complexities of algorithms is compared. These complexities are presented with respect to number of samples only.	33
2.2	FiRE is fast. Execution time (in minutes) collected for the four methods with cell counts varying from 1k to ~68k.	33
3.1	Run-time complexities of algorithms is compared. These complexities are presented with respect to the number of samples only.	43
3.2	The performance of FiRE.1 [53], FiRE [67], and HBOS [45] is evaluated on 5 different clusters. A cluster consists of datasets with similar distributions of <i>o-score</i> . Different clusters consist of a different count of datasets. For every cluster, the performances have been compared from the context of all evaluation measures and graded using Friedman ranking. The lowest value of Friedman ranking across methods for a given measure is boldfaced.	50
3.3	Summary of the large datasets	52
3.4	The performances of FiRE.1 [53], FiRE [67], and HBOS [45] are compared on 4 large datasets. The values of the following evaluation measures are reported: <i>Adjusted AP</i> , <i>Adjusted P@n</i> , <i>AP</i> , <i>P@n</i> , and <i>ROC AUC</i> . A method with the highest value of evaluation measure for a given dataset is boldfaced.	53

4.1	Time complexities of algorithms is compared. This table presents the complexity to process the N samples from a stream. The base estimators are as per the default parameters of the corresponding classes in <code>scikit-multiflow</code> package. In the table N represents number of samples, d represents number of dimensions, L represents number of estimators, C represents the number of classes, w is the window size, k is the number of trials coming from Poisson distribution, and s is the oversampling rate. To be noted, these are the simplified estimates of the time complexity.	63
4.2	Description of datasets.	65
4.3	Error (in %) is reported to compare the performance of Enhash [66] with other methods. For a given dataset, the method with the least error is in boldface. Due to implementation constraint, Learn ⁺⁺ .NSE could not run for the outdoorStream dataset.	68
4.4	KappaM is tabulated to compare the performances of the methods. For a given dataset, the method with the highest value of KappaM is in boldface.	68
4.5	KappaT is reported to compare the performances of the methods. The highest value of KappaT in each row is highlighted.	69
4.6	The running time of different methods is compared using Time (in hrs). The method with the fastest speed is highlighted for every dataset. . . .	69
4.7	The memory consumption is measured in terms of RAM-hours. The method with the least value of RAM-hours is highlighted for every dataset.	69
4.8	Ablation study of Enhash. The performance of Enhash is compared with its two different variants- 1. Enhash with $\lambda = 0$ (referred to as Enhash-lambda0), and 2. Enhash when ties in <i>concept class</i> assignments are not broken by considering the distance of an incoming sample from the mean of classes in the bucket (referred to as Enhash-noWeights).	71

List of Abbreviations

This document is incomplete. The external file associated with the glossary ‘acronym’ (which should be called `main.acr`) hasn’t been created.

Check the contents of the file `main.acn`. If it’s empty, that means you haven’t indexed any of your entries in this glossary (using commands like `\gls` or `\glsadd`) so this list can’t be generated. If the file isn’t empty, the document build process hasn’t been completed.

Try one of the following:

- Add `automake` to your package option list when you load `glossaries-extra.sty`.

For example:

```
\usepackage[automake]{glossaries-extra}
```

- Run the external (Lua) application:

```
makeglossaries-lite.lua "main"
```

- Run the external (Perl) application:

```
makeglossaries "main"
```

Then rerun \LaTeX on this document.

This message will be removed once the problem has been fixed.

Chapter 1

Introduction

The process of identifying, and where appropriate, removing anomalous observations from data, is referred to as *outlier detection* [58]. Most commonly, *anomaly detection* is used interchangeably with outlier detection. The concept of outlier detection is widely used to identify faulty engines to avoid undesirable consequences in the future, outlying observations in patients' medical records to detect the possibility of a disease, anomalous trends in prices of a stock to book profits or avoid losses, unusual patterns in credit card transactions to identify possible theft, etc. In effect, outlier detection plays an important role in several analytical tasks. Outlier detection techniques may be supervised or unsupervised. We focus on unsupervised anomaly detection techniques. In scenarios where the complete dataset may be loaded into RAM for mining, *offline algorithms* are sufficient. There may be scenarios where RAM is limited, e.g. IoT devices, or where the distribution of a dataset may evolve or change with time; in such cases, online algorithms are necessary. In non-stationary environments, algorithms must adapt to new distributions as well. The process of learning about changes in the data distribution in streaming environments is referred to as *concept drift detection* [29].

1.1 Scope and objectives

For both streaming and non-streaming environments, we identify rarity/outlierness as the flip side of density around the samples. Samples or points with sparser neighborhoods are more likely to be rare, as against those with dense neighborhoods. With

increasing dimension, finding absolute nearest neighbors becomes prohibitive. Hence, to avoid the *curse of dimensionality* [94], approximate nearest neighbors are computed. There have been some attempts in the past to use the local density around the sample as the measure of its rarity [13]. We expedite the process by finding the neighbors in constant time using the concept of hashing. Hashing methods are widely used for several practical applications such as data mining [7, 118], audio-video fingerprinting [93, 126], identification of copy videos [35], clustering of large single-cell data [113, 114]. The primary reason being that hashing techniques identify the approximate nearest neighbor(s) of a query in $O(1)$ time. We exploit hashing to identify outliers quickly and efficiently amongst several thousands of samples in high-dimensional spaces. We briefly discuss about *LSH (Locality Sensitive Hashing)* and its variants in the subsequent section. This is followed with a brief background and the importance of the problem (*outlier detection* and *concept drift detection*); the motivation to propose a new technique for the same.

1.2 Locality Sensitive Hashing

Indyk and Motwani [44, 60] introduced *LSH (Locality Sensitive Hashing)* to identify approximate nearest neighbors. The key idea behind the concept is to use hash functions such that similar objects/samples have a higher probability of collision than those samples which are far apart. Then, the points in the same bucket represent each other's neighborhood. The hash functions are chosen so that they reduce the complexity of objects owing to their dimensionality while preserving the inter-point distances within a relative error of ϵ (Johnson-Lindenstrauss lemma) [86]. Formally, LSH is defined as follows:

A family \mathcal{H} is defined for a metric space $\mathcal{M} = (M, d)$, a threshold $R > 0$ and an approximation factor $c > 1$. It is a family of functions $h : M \rightarrow S$ which maps elements from the metric space to a bucket $s \in S$. The family is called (R, cR, P_1, P_2) -sensitive if for any two points $p, q \in \mathbb{R}^d$

- if $\|p - q\| \leq R$ then $\Pr_{\mathcal{H}}[h(p) = h(q)] \geq P_1$
- if $\|p - q\| \geq cR$ then $\Pr_{\mathcal{H}}[h(p) = h(q)] \leq P_2$

For LSH family \mathcal{H} to be useful, it should satisfy $P_1 > P_2$. In effect, an LSH technique

is a distribution on a family \mathcal{H} of hash functions, such that for any pair of objects p , and q

$$Pr_{h \in \mathcal{H}}[h(p) = h(q)] = sim(p, q),$$

where $sim(p, q) \in [0, 1]$ is some similarity function defined on the collection of objects [22]. We briefly discuss some of the LSH-based techniques that find approximate nearest neighbors in high-dimensional spaces [27, 115], even when the intrinsic dimensionality is high. These methods represent samples via compact representation such that inter-point distances in the original feature space are well-approximated.

1.2.1 Sketching

The sketch construction algorithm [134] involves randomly picking a threshold for a given feature and assigning it a bit. If the value of a feature is greater or smaller than a given threshold, then bit 1 or bit 0 is assigned, respectively. The sketches constructed using this technique result in bit vectors. Let B be the sketch size in bits. The similarity between objects $sim(p, q)$ is then computed as the measure of similarity between their corresponding sketches. There exist several evidences that show that sketches constructed using random projections can be used to approximate l_1 distance on the feature vectors with the Hamming distance on their sketches [89].

1.2.2 Binary hash

Binary hash [22, 130] involves random projection of a sample x by picking B random vectors w_i , where $i \in \{1, \dots, B\}$ (from the Gaussian distribution). The bit vector is then assigned to x on the basis of $sign(w_i^T x)$, where $i \in \{1, \dots, B\}$. The probability of two samples hashing into the same bucket is determined by the cosine similarity between them in the original feature space.

1.2.3 Projection hash

Projection hash [115] involves linear projection of a sample, followed by assignment to the bucket via quantization. For linear projection of a sample x , B random vectors w_i , where $i \in \{1, \dots, B\}$ are chosen from the Gaussian distribution and a bias $bias$ from

the uniform distribution over $[-bin-width, bin-width]$, where $bin-width$ is the quantization width. The hash code is computed as $\lfloor (w_i^T x + bias) / bin-width \rfloor$, where $i \in \{1, \dots, B\}$.

1.3 Outlier detection

1.3.1 Outlier detection: Definition

The commonly used notions of outliers are as follows:

- “An outlying observation, or outlier, is one that appears to deviate markedly from other members of the sample in which it occurs [50].”
- According to Hawkins [55], an outlier is “an observation which deviates so much from other observations as to arouse suspicions that it was generated by a different mechanism.”
- “An object O in a dataset T is a $DB(p, D)$ -outlier if at least fraction p of the objects in T lies greater than distance D from O [73].”

1.3.2 Outlier detection: Use cases

Outlier detection is widely used across several applications to extract samples that distinct from the majority population. In specific scenarios, these samples act as noise, while in other cases, they may be used to extract some useful hidden phenomena. The most critical application of outlier detection is identifying anomalous patterns in medical diagnoses to identify brain tumor [100], cancerous masses in mammograms [121], etc. It can also be used to monitor industrial production and point out defective manufacturing products [46].

1.3.3 Outlier detection: Existing techniques

Several algorithms have been proposed in the recent past to identify outliers. They may be broadly categorized as supervised and unsupervised algorithms. However, supervised algorithms are more expensive than unsupervised algorithms. Also, supervised algorithms are particularly restrictive in class-imbalance problems [62].

We discuss in detail some of the widely used unsupervised methods that provide outlier scores. A score enables a qualitative comparison of the concerned methods. The Distance-based outlier score (DB-outlier score) [73] modifies the conventional definition of distance-based outlier detection, to rank points based on their outlierness values. The number of points present within a given *distance* from a given point determines its rank. A higher rank indicates a higher degree of sparsity around a data point. However, for high dimensional points, it is very difficult to choose an appropriate value of *distance*.

k NN (k^{th} Nearest Neighbor) [101] identifies outliers using the distance of a point to its k^{th} nearest neighbor. The longer the distance, the higher is the rank. k NNW (k NN-weight) [4] is an extension of k NN that is less sensitive to the choice of k . It also scales linearly for points in high dimensional spaces by using the Hilbert space-filling curve. k NNW maps points to a d -dimensional hypercube $D = [0, 1]^d$. A Hilbert space-filling curve maps this hypercube to the interval $I = [0, 1]$. This facilitates a quick search of k nearest neighbors of a point, by identifying its predecessors and successors on I . It considers the sum of distances to k nearest neighbors as the weight of a point p . The points with high values of weights are the potential outliers.

LIC (Local Isolation Coefficient) [141] is defined as the sum of the distance of the farthest point in the k -neighborhood of p ($k\text{-dist}(p)$), and the average distance of points in the k -neighborhood from p ($LDS_k(p)$). For points in a dense cluster, both $k\text{-dist}(p)$ and $LDS_k(p)$ are small and hence, LIC is also small.

LOF (Local Outlier Factor) [13] considers only a restricted neighborhood to identify outliers, and is, therefore, more suitable for local outlier detection. It assigns a degree of outlierness to every point, and hence, called as local outlier factor. For a given point p , it defines $\text{dist}_k(p)$ as the distance between p and its k^{th} NN. The local neighborhood of p , $N_k(p)$, consists of all points with distance less than or equal to $\text{dist}_k(p)$. It calculates the *reachability* to every point in its k -neighborhood $N_k(p)$, $p' \in N_k(p)$, as follows.

$$\text{reachability}_k(p \leftarrow p') = \max\{\text{dist}_k(p), \text{dist}(p, p')\} \quad (1.1)$$

In the above (1.1), $\text{dist}(p, p')$ is an L_P distance. Local reachability density of point p , $\text{lrd}(p)$, is defined as the ratio of cardinality of $N_k(p)$ and the sum of *reachability* to points

in $N_k(p)$. For a given point p , $LOF(p)$ is calculated as follows.

$$LOF_k(p) = \frac{\sum_{o \in N_k(p)} \frac{lrd(o)}{lrd(p)}}{|N_k(p)|} \quad (1.2)$$

Intuitively, a point p with lower value of $lrd(p)$, and higher values of lrd of points in $N_k(p)$ is assigned higher values of LOF . Simplified-LOF [111] simplifies the definition of local reachability density in LOF. It redefines it as the inverse of $dist_k(p)$ for a given point p .

LDOF (Local Distance-based Outlier Factor) [144] is an extension of LOF for identification of outliers in scattered datasets. $LDOF$ is the ratio between $LDS_k(p)$ and the average of pairwise distances between points in k -neighborhood of p . Points with $LDOF > 1$ are more likely to be outliers. INFLO (INFLuenced Outlierness) [64] considers both the k -neighborhood of p ($N_k(p)$), and the reverse neighborhood of p ($RNN_k(p)$) to estimate $lrd(p)$. $RNN_k(p)$ refers to the collection of points for which p exists in their k -neighborhood. The combined space of $N_k(p)$ and $RNN_k(p)$ is collectively called as k -influenced space for p ($IS_k(p)$). For a given point p , $INFLO_k(p)$ is calculated as follows.

$$INFLO_k(p) = \frac{lrd_{avg}(IS_k(p))}{lrd(p)}, \text{ where } lrd_{avg}(IS_k(p)) = \frac{\sum_{o \in IS_k(p)} lrd(o)}{|IS_k(p)|} \quad (1.3)$$

INFLO uses the same definition of $lrd(p)$ as in Simplified-LOF.

LDF (Local Density Factor) [83] incorporates LDE (Local Density Estimate), a kernel density estimate (KDE), to identify outliers. $LDE(p)$ is computed as follows.

$$LDE(p) = \frac{\sum_{o \in N_k(p)} \frac{1}{(2\pi)^{\frac{d}{2}} (h \times dist_k(o))^d} \exp\left(-\frac{(reachability_k(p \leftarrow o))^2}{2 \times (h \times dist_k(o))^2}\right)}{|N_k(p)|} \quad (1.4)$$

In the above (1.4), h represents a fixed bandwidth. $LDF(p)$ is calculated as

$$LDF(p) = \frac{\sum_{o \in N_k(p)} \frac{LDE(o)}{|N_k(p)|}}{LDE(p) + c \times \sum_{o \in N_k(p)} \frac{LDE(o)}{|N_k(p)|}} \quad (1.5)$$

In (1.5), c is a scaling constant. The higher the value of $LDF(p)$, the more likely it is to be an outlier. The kernel density estimator chosen by LDF does not integrate to

1, an essential property of any such estimator. To fix this, KDEOS (Kernel Density Estimation Outlier Scores) [110] incorporates such estimators in LOF, which preserves the said property for every point. $KDE_k(p)$ for a given point p is computed as follows.

$$KDE_k(p) = \frac{1}{N} \sum_{o \in N_k(p)} K_{h(p)}(p - o), \text{ where} \quad (1.6)$$

N is the dataset size, and $K_{h(p)}(\cdot)$ is the kernel function with bandwidth $h(p)$, which is defined as follows.

$$h(p) = \min\{\text{mean}_{o \in N_k(p)} \text{dist}(p, o), \epsilon\} \quad (1.7)$$

LoOP (Local Outlier Probabilities) [78] makes LOF less amenable to the choice of k for the estimation of local reachability density. To achieve this, LoOP conceptualizes a scoring method independent of data distribution and returns the probability of each point being an outlier.

COF (Connectivity-based Outlier Factor) [120] redefines the notion of reachability as the average chaining distance (*ac-dist*). It differentiates between points with low density and isolated points. Let $G = \langle p_1, p_2, \dots, p_N \rangle$, which consists of all points. Assume two disjoint sets $A, B \subseteq G$ and $A \cap B = \phi$. COF defines the notion of distance between A and B as

$$\text{dist}(A, B) = \min\{\text{dist}(x, y) : x \in A \ \& \ y \in B\} \quad (1.8)$$

Let an ordered set of points $s = \langle p_1, p_2, \dots, p_r \rangle$, termed as set based nearest path or an SBN-path on G from p_1 . An SBN-trail with respect to an SBN-path s is a sequence $\langle e_1, e_2, \dots, e_{r-1} \rangle$ such that for all $1 \leq i \leq r - 1$, $e_i = (o_i, p_{i+1})$, where $o_i \in \langle p_1, p_2, \dots, p_i \rangle$. So, *ac-dist* from p_1 to $G - \{p_1\}$ is defined as

$$\text{ac-dist}_G(p_1) = \sum_{i=1}^{r-1} \frac{2(r-i)}{r(r-1)} \text{dist}(e_i) \quad (1.9)$$

Equation (1.8) is applicable to e_i since e_i is a sequence. Isolated points will have higher values of *ac-dist* than points with low density. Now, *COF* at p with respect to its

k -neighborhood is defined as

$$COF_k(p) = \frac{|N_k(p)| \times ac-dist_{N_k(p)}(p)}{\sum_{o \in N_k(p)} ac-dist_{N_k(o)}(o)} \quad (1.10)$$

ODIN (Outlier detection using Indegree Number) [54] utilizes directed k NN graphs to identify outliers. Every point represents a vertex, and an edge connects a pair of nearest neighbors. For every point, there are exactly k outgoing edges to its nearest neighbors. The resultant in-degree of the vertex is used to rank outliers. A point with a lower in-degree is more likely an outlier.

FastABOD (Fast Angle-Based Outlier Detection) [80] has been proposed as an outlier detection approach for points in high-dimensional spaces. It handles the curse of dimensionality by replacing the distance-based approach with an angle-based one. *ABOF* (*Angle-based outlier factor*) is defined as the variance over the angles between the difference vectors of a point p to the remaining points in a given dataset. FastABOD approximates *ABOF* and computes the variance in angles between the difference vectors of a point p and $N_k(p)$ only. Points with lower values of *ABOF* are potential outliers. SOD (Subspace Outlier Degree) [79] solves the problem of identifying outliers in high-dimensional spaces by identifying relevant attributes. For every point p , it defines its reference set of points $R(p)$. For $R(p)$, it computes its variance along every attribute. The variance along an attribute i is independent of other attributes. An attribute i is relevant for $R(p)$ if its variance is lower than the expected variance. The resultant relevant attributes define subspace hyperplane $H(R(p))$. The distance of p from $H(R(p))$ is used to determine its degree of outlierness. A value near to 0 indicates that point p fits well into $H(R(p))$.

HBOS (Histogram-based Outlier Score) [45] is an extremely fast unsupervised outlier detection approach. It assumes independence of features for faster computation. HBOS constructs an individual histogram for every feature or dimension (d) in data. The height of each bin represents the density of points falling into that bin. These values are converted into probabilities by normalizing them using the dataset size. The outlier

score for each data point is computed as

$$HBOS(p) = \sum_{i=1}^{i=d} \log \left(\frac{1}{hist_i(p)} \right), \text{ where} \quad (1.11)$$

$hist_i(p)$ is the density of point p in dimension i , normalized by the number of samples.

The overall categorization of various methods can be summarized as follows 1.1:

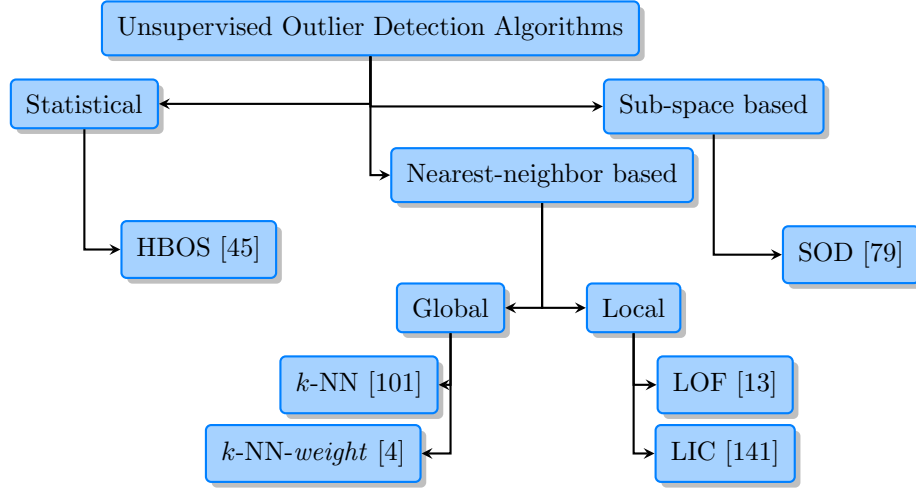


Figure 1.1: Overall categorization of well-known unsupervised anomaly detection algorithms. The three broad categories are statistical, sub-space based, and nearest-neighbor based.

1.3.4 Outlier detection: Motivation

To date, several methods have been proposed that identify outliers. However, in general, methods do not scale with increasing number of samples N . Methods such as k NN [101], ODIN [54], LOF [13], Simplified-LOF [111], INFLO [64], LoOP [78], LDF [83], LIC [141], DB-outlier score [73], and KDEOS [110] require $O(N^2)$ to identify k nearest neighbors (NNs). This may be reduced to $O(N \log N)$ if the dataset is indexed. COF [120], LDOF [144], and FastABOD [80] require an additional $O(k^2)$ computations per point. Therefore, they require an overall running time of $O(N \log N + N \times k^2)$. Very few methods scale well with increasing dimensions d . SOD [79] has an overall run-time complexity of $O(d \times N^2)$, where d is the total number of features. This may be reduced to $O(d \times N \log N)$ if an indexed structure is used to find NNs. Also, there are too scarce methods with linear run-time complexity, such as Isolation Forest [87], RS-Hash [65],

and HBOS [45] (for fixed bin widths). For dynamic bin widths, HBOS has $O(N \log N)$ complexity. HBOS constructs a histogram for every feature independently and then combines them to determine the density of every point. However, it does not consider the possibility of irrelevant/redundant features.

The inability of the state-of-the-art algorithms to scale to large datasets poses a great challenge, especially for biological applications. One prevalent use-case is that of identification of minor cell types amongst thousands of single cells. These cell types have several profound applications, such as pathogenesis of cancer, angiogenesis in cancer and other disorders, etc. These rare cells correspond to the group of global outliers.

There is another group of outliers called as local outliers, that are unusual only to a local section of the data [16]. A dataset may consist of local or global or a combination of outliers. Till date, there have been very limited efforts to quantify a given dataset on the basis of the presence of outlier sub-categories.

1.3.5 Outlier detection: Proposed technique

We propose hashing based techniques to detect outliers in linear time. The proposed method uses an ensemble of different subspaces to determine outliers. FiRE (Finder of Rare Identities) is a *sketching* based algorithm that detects global outliers. FiRE has been employed to detect rare cells in a single-cell study with approx. 68k cells expressed in approx. 32k space of genes. An extension of FiRE, FiRE.1, works well for the identification of local outliers as well. An extensive comparison of FiRE.1 has been shown with 18 state-of-the-art outlier detection algorithms on a diverse collection of 1000 datasets. We also propose a scoring criterion that assigns a value to a dataset based on it's outliers' local or global nature.

The notion of an outlier may also change with time, particularly in non-stationary environments. This is the motivation for the next chapter of the thesis, that focusses on detecting changes in data distributions over time.

1.4 Concept drift detection

1.4.1 Concept drift detection: Definition and use cases

During classification, a change in the distribution of data is referred to as the *concept drift* problem [41]. Let $p(c|x) = p(x|c)p(c)/p(x)$ be the Bayes posterior probability of a class that an instance x belongs to. Then *concept drift* can formally be defined as the one where $p_{t+1}(c|x) \neq p_t(c|x)$, i.e., the posterior probability changes over time. A shift in the likelihood of observing a data point x within a particular class, and thus, alteration of class boundaries is referred to as *real concept drift*. This involves *replacement learning*. A concept drift without an overlap of true class boundaries is referred to as *virtual concept drift*. This requires *supplemental learning*. An example of *real concept drift* involves a change in user's interests in news articles, while the underlying distribution of news articles remains the same. On the other hand, *virtual concept drift* refers to the scenario when the user's interests remain the same, but the underlying distribution of new articles changes with time. A drift may be *incremental*, *abrupt* or *gradual*.

1.4.2 Concept drift detection: Existing techniques

In this section, we discuss some of the widely used ensemble learners for drift detection.

Learn++ [99] is an *Adaboost* [40, 106, 107] inspired algorithm, that generates an ensemble of weak classifiers, each trained on a different distribution of training samples. The multiple classifier outputs are combined using weighted majority voting. For incremental learning, *Learn++* updates the distribution for subsequent classifiers such that instances from new classes are given more weights.

While *Learn++* is suitable for incremental learning, *Learn⁺⁺.NSE* [33] employs a passive drift detection mechanism to handle non-stationary environments. If the data from a new *concept* arrives and is misclassified by the existing set of classifiers, then a new classifier is added to handle this misclassification. *Learn⁺⁺.NSE* is an ensemble-based algorithm that uses weighted majority voting, where the weights are dynamically adjusted based on classifiers' performance.

Accuracy-Weighted Ensemble [129] is an ensemble of weighted classifiers where the weight of a classifier is inversely proportional to its expected error.

Additive Expert Ensemble [75] uses a weighted vote of experts to handle *concept drift*. The weights of the experts that misclassify a sample are decreased by a multiplicative constant $\beta \in [0, 1]$. In case the overall prediction is incorrect, new experts are added as well.

Dynamic Weighted Majority (DWM) [74] dynamically adds and removes classifiers to cope with *concept drift*.

Online bagging and boosting [96] ensemble classifiers are used in combination with different algorithms such as *ADWIN (ADaptive WINdowing)* [9] for *concept drift* detection. ADWIN dynamically updates the window by growing it when there is no apparent change, and shrinking it when the data evolves. In general, bagging is more robust to noise than boosting [30, 97]. Henceforth, we discuss methods based on online bagging, that approximates batch-bagging by training every base model with K copies of a training sample, where $K \sim \text{Poisson}(1)$. We refer to the combination of online bagging classifiers with ADWIN as *Online Bagging-ADWIN*.

Leveraging bagging [10] exploits the performance of bagging by increasing randomization. Resampling with replacement is employed in online bagging using $\text{Poisson}(1)$. Leveraging bagging increases the weights of this resampling by using a larger value of λ to compute the *Poisson* distribution. It also increases randomization at the output by using output codes.

Online SMOTE Bagging [127] oversamples a minor class by using SMOTE [23] at each bagging iteration to handle class imbalance. SMOTE generates synthetic examples by interpolating minor class examples.

ARF (Adaptive Random Forest) [48] is an adaptation of Random Forest [12] for evolving data streams. It trains a background tree when there is a warning and replaces the primary model if drift occurs.

1.4.3 Concept drift detection: Motivation and proposed technique

For drift detection in non-stationary environments, there are mainly two constraints: memory and time. For specific applications such as those related to IoT devices, there is only a limited main memory. A device can accommodate a limited amount of data,

and the model size must be reasonable as well. To accommodate drift, the model must be able to update its parameters, and hence, predict (accordingly) almost instantaneously. For any model to be acceptable, it must have a reasonable performance within constraints (as mentioned above). The most popular methods for the detection of drifts in streaming environments have been ensemble learners [10, 33, 48, 74, 75, 99, 127, 129]. An ensemble method selectively retains few learners to maintain prior knowledge (since new information may be noise), discards, and adds new learners to accommodate new information.

We propose a fast, ensemble learner *Enhash*, based on the concept of hashing that inserts an incoming sample, updates the model parameters, and predicts the class in $O(1)$ time. We show empirically on 6 artificial and 4 real datasets, the superiority of the proposed method Enhash in terms of both speed and performance. The datasets consist of various kinds of drift. The closest competitors of Enhash in terms of performance had significantly large requirements for RAM-hours. Thus, Enhash offers a perfect mix of good performance and superior run times.

1.5 Organization of the thesis

In this thesis, we begin with the problem of identifying rare samples in a dataset. These may be outliers in some contexts and ignored, but in many scenarios, their identification is of critical use. One high impact application is identifying rare cells in sc-RNA data corresponding to thousands of cells. Circulating tumour cells, cancer stem cells, endothelial progenitor cells, antigen-specific T cells, invariant natural killer T cells, etc. are examples of rare cells, whose identification is challenging yet potentially of great significance. For example, Circulating Tumor Cells (CTCs) offer unprecedented insights into the metastatic process with real-time leads for clinical management [77]. Chapter 2 discusses our algorithm for the identification of rare samples, with a focus on sc-RNA data by way of illustration. We propose a high-speed algorithm named as FiRE in chapter 2. FiRE identifies dendritic cell types amongst several thousands of human blood cells. In a single cell sequencing dataset, local outliers act as noise. We propose an extension of FiRE, FiRE.1, in chapter 3 that identifies both local and global outliers. Chapter 3 assesses the relative performance of several well-known outlier detection algo-

rithms. The methods are compared from the perspective of their ability to detect local and global outliers as well. For the identification of outliers in non-stationary environments, we propose Enhash in chapter 4. Enhash accommodates the concept drift and identifies outliers when samples arrive in an online fashion. The thesis concludes with a chapter containing concluding remarks and scope for future work.

Chapter 2

Identification of Rare Events^{*}

2.1 Introduction

Rare events are outliers, that are not noises or erroneous readings but are generated from co-incidental or occasional processes that are valid in the problem/domain contexts. Events generated via such phenomenons tend to cluster themselves. The clusters of such events are fewer and warrant different treatment from a generic outlier. Rare event identification finds widespread application, e.g. detection of credit card fraud or credit-to-GDP gap [25] in the financial domain; or identification of malignant cells [76], and identification of pandemic-causing virus strains, in the medical domain. Sociology and astronomy have benefited from rare event detection techniques as well [68, 145].

In biology, one important use case of rare event detection is minor cell type identification. These minor cell types form small clusters and do not merely exist as singletons. These minor/ rare cell types have profound significance in biological processes. In conventional bioinformatics analysis, the abundant cell types overshadow the presence of minor cell types, and they are not included in the downstream analysis. Thus, depriving the studies of benefiting from the information provided by rare cells. We, therefore, propose an algorithm that overcomes the shortcomings of the current state-of-the-art technologies and detects rare cell types.

Transcriptome analysis of individual cells is now possible thanks to the unrelenting

^{*}The work presented in this chapter has been published as a research paper titled “*Discovery of rare cells from voluminous single cell expression data*” in Nature Communications (2018).

advancement of technology over the past few years [125]. Cells, the fundamental building blocks of complex tissue, are formed in the presence of a variety of stimuli that influence their identity. In contrast to bulk RNA-sequencing, scRNA-seq (single-cell RNA sequencing) examines the average expression-signature of genes in a population of heterogeneous cells at the level of individual cells.

Processing hundreds of thousands of single cells is necessary for thorough characterization of all main and minor cell types in a complex tissue [112]. In other words, the likelihood of detecting small cell subpopulations in a tissue is improved by using bigger sample numbers. It is mostly due to failure at the synthesis step, which prevents a significant percentage of transcripts that are cell-type specific from being discovered during sequencing. As a result, cell types represented by a small number of cells frequently fall short of having a significant impact on the cell type detection regime. The recent development of droplet-based transcriptomic systems has made it possible to profile tens of thousands of individual cells simultaneously for a substantially lower cost per cell. Numerous research has been published to date, with reported transcriptomes with ranging from thousands to hundreds of thousands of cells [15, 82, 90, 118, 148].

Rare cell discovery has been a commonplace element in the pipeline for downstream analysis since the development of single-cell transcriptomics. Minor cell types in an organism are represented by rare cells. Even a singularity (outlier cell) may warrant attention when there are hundreds of profiled cells. However, the emphasis now turns to the finding of minor cell-types rather than merely singletons due to the rise in throughput capacity. Circulating tumour cells, cancer stem cells, endothelial progenitor cells, antigen-specific T cells, invariant natural killer T cells, etc. are examples of rare cell types. Rare cell populations play a significant role in the pathogenesis of cancer, modulating immunological responses, angiogenesis in cancer and other disorders, etc. despite their low abundance. Antigen-specific T cells are crucial to the formation of immunological memory [3, 92, 116]. EPCs (Endothelial Progenitor Cells), which originate from the bone marrow, have proven to be reliable biomarkers of tumor angiogenesis [24, 81]. Stem cells have an ability to replace damaged cells, and to treat diseases like Parkinson's, diabetes, heart diseases, etc. [61]. CTCs (Circulating Tumor Cells) offer unprecedented insights into the metastatic process with real-time leads for clinical management [77].

Algorithms for detecting rare cell transcriptomes are scarce. Prominent among these are RaceID [51] and GiniClust [63]. For the purpose of identifying outlier expression patterns, RaceID employs a parametric statistical technique that is computationally intensive. It uses unsupervised clustering as an intermediate step to define populous cell types, which in turn are used to determine outlier events (cells). GiniClust, on the other hand, employs a rather simple two-step algorithm. It starts by choosing informative genes based on the Gini index [43]. It then applies a density-based clustering method, DBSCAN [36], to discover outlier cells. Notably, to discriminate between major and minor cell types, both RaceID and GiniClust employ clustering. In fact, these algorithms involve the computation of pair-wise distances between cells. Both of these algorithms are memory inefficient and sluggish for huge scRNA-seq data due to a number of important design decisions.

We propose FiRE, a conspicuously fast algorithm, to calculate the density around each subjected multi-dimensional data point. The workhorse algorithm used to accomplish this is Sketching [89, 133]. FiRE, which, in contrast to other methodologies, assigns a rareness score to each sample. In the context of rare cells, this is a score based on each cell’s individual expression profile, thus giving the user a choice for focusing downstream analyses only on a small set of potentially rare cells. However, it must be noted that we use clustering to group these rare cells. We used the dropClust [113] technique to cluster these potential rare cells detected by FiRE. Outlier cells, if any, get submerged into the minor cell clusters since dropClust does not give any special treatment to outliers. Although, dropClust itself removes poor quality cells and genes.

On a variety of real and simulated datasets, we assessed FiRE. We also demonstrated the efficiency of FiRE in delineating human blood dendritic cell subtypes using a large scRNA-seq data of human blood cells.

2.2 Overview of FiRE

As a preliminary step for identifying unusual cells, both RaceID and GiniClust make use of clustering in some way. By its very nature, clustering frequently depends on a variety of delicate characteristics and performs poorly when data point densities vary. Another major problem is to decide the resolution of group identities. Multi-level clustering is

frequently necessary since tiny clusters are frequently missed during the initial pass [15]. This occurs because other significant cell types affect a dataset’s expression variance. We questioned whether it was possible to create a novel, unified approach that directly estimates a cell’s rarity without using clustering (multidimensional data point).

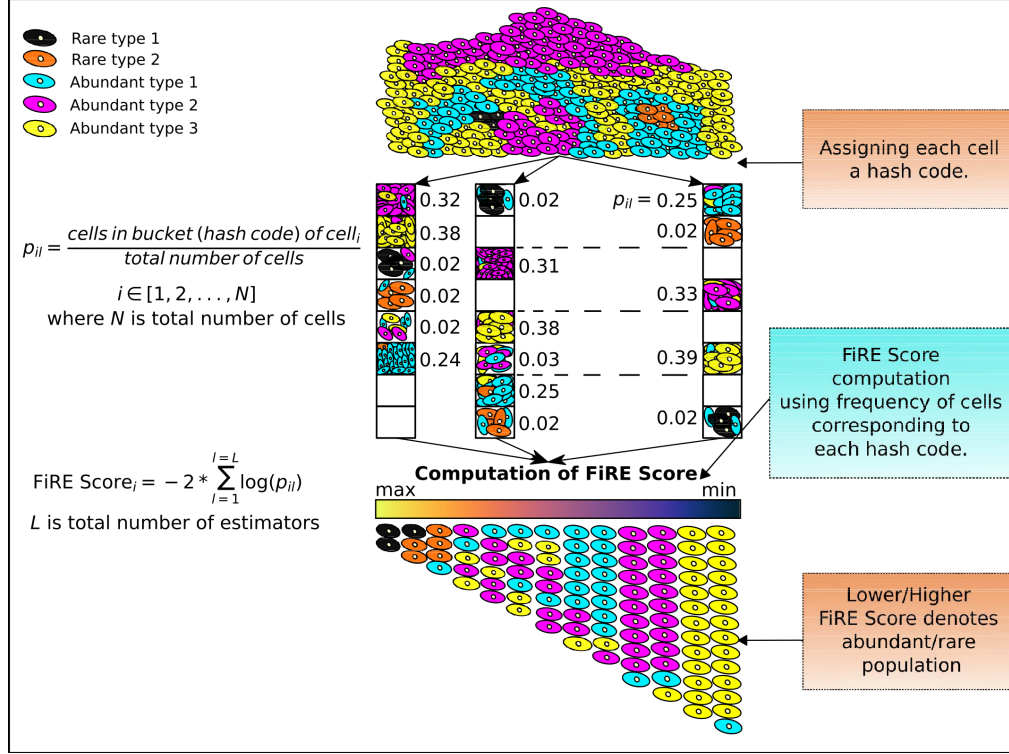


Figure 2.1: Overview of FiRE. The first step is to assign each cell to a hash-code. As numerous similar cells can share the same hash-code, it is possible to think of a hash-code as an imagined bucket. The phase of creating the hash-code is repeated L times to test the reliability of rarity estimates. The chance that any point will fall into the bucket of a given cell i and estimator l is calculated as p_{il} . These probabilities are combined in the algorithm’s second phase to get an estimate of how rare each cell is.

To circumvent the above issues, we propose FiRE to identify rare cell types. Design of FiRE is inspired by the observation, that rareness estimation of a particular data point is the flip side of measuring the density around it. The algorithm capitalizes on the Sketching technique [89, 133], a powerful technique for low dimensional encoding of a large volume of data points. It works by randomly projecting points to low dimensional bit signatures (hash code), such that the weighted L_1 -distance between each pair of points is approximately preserved. The computation involved in the creation of hash codes is linear w.r.t. the number of individual transcriptomes. A hash code can be

imagined as a bucket, that tends to contain data points which are close by in the concerned hyper-dimensional space. The cell originating from a large cluster shares its bucket with many other cells, whereas a rare cell shares its bucket only with a few. To this end, FiRE uses the populousness of a bucket as an indicator of the rareness of its resident data points. To ward off biases, FiRE uses several such rareness estimates, to arrive at a consensus rareness score for each of the studied cells. This score is termed as the FiRE-score. The section 2.2.1 contains an elaborate explanation of the various steps involved in FiRE. Figure 2.1 depicts a visual interpretation of FiRE.

2.2.1 Steps involved in FiRE

Let $X \in \mathbb{R}^d$ represent an input space. Let S contains N data points drawn independently and identically from the distribution D over X . Assume, $U[a, b] = \frac{1}{b-a}$ represents a uniform distribution. Let $S_j^{(i)}$ represents j -th feature of i -th sample. Let, $\forall j \in \{1, \dots, d\}$, $mi_j = \min_{i \in \{1, \dots, N\}} S_j^{(i)}$ and $ma_j = \max_{i \in \{1, \dots, N\}} S_j^{(i)}$. Let, L , M , and H are integers and H is a prime number as well.

FiRE is a two-step algorithm. In the first step, it follows the Sketching [135] process. FiRE randomly selects M values with replacement from $\{1, \dots, d\}$. Say $_ind^{(l)}$, where $1 \leq l \leq L$, represents this set. FiRE projects S onto $_ind^{(l)}$ for every l . Say projected data is P_l . For a P_l , FiRE generates a random threshold vector $_th^{(l)}$ where $_th_j^{(l)} \sim U[mi_{_ind_j^{(l)}}, ma_{_ind_j^{(l)}}]$, where $1 \leq j \leq M$. Every data point in P_l is then converted into a bit stream by thresholding it with $_th^{(l)}$. Let the thresholded data be denoted by T_l ; then, bit j of i -th sample is generated as follows.

$$(T_l)_j^{(i)} = \begin{cases} 1, (P_l)_j^{(i)} \geq _th_j^{(l)} \\ 0, \text{otherwise} \end{cases} \quad (2.1)$$

Further, FiRE samples M elements with replacement from $\mathbb{I}^+ \cup \{0\}$. Say, $_pr^{(l)}$ represents this set. Hash index $_index_i^{(l)}$ for each data point is computed by taking the dot product of their bit vector $T_l^{(i)}$ with $_pr^{(l)}$, and modulo it with H .

$$_index_i^{(l)} = \sum_{j=1}^{j=M} \left((T_l)_j^{(i)} * _pr_j^{(l)} \right) \% H \quad (2.2)$$

In the second step, the neighborhood information is collected for every data point. All data points which map to the same hash index as that of element i construct its neighborhood. Probabilistic neighborhood $neighborhood_i^{(l)}$ is defined as

$$neighborhood_i^{(l)} = \frac{\text{Total data points with hash index } index_i^{(l)}}{N} \quad (2.3)$$

For every data point, this information is combined across L and $FiRE$ -score of each data point, $FiRE\text{-}score_i$, is computed as follows.

$$FiRE\text{-}score_i = -2 \sum_{l=1}^L \log neighborhood_i^{(l)}, \forall i \in \{1, \dots, N\} \quad (2.4)$$

The sparser the neighborhood of a point, the higher the value of $FiRE$ -score. Hence, points with higher values of $FiRE$ -score represent potential outliers. Algorithm 1 gives the pseudo-code of FiRE.

2.3 Results

2.3.1 Experimental setup

2.3.1.1 Description of datasets

For the various analyses, we used four publicly available scRNA-seq datasets.

For a simulation experiment of artificially planted rare cells, we used 293T and Jurkat cells data containing a total of ~ 3200 cells, with an almost equal number of representative transcriptomes of each type. The cells were mixed *in vitro* at equal proportions. Authors of the study resolved the cell types bioinformatically exploiting their SNV profiles [148].

We used a large scale scRNA-seq data containing expression profiles of $\sim 68k$ PBMCs (peripheral blood mononuclear cells), collected from a healthy donor [148]. Single cell expression profiles of 11 purified subpopulations of PBMCs were used as a reference for cell type annotation. Both 293T-Jurkat cells and PBMC datasets are available for download from 10xgenomics.com (<https://support.10xgenomics.com/single-cell-gene-expression/datasets>).

Algorithm 1 FiRE

```
1: function FiRE(Input: dataset) # nSamples x nFeatures
2:    $nSamples \leftarrow$  Number of data samples(cells)
3:    $nFeatures \leftarrow$  Number of features(genes)
4:    $X[nSamples][nFeatures] \leftarrow$  dataset
5:    $L \leftarrow$  Number of runs
6:    $M \leftarrow$  Number of dimensions to be sampled
7:    $H \leftarrow$  Number of bins
8:    $bins[L][H][.] \leftarrow$  Keeps the bin details across runs
9:    $neighborhood[nSamples][L] \leftarrow$  Stores the size of the neighborhood of each sample
10:   $scores[nSamples] \leftarrow$  Stores the score for each sample
11:   $mi \leftarrow \min(X)$ 
12:   $ma \leftarrow \max(X)$ 
13:  for  $i = 1$  to  $L$  do
14:     $\_index[nSamples] \leftarrow [0]$  # Keeps the bin index for all the sample points for the current run.
15:    for  $j = 1$  to  $M$  do
16:       $\_ind \leftarrow \text{randomInt}(\text{low} = 1, \text{high} = nFeatures, \text{dist} = \text{"Uniform"})$ 
17:       $\_th \leftarrow \text{randomFloat}(\text{low} = mi, \text{high} = ma, \text{dist} = \text{"Uniform"})$ 
18:       $\_pr \leftarrow \text{randomInt}(\text{low} = 1, \text{high} = \text{maxInt}, \text{dist} = \text{"Uniform"})$ 
19:      for  $k = 1$  to  $nSamples$  do
20:         $\_v \leftarrow 0$ 
21:        if  $X[k][\_ind] \geq \_th$  then
22:           $\_v \leftarrow 1$ 
23:        end if
24:         $\_index[k] \leftarrow \_index[k] + \_pr * \_v$ 
25:      end for
26:    end for
27:    for  $k = 1$  to  $nSamples$  do
28:       $\_index[k] \leftarrow \_index[k] \% H$ 
29:       $bins[i][\_index[k]].append(k)$ 
30:    end for
31:  end for
32:  for  $i = 1$  to  $L$  do
33:    for  $j = 1$  to  $H$  do
34:       $\_b \leftarrow bins[i][j]$ 
35:       $\_l \leftarrow \text{length}(\_b)$ 
36:      for  $k = 1$  to  $\_l$  do
37:         $neighborhood[\_b[k]][i] \leftarrow \log(\_l/nSamples)$ 
38:      end for
39:    end for
40:  end for
41:  for  $k = 1$  to  $nSamples$  do
42:     $\_t \leftarrow 0$ 
43:    for  $i = 1$  to  $L$  do
44:       $\_t \leftarrow \_t + neighborhood[k][i]$ 
45:    end for
46:     $scores[k] \leftarrow -2 * \_t$ 
47:  end for
48:  return  $scores$ 
49: end function
```

We applied FiRE on a publicly available ~ 2.5 k mouse ESCs (embryonic stem cells) data [70] (GSE65525). Mouse embryonic cells were sequenced at different points after the removal of leukemia inhibitory factor (LIF). Similar to Jiang *et al.* [63], we used Day 0 data where stem cells were undifferentiated. Data contained a total of 2509 cells.

Our fourth scRNA-seq data contained single cell expression profiles of mouse intestinal organoids [51] (GSE62270). A set of 288 organoid cells were randomly selected and sequenced using a modified version of the cell expressions by linear amplification and sequencing (CEL-seq) method. UMI identifiers were used to count transcripts.

2.3.1.2 Data preprocessing

Mouse ESCs and mouse small intestine datasets were screened for low quality cells. For mouse ESC data, cells having more than 1800 detected genes were selected for analysis. For the intestine dataset, the cutoff for the number of detected genes was set at 1200. The remaining data were already filtered.

For each dataset, genes which had a read count exceeding 2 in at least three cells, were retained for downstream analysis. Each scRNA-seq data was normalized using median normalization. The thousand most variable genes were selected, based on their relative dispersion (variance/mean) with respect to the expected dispersion across genes with similar average expression [148]. The normalized matrix was then \log_2 transformed after the addition of 1 as a pseudo count.

2.3.1.3 IQR-thresholding-criteria for selection of cells for further downstream analysis

FiRE marks a cell as rare if its FiRE-score is $\geq q3 + 1.5 \times \text{IQR}$, where $q3$ and IQR denote the third quartile and the inter-quartile range (75th percentile - 25th percentile), respectively, of the number of FiRE scores across all cells.

2.3.1.4 F_1 score computation for the simulation study

Both RaceID [51] and GiniClust [63] provide a binary prediction for rare cells. The contamination parameter in `scikit-learn` package implementation of LOF gives a threshold for the identification of outliers. In a two-class experiment (293T and Jurkat cells), it

is straightforward to construct a confusion matrix. The F_1 score on a confusion matrix can easily be computed as follows.

$$F_1 \text{ score} = 2 \frac{\text{precision} \times \text{recall}}{\text{precision} + \text{recall}}$$

For the simulation experiment, rare cells were considered ones whose FiRE scores satisfied the IQR-thresholding-criterion.

For all algorithms, the F_1 score has been calculated with respect to the minor population of the Jurkat cells.

2.3.1.5 Parameter value selection for FiRE

The process of hashing cells to buckets is repeated L times. For obvious reasons, a large value of L ensures rareness estimates with low variance.

For every estimator, the Sketching technique randomly sub-samples a fixed set of M features. While a very small choice of M requires a commensurately large number of estimators, a very large M might make the FiRE scores sensitive to noisy expression readings.

For all experiments, the hash table size, i.e., H was set 1017881. It should be a prime number large enough to avoid unwanted collisions between dissimilar cells. In practice, H is chosen to be a prime number greater than ten times of the number of items to be hashed.

On two independent datasets, we experimented with different values of L and M . We found $L = 100$ and $M = 50$ were a reasonably good choice to be considered as default values of L and M , respectively (Figure 2.2).

2.3.1.6 Identification of Differential Genes

A traditional Wilcoxon’s rank sum test was used to identify differentially expressed (DE) genes with an FDR cutoff of 0.05 and an inter-group absolute fold-change cutoff of 1.5. Fold-change values were measured between group-wise mean expression values of a given gene. We qualified a gene to be a cell-type specific one if it was found differentially up-regulated in a particular cluster, as compared to each of the remaining clusters.

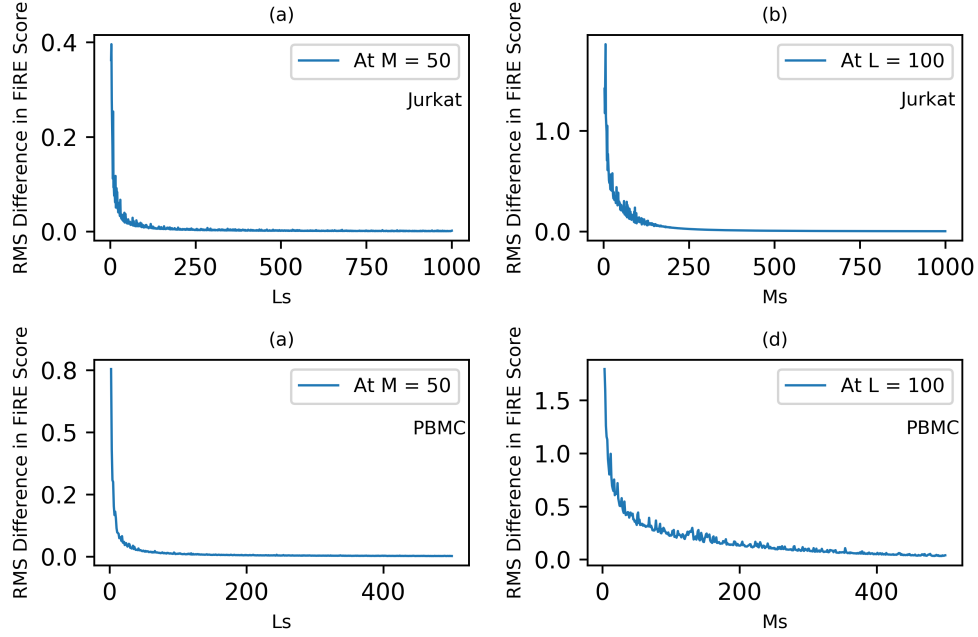


Figure 2.2: Stability of FiRE. (a),(c) RMS (Root Mean Square) difference in values of FiRE-score of every cell between two successive estimators. For calculation of RMS, FiRE-score is averaged across multiple seeds and normalized by the value of L . (b),(d) RMS difference in values of FiRE-score between two successive values of M . For calculation of RMS, FiRE-score is averaged across multiple seeds and normalized by the value of M . (a)-(b) RMS has been shown on a simulated dataset consisting of a mixture of Jurkat and 293T cells [148]. (c)-(d) RMS has been shown on $\sim 68k$ Peripheral Blood Mononuclear Cells (PBMCs) [148].

2.3.1.7 Simulation experiment to assess FiRE's sensitivity to DE genes

To analyze the sensitivity of FiRE to cell type identity, we generated an artificial scRNA-seq data using the `splatter` R package [143]. The following command was used to generate this data:

```
splatSimulate(group.prob = c(0.95, 0.05), method = 'groups', verbose =
F, batchCells = 500, de.prob = c(0.4, 0.4), out.prob = 0, de.facLoc=0.4,
de.facScale = 0.8, nGenes = 5000)
```

The generated dataset had 500 cells and 5000 genes per cell. Out of the 500 cells, 472 cells represented the major cell-type, whereas 28 cells defined the minor one.

Genes for which expression counts exceeded 2 in at least three cells were considered for analysis. The filtered data was \log_2 transformed after adding 1 as a pseudo count. On the transformed data, differential genes were detected using Wilcoxon's rank sum

test with an FDR cutoff of 0.05 and as an inter-group absolute value of fold change cut-off of 2.32 ($\log_2(5)$). The differentially expressed genes, which were 180 in number, were removed from the data and kept as a separate set. Genes with a p-value of more than 0.05, 2387 in number, were kept as a separate set of non-differential genes.

2.3.2 FiRE discovers cells with varying degrees of rareness

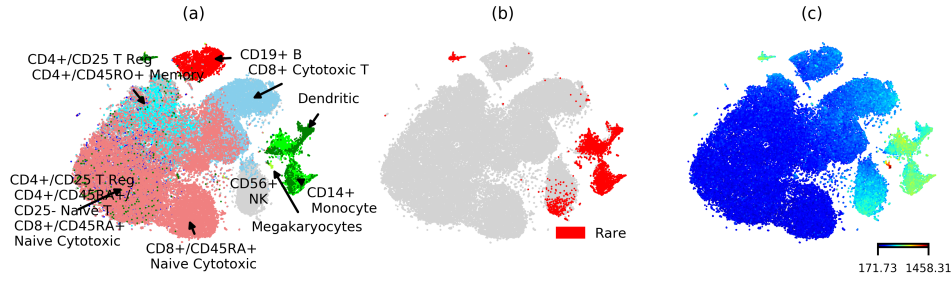


Figure 2.3: Performance evaluation of FiRE on Peripheral Blood Mononuclear Cells (PBMCs). (a) t-SNE based 2D embedding of the data with color coded cluster identities as reported by Zheng and colleagues [148]. (b) Rare population identified by FiRE using IQR-thresholding-criteria. (c) Heat map of FiRE scores for the individual PBMCs. The cluster of megakaryocytes (0.3%), the rarest of all the cell types are assigned the highest FiRE scores.

FiRE assigns a continuous score to each cell, such that outlier cells and cells originating from the minor cell populations are assigned higher values in comparison to cells representing major sub-populations. A continuous score gives users the freedom to decide the degree of the rareness of the cells, to be further investigated. To illustrate this, we applied FiRE on a scRNA-seq data containing $\sim 68k$ Peripheral Blood Mononuclear Cells (PBMCs), annotated based on similarity with purified, well known immune cell sub-types [148] (Section 2.3.1.1). The authors of the study performed unsupervised clustering of the cells and annotated the clusters based on previously known markers (Figure 2.3a). We overlaid FiRE scores on the 2D map reported as part of the study (Figure 2.3c). The top 0.25% highest FiRE scores exclusively corresponded to the smallest, unambiguously annotated cluster harboring megakaryocytes (Figure 2.4a). Of note, megakaryocytes represent only 0.3% of the entire set of the profiled cells. As we increased the proportion from 0.25% to 2.0% and subsequently 5.0%, the next batches of minor cell sub-types made their way into the extended set of rare cells. These include

sub-classes of monocytes and dendritic cell sub-types (Figures 2.4b and 2.4c). The case study highlights the utility of FiRE in discovering cells with varying degrees of rareness.

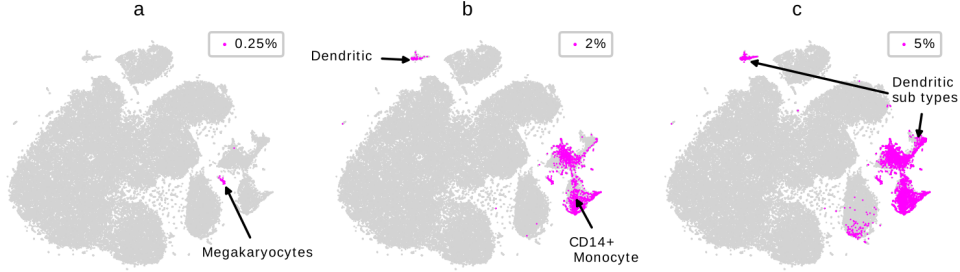


Figure 2.4: In the $\sim 68k$ PBMC data [148], the appearance of minor cell populations with varying degrees of rarity is accompanied by a rise in the number of chosen rare cells. Figures (a)-(c) demonstrate, respectively, the top 0.25%, 2%, and 5% cells chosen based on FiRE scores.

While a continuous score is helpful, sometimes a binary annotation about cell rarity eases out the analysis. To this end, we introduced a thresholding scheme using the properties of the score distribution (Section 2.3.1.3). Figure 2.3b highlights cells in the $\sim 68k$ PBMC data, which are detected as rare going by the threshold based dichotomization. As expected, a majority of the detected rare cells originated from known minor cell types such as megakaryocytes, dendritic cells, and monocytes.

It should be noted that unlike GiniClust and RaceID, FiRE refrains from using clustering as an intermediate step to pinpoint the rare cells. Clustering is done in a later phase for delineating minor cell types from the detected rare cells.

2.3.3 FiRE detects artificially planted rare cells with high accuracy

We designed a simulation experiment to evaluate the performance of FiRE in the presence of ground truth information pertaining to cell-type identity. For this, we used a scRNA-seq data comprising 293T and Jurkat cells combined *in vitro* in equal ratio (Section 2.3.1.1) [148]. The authors exploited the SNV (Single Nucleotide Variant) profile of each cell to determine its lineage. We considered this genotype based annotation scheme to be near confirmatory. With this data, we mimicked the rare cell phenomenon by bioinformatically diluting Jurkat cell proportion in the data. We varied the propor-

tion of Jurkat cells between 0.5% and 5%. Besides GiniClust and RaceID, we compare FiRE with a rare event detection algorithm called Local Outlier Factor or LOF. LOF is a widely used algorithm in the field of data mining. The performance of various methods was measured using F_1 score (Section 2.3.1.4) with respect to the minor population of the Jurkat cells. F_1 score reflects the balance between precision and sensitivity. FiRE clearly outperformed LOF [13], RaceID [51] and GiniClust [63] on each of the test-cases (Figure 2.5a). Notably, RaceID and GiniClust report dichotomized predictions for rare cells, whereas FiRE and LOF offer both continuous scores and binary prediction. FiRE implements an IQR-based-thresholding technique for the dichotomization (Section 2.3.1.3).

We took a closer look at working of the methods at a rare cell concentration of 2.5%. We found FiRE scores of the rare cells to be unambiguously higher compared to the abundant cell type (Figure 2.5c). Figures 2.5d- 2.5g mark the rare cells detected by each of the algorithms. Among all algorithms, FiRE displayed the highest level of congruence with the known annotations (Figure 2.5h). Further, congruence between methods has also been depicted in Figure 2.6.

To evaluate the performance of the techniques, we used two additional datasets: $\sim 2.5k$ Embryonic Stem Cells (ESCs) [70], and 288 mouse intestinal organoids cell data [51] (Section 2.3.1.1). FiRE and LOF could identify Zscan-4 enriched, 2C-like cells, as stated by the authors of the GiniClust algorithm [63] (Figure 2.7a). In addition, FiRE had the least overlap with RaceID, which could not identify the 2C-like cell type. Figure 2.7b depicts the performance of the various methods in identifying rare cell types in the secretory lineage of mouse small intestine, as reported by the authors of the RaceID algorithm. Both FiRE and LOF could detect almost all of the designated rare cell types, including the goblet, tuft, paneth, and enteroendocrine cells. GiniClust could detect only a fraction of these cells.

2.3.4 FiRE is sensitive to cell type identity

A simulation study was designed to analyze the robustness and sensitivity of FiRE-score with respect to the number of differentially expressed genes. We first generated an artificial scRNA-seq data consisting of 500 cells and two cell types. The minor cell

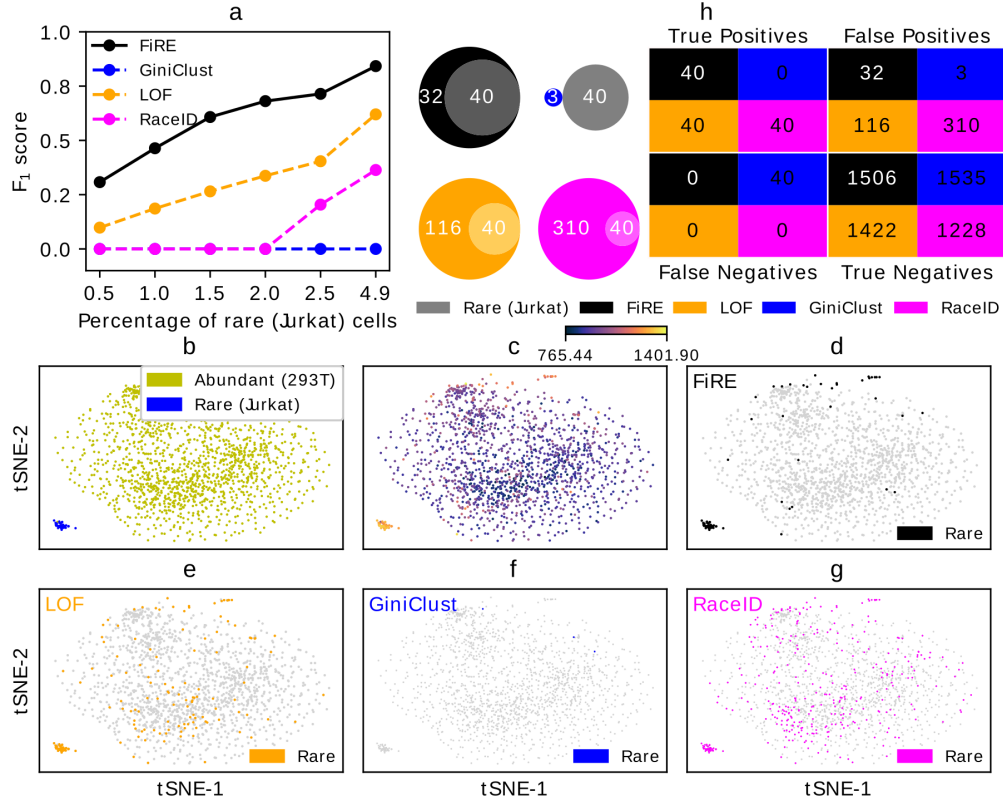


Figure 2.5: Minor cell types' detectability in a simulated dataset with a mixture of Jurkat and 293T cells (known annotations) [148]. (a) F_1 scores were determined relative to the rare (Jurkat) population, while bioinformatically altering the percentage of artificially planted rare cells. It is noteworthy that both FiRE and LOF [13] use a threshold to their continuous scores for zeroing on the rare cells. On the other hand, GiniClust [63] and RaceID [51] offer binary annotations for cell-rarity. (b) t-SNE based 2D embedding of the cells with color-coded identities. (c) FiRE-score intensities were displayed on the t-SNE based 2D map. Figures (d)-(g) demonstrate the rare cells detected by various algorithms. (h) Congruence of methods with known annotations. Note: Results shown in Figures (b)-(h) correspond to a rare cell concentration of 2.5%.

type represented about 5% of the total population (Section 2.3.1.7). We kept aside the DE genes selected through a stringent criterion. For every iteration of the experiments, we replaced a fixed number of non-DE genes by pre-identified DE genes. We varied the count of differentially expressed genes between 1 to 150 to track the sensitivity of FiRE in detecting the minor population.

With the given set of differentially expressed genes, FiRE scores were obtained and used for computing the ROC-AUC with respect to the minor population. For every count of differentially expressed genes, the aforementioned process was repeated 1000 times to report an average ROC-AUC (Figure 2.8).

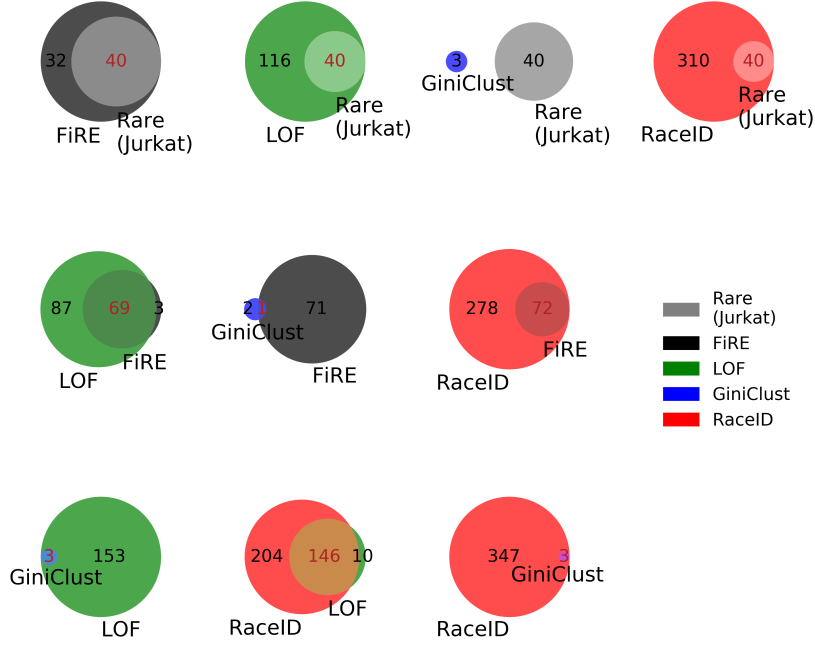


Figure 2.6: Congruence of methods with known annotations and congruence between pairs of methods on a simulated, scRNA-seq data consisting of 293T and Jurkat cells mixed *in vitro* in equal proportion [148].

With a small number of DE genes, FiRE struggled to detect the minor cell population. However, FiRE predictions improved sharply when 20 or more DE genes were introduced. It reflects the robustness of FiRE against noise. A plausible explanation for the same could be that a small number of differential genes fail to stand out in the presence of cell-type specific expression noise (biological plus technical).

2.3.5 FiRE is scalable and fast

Both RaceID and GiniClust are slow and incur significant memory footprints. For both these methods, clustering takes $O(N^2)$ time, where N is the number of cells. RaceID additionally spends enormous time in fitting parametric distributions for each cell-gene combinations. On the other hand, LOF requires a large number of k-nearest neighbor queries to assign an outlieriness score to every cell. FiRE, on the other hand, uses Sketching [133], a randomized algorithm for converting expression profiles into bit strings

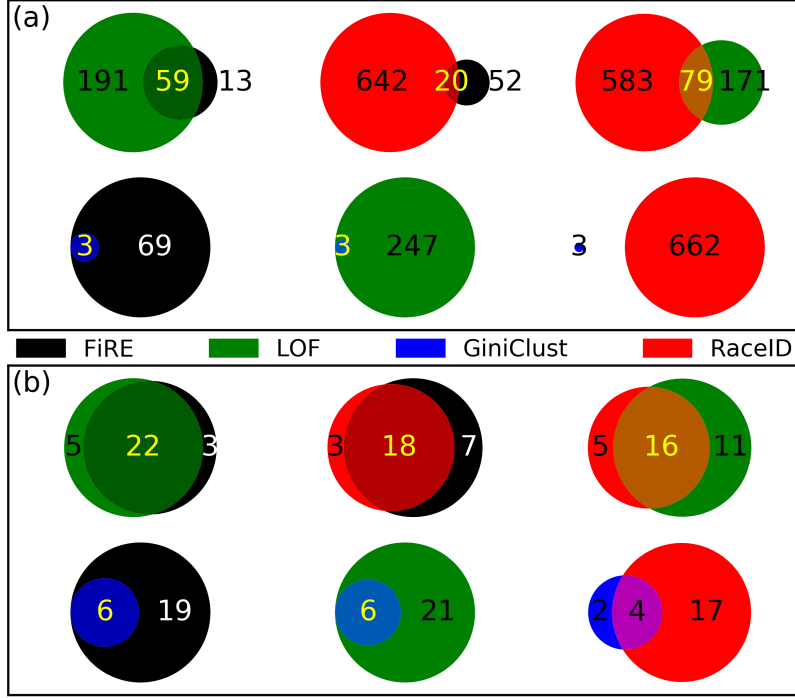


Figure 2.7: Congruence of methods using Venn diagrams. (a),(b) Performance comparison of FiRE, GiniClust [63], RaceID [51] and LOF [13] as per the rare cells identified by them. (a) Performance comparison of methods above on Embryonic Stem Cells (ESCs) data [70]. FiRE could easily identify the Zscan-4 enriched, 2C-like cell cluster as reported by Jiang *et al.* [63]. Also, the FiRE predicted rare cells had the least overlap with the ones predicted by RaceID, which could not identify those 2C-like cells. (b) Performance on mouse small intestine cells [51]. FiRE could identify the rare cell types in the secretory lineage, which consisted of goblet, enteroendocrine, paneth and tuft cells (as discussed in Grun *et al.* [51]).

while preserving the weighted L_1 distance between data points. The main advantage of randomized algorithms is, that they usually save a lot of computational time. FiRE generates a rareness estimation of N cells in linear, i.e., $O(N)$ time, where the constant is $L \times M$.

FiRE does two passes over the dataset. To quantify the time complexity of the first pass of FiRE, let us assume a dataset of N cells represented in d dimensions. In sketching technique, hash value computation requires two steps 1. thresholding of sub-spaced feature vector and 2. linear combination of thresholded vectors. Assume that L such hash values are generated. Thus, to perform sketching, L random estimators of M dimensions would be generated. Both of the aforementioned steps require $O(M)$ computations for an estimator. Expanding this estimate for each estimator and every

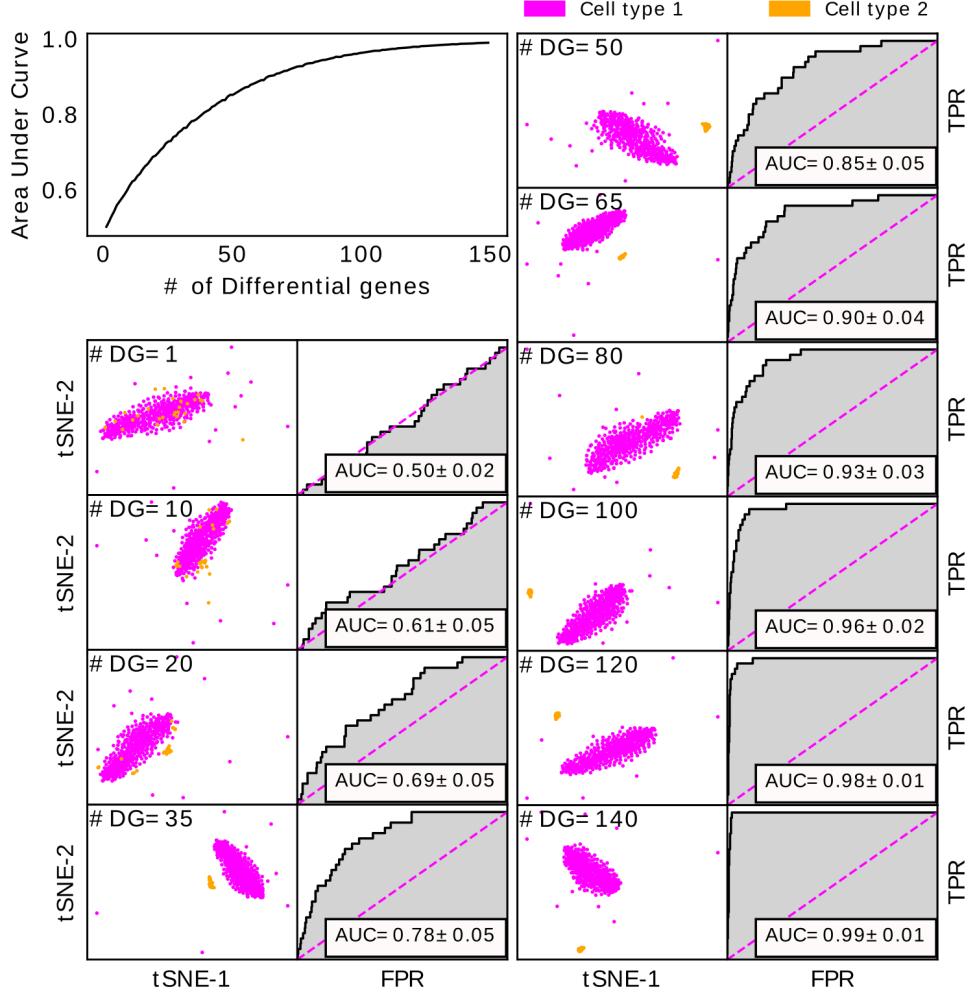


Figure 2.8: Sensitivity of FiRE to cell type. As soon as there are enough differentially expressed genes to create a small cluster that represents the minor cell subpopulation, fire begins properly identifying the minor cell type on scRNA-seq data generated using the R tool `splatter` [143]. The succeeding ROC-AUC plots use the figure in the upper-left corner as their legend. Each t-SNE and ROC figure pair represents one of the 1000 times the experiment was run with respect to a particular set of differentially expressed genes. Cell-group annotations were used in the ROC-AUC study, and individual cells were given FiRE ratings.

sample, the total time required to compute the hash value is $O(N \times L \times M + N \times L \times M) \approx O(N \times L \times M)$. Now, to limit the range of hash value, a modular operation is also performed that can be completed in constant time for every sample. Thus, the total time to hash the dataset is given by $O(N \times L \times M + N) \approx O(N \times L \times M)$. Assuming that total number of possible hash values are H . Further assume that these hash values are represented in a form of an array of size H and every element in that

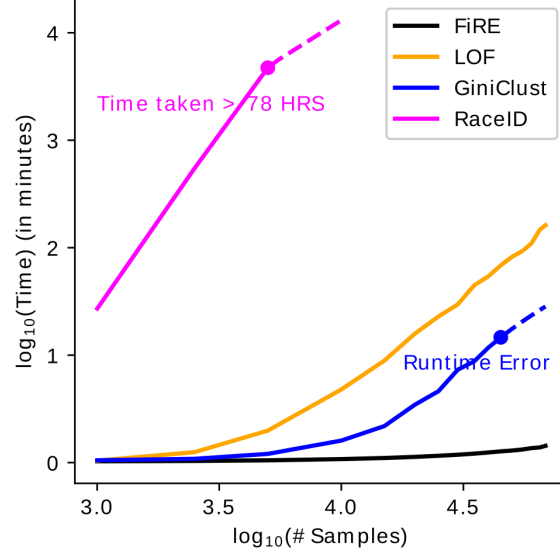


Figure 2.9: FiRE is fast. Execution time collected for the four methods with cell counts varying from 1k to ~68k.

array can be accessed in constant time. Interleaving the counting of number of samples sharing same hash value will require additional $O(N \times L)$ time. Now, in the second pass, the final rarity score is computed. This computation of final score will require consulting the hash values of one sample across L estimators that can be completed in $O(L)$ time, and for N samples this time would be $O(N \times L)$. Thus, total time to compute the rarity score (combining both first pass and second pass) can be given by $O(N \times L \times M + N \times L + N \times L) \approx O(N \times L \times M)$. It can be argued that the L and M are the constants for an algorithm run. Thus, the effective complexity of score computation is $O(N)$.

We tracked the time taken by LOF, RaceID, GiniClust, and FiRE, while varying the input data size (Figure 2.9, Table 2.2, 2.1) on a single core of a machine with a clock speed of 1.9 GHz, and 1024 GB DDR4-1866/2133 ECC RAM. FiRE turned out to be remarkably faster as compared to LOF, RaceID, and GiniClust. For FiRE, we recorded ~26 seconds on the ~68k PBMC data. GiniClust reported a runtime error, when the input expression profiles increased beyond ~45k, while RaceID took ~79 hours for just 5k cells.

Table 2.1: Run-time complexities of algorithms is compared. These complexities are presented with respect to number of samples only.

Algorithm	Complexity	Remarks
FiRE [67]	$O(N)$	
LOF [13]	$O(N^2)$, $O(N \log N)$	Tree based approaches can be used to speed-up the nearest neighbor searches.
GiniClust [63]	$O(N^2)$	
RaceID [51]	$O(N^2)$	Although the complexity is same as GiniClust, it has a very large constant associated with the big O notation, because it also learns multiple parametric distributions.

Table 2.2: FiRE is fast. Execution time (in minutes) collected for the four methods with cell counts varying from 1k to $\sim 68k$.

Samples	FiRE time (min.) [67]	LOF time (min.) [13]	GiniClust time (min.) [63]	RaceID time (min.) [51]
1000	0.0289066871	0.0442489147	0.0517063022	26.14682858
2500	0.0365521709	0.250727284	0.085117805	544.0205631
5000	0.0502097885	0.985178566	0.2058585723	4729.290497
10000	0.0783540368	3.79507608	0.6036896904	-
15000	0.1040728211	7.898171449	1.187051054	-
20000	0.1308689475	14.83272862	2.456504417	-
25000	0.1575588862	21.9108673	3.621491746	-
30000	0.1842079679	28.68896627	6.329408483	-
35000	0.2123669028	43.65191623	7.754190397	-
40000	0.2424690485	53.09929506	10.74303849	-
45000	0.2728209337	67.55955516	13.65257459	-
50000	0.2950131019	81.28970995	-	-
55000	0.3231681029	91.62621465	-	-
60000	0.3635717352	108.2481951	-	-
65000	0.3853084048	145.867392	-	-
68579	0.4325375557	160.8379446	-	-

2.3.6 FiRE resolves heterogeneity among dendritic cells

Dendritic Cells (DCs) play a central role in antigen surveillance. DCs are among the rarest immune cell types, constituting about 0.5% of the PBMCs [37]. A recent study by Villani and colleagues delineated six different sub-types of dendritic cells, by analyzing the expression profiles of a Fluorescence-activated cell sorting (FACS) sorted population of dendritic cells and monocytes. The several DC sub-types reported by the authors are as follows : $CD141^+$ DCs (DC1), $CD1C^+_{-A}$ cDCs (DC2), $CD1C^+_{-B}$ cDCs (DC3), $CD1C^-CD141^-$ (DC4), DC5, and plasmacytoid DCs (DC6, pDCs) [124].

We asked if some of the dendritic cell sub-types could be identified in unfractionated PBMC data. To this end, we applied FiRE on $\sim 68k$ PBMC data. FiRE reported a total of 4238 rare cells, which we then clustered using dropClust [113]. Out of the 13 clearly

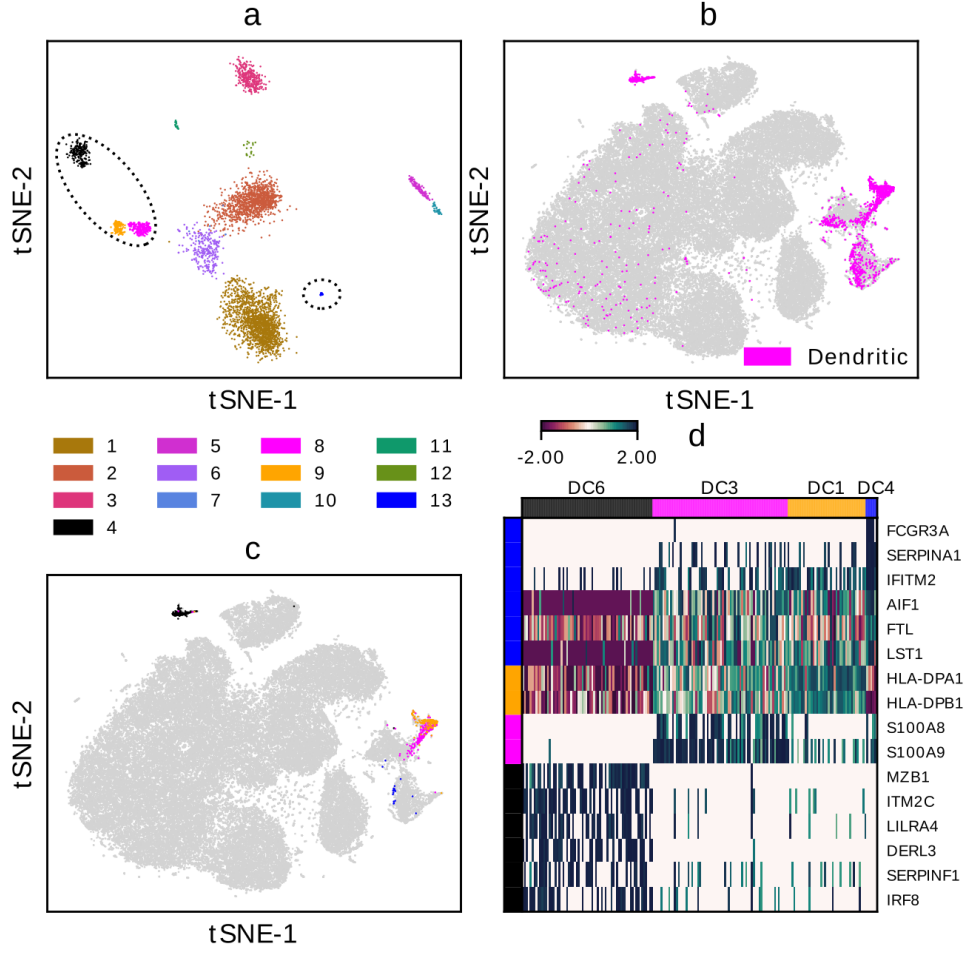


Figure 2.10: FiRE-defined dendritic cell heterogeneity in human blood. (a) t-SNE based 2D plot of rare cells detected by FiRE. Cells are color coded based on their cluster identity as determined by dropClust. (b) Dendritic cells, annotated by the authors, are highlighted in the 2D map adopted from Zheng *et al* [148]. (c) Dendritic cell sub-types detected from FiRE-reported rare cells are color-coded as per Figure (a). (d) Characterization of dendritic cell sub-types using markers reported by Villani and colleagues [124].

distinguishable clusters R1-R13, R4, R8, R9, and R13, exclusively consisted of dendritic cells as per the annotations provided by Zheng and colleagues [148] (Figures 2.10a, 2.10c, Figure 2.11). For these 4 DC clusters, we conducted differential expression analysis to find the cell types specific genes (Section 2.3.1.6). Upon overlaying our differential genes with the ones reported by Villani and colleagues, we could confidently resolve four (DC1, DC3, DC4, DC6) out of the six sub-types reported by Villani *et al*. (Figure 2.10d).

To summarize, when applied to the ~68k PBMC data, FiRE helped in delineating four distinct DC subtypes, of which DC1, DC3, and DC4, were unresolved by the un-

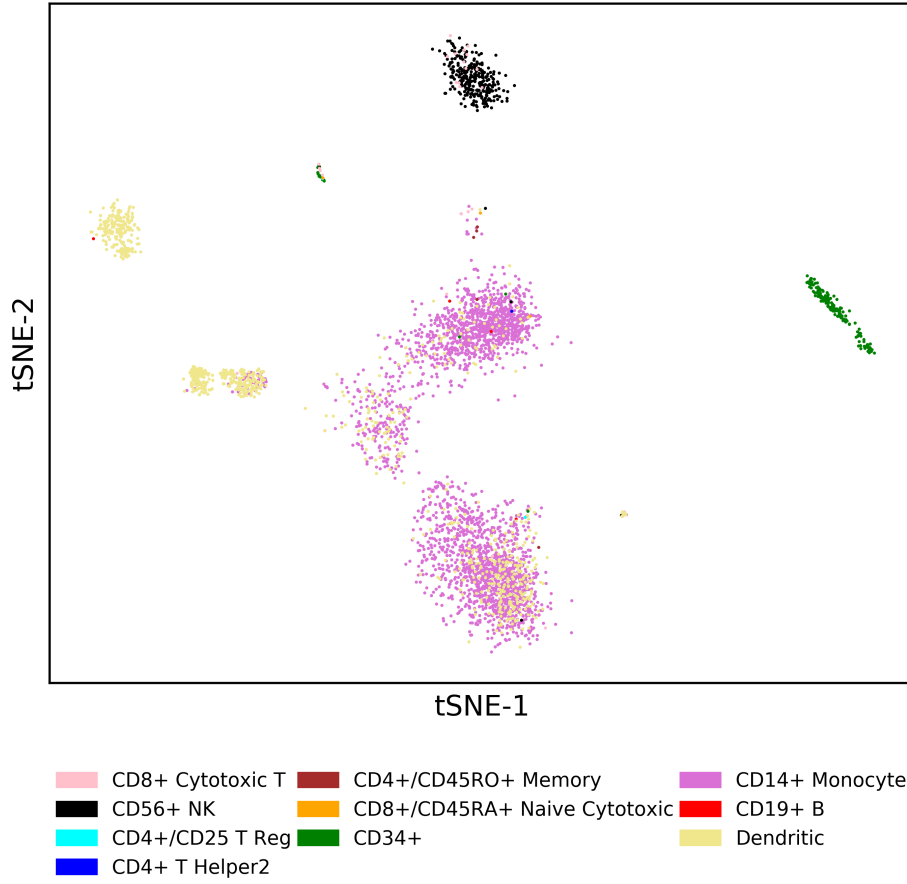


Figure 2.11: 2D embedding of rare cells detected by FiRE on ~68k PBMCs. Cells are color coded based on the cell type annotations reported by Zheng [148].

supervised clustering used in the original study [148]. Notably, in the t-SNE based 2D embedding, these cell types were visually co-clustered within themselves or the monocytes.

2.4 Conclusions

Of late, single cell transcriptomics has considerably refined our understanding about the true nature of cellular phenotype. It has also accelerated the discovery of new cell types. Most of these new cell types are rare since it's quite improbable for an abundant cell type to remain unobserved for a very long time. A truly rare cell type can only be

found by profiling several thousands of cells [112]. While technological advances over the past years have enabled us to perform ultra high-throughput single cell experiments, scalable methods for rare cell detection are nearly non-existent. FiRE attempts to fill that gap, with a number of pragmatic design considerations. Most notable among these is its ability to avoid clustering as an intermediate step. A typical clustering technique is not only time consuming, but also incapable of comprehensively charting the minor cell types in a complex tissue on a single go [15].

While RaceID [51] and GiniClust [63] offer binary predictions, FiRE gives a rareness score to every individual expression profile. We demonstrated how these scores might help the user focus their downstream analyses on a small fraction of the input scRNA-seq profiles. A score is particularly helpful since a number complex techniques such as pseudo-temporal analysis [122], shared the nearest neighborhood based topological clustering [139] etc. are applicable only on a few hundreds of cells.

FiRE makes multiple estimations of the proximity between a pair of cells, in low dimensional spaces, as determined by the parameter M . The notion of similarity for LOF [13], on the other hand, is confounded by the arbitrary scales of the input dimensions. As a result, even though LOF consistently outperforms RaceID and GiniClust, it struggles to match the performance of FiRE.

FiRE, in principle, does not discriminate between an outlier and cells representing minor cell-types. We adhered to dropClust [113] for clustering of rare cells detected by FiRE. dropClust [113] does not administer any special treatment to outliers. As a result, outlier cells, if any, get submerged into the minor cell clusters. However, one may wish to use hierarchical or density based clustering techniques to flag outlier cells. A new version of FiRE will be compared against other state-of-the-art techniques such as scanpy [137], Seurat [105], scAIDE [138], MicroCellClust [42], etc.

FiRE took ~ 26 seconds to analyze a scRNA-seq dataset containing $\sim 68k$ expression profiles. Such unrivaled speed, combined with the ability to pinpoint the truly rare expression profiles, makes the algorithm future proof.

Outliers may also signal anomalous samples, or samples pointing to anomalies. Identifying anomalies requires identifying both local and global outliers. In the next chapter, we discuss an extension of FiRE and its application to anomaly detection.

Chapter 3

Linear Time Identification of Local and Global Outliers^{*}

3.1 Introduction

Anomaly detection refers to the problem of finding patterns in data that do not conform to expected behavior [21, 72]. Anomaly detection has innumerable practical applications, including credit card fraud detection [117], fault detection [146], rare cell type detection in large scale gene expression data, and system health monitoring [142]. Outlier detection methods may be supervised [98], semi-supervised [49, 140], or unsupervised [17, 46]. Unsupervised methods are the most popular, because of the challenges in gathering annotated anomaly examples. Outliers may be treated as global, that are eccentric and irregular relative to the entire set of data points; or local, that are unusual only to a local section of the data [16].

To date, several studies have reviewed anomaly detection algorithms [58, 149]. However, little has been reported in the direction of comprehensive performance evaluation of widely used methods [17, 47] on several annotated datasets. The most comprehensive work in this context is by Campos and colleagues [17], who reported a comparison of 12 well known methods [4, 13, 54, 64, 78, 80, 83, 101, 110, 111, 120, 144] on about 1000 datasets.

^{*}The work presented in this chapter has been published as a research paper titled “*Linear time identification of local and global outliers*” in Neurocomputing (2021).

The existence of local and global outliers is well recognized, but there has been little visible effort to assess the relative performance of existing methods for their ability to detect outlier sub-categories. We propose a scoring criterion that assigns a value to a dataset based on its outliers' local or global nature. This measure is used to classify datasets based on their global and local outlier compositions. The analysis reveals varied performance with different algorithms.

In this study, we incorporate the Finder of Rare Entities (FiRE) (discussed in the previous chapter). FiRE was proposed as a linear time hashing-based algorithm first envisaged for identifying rare cells. In molecular biology, rare cells are analogous to global outliers, whereas sequencing artifacts and biological noise dominate the emergence of local outliers. In this study, we propose an extension of FiRE, referred to as *FiRE.1* in the sequel, that also takes into account local outliers.

Subspace outlier degree (SOD) [79] was proposed to tackle the problem of outlier detection in high dimensional data. We also considered the histogram-based outlier score (HBOS) [45], which is a linear time outlier detection algorithm. Two more algorithms based on k nearest neighbors namely local isolation coefficient (LIC) [141] and distance-based outlier score (DB-outlier score) [73] are also included for comparisons. These 6 algorithms, including FiRE and FiRE.1, are compared with 12 algorithms evaluated by Campos [17] for comparing different algorithms.

3.2 FiRE.1: FiRE for local outliers

In FiRE, a threshold divides the given dimension into two parts. Thus, the resultant bit vector of length M is composed of 0s and 1s. As a result, the maximum possible unique hash indices for a given value of M are 2^M in number. For low-dimensional data, if $M \leq d$, we will end up with a small number of hash indexes. Hence, small variations in data are not adequately captured, as shown in Figure 3.1. Figure 3.1(a) contains both local and global outliers. For $M = 2$, maximum possible hash indexes is 4. As shown in Figure 3.1(b), high values of *FiRE-score* are assigned to global outliers. However, local outliers are missed. In contrast, when $M > d$ in Figure 3.1(c), local outliers are also captured.

Thus, one limitation of FiRE is its dependence on M , to decide the number of bins in

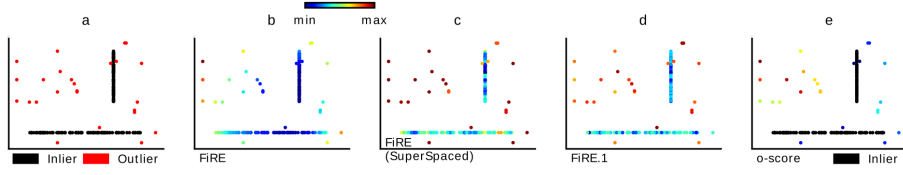


Figure 3.1: Performance of FiRE and FiRE.1 on a simulated dataset with local and global outliers (the illustration is inspired by [79]). (a) A 2-dimensional simulated dataset containing both local and global outliers. (b) Distribution of $FiRE\text{-score}$ when $M = 2$. Global outliers are well captured and have high values of $FiRE\text{-score}$. On the other hand, local outliers deviating marginally from a local population are not captured. (c) Distribution of $FiRE\text{-score}$ when $M > d$ ($M = 100$). In addition to global outliers, local ones are also identified since sufficient hash indexes account for minor differences between local outliers and their local population. (d) FiRE.1 identifies both local and global outliers. (e) Variation of outlieriness criterion $o\text{-score}$ on different types of outliers. For global outliers, the values are high and vice-versa.

which data points need to be segregated. As a result, very few bins are created for low-dimensional data, leading to insufficient granularity in the bins needed to identify local outliers. Hence, FiRE’s performance falls on datasets with local outliers. To overcome this, we propose FiRE.1, that replaces the sketching process with a projection hash. The hash index $h_i^{(l)}$ for sample i is computed as follows.

$$h_i^{(l)} = \lfloor \frac{1}{bin\text{-}width} \sum_{j=1}^{j=M} (P_l)_j^{(i)} * t_j^{(l)} + bias_l \rfloor \quad (3.1)$$

In (3.1), $bias_l \sim U[-bin\text{-}width, bin\text{-}width]$ [115]. Figure 3.2 represents an overview of FiRE.1 steps. For a given value of M , sub-spaced points are projected onto a line by using a dot product with a randomly chosen vector $t^{(l)}$. The projected values are divided into equally spaced bins, determined by $bin\text{-}width$, that controls the bin size. The total number of bins in FiRE.1 is notionally infinite. The smaller value of $bin\text{-}width$ allows the points to get distributed across a large number of bins. Consequently, a smaller bin-width is preferable for datasets with more local outliers. In contrast to FiRE, FiRE.1 provides explicit control over bin width (Figure 3.1(d)).

After dividing points into bins, (2.3) is used to compute the neighborhood of every point probabilistically. Similar to FiRE, (2.4) is used to compute the rareness score of every point. Points with high $FiRE\text{-score}/FiRE.1\text{-score}$ lie in sparser neighborhoods

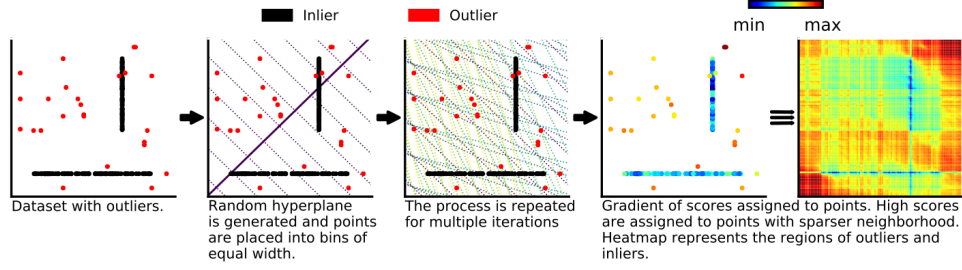


Figure 3.2: An overview of FiRE.1 on a simulated dataset. The heatmap depicts FiRE.1 approximated regional densities.

and are more likely to be outliers. Algorithm 2 describes the working of FiRE.1.

The overall space requirement of FiRE.1 is $L \times (2M + N)$. FiRE.1 needs $L \times M$ space to store the weight matrix and $L \times M$ space to store the sub-spacing matrix. It needs $L \times N$ space to store hash indices of every point.

Algorithm 2 FiRE.1

Input: Data points $(x^{(1)}, x^{(2)}, \dots, x^{(N)})$, $x^{(i)} \in S$, $S \subseteq \mathbb{R}^d$

$L \leftarrow$ Number of projectors

$M \leftarrow$ Size of subspace

$bin-width \leftarrow$ Width of each bin

Initialize: For every projector $l \in \{1, \dots, L\}$

$h^{(l)} \leftarrow N$ size array for hash indexes.

$m^{(l)} \leftarrow M$ size array for selected dimensions.

$t^{(l)} \leftarrow M$ size array for weights.

$bias_l \leftarrow$ Scalar for generated bias.

$mi_j \leftarrow \min_{i \in \{1, \dots, N\}} S_j^{(i)} \quad \forall j \in \{1, \dots, d\}$

$ma_j \leftarrow \max_{i \in \{1, \dots, N\}} S_j^{(i)} \quad \forall j \in \{1, \dots, d\}$

Run:

for $l \in \{1, \dots, L\}$

$m^{(l)} \leftarrow$ Randomly sampled M dimensions from d with replacement.

$P_l \leftarrow$ Projected data from S onto $m^{(l)}$.

$t_j^{(l)} \sim U[mi_{m_j^{(l)}}, ma_{m_j^{(l)}}] \quad \forall j \in \{1, \dots, M\}$

$bias_l \sim U[-bin-width, bin-width]$

$h_i^{(l)} = \lfloor \frac{1}{bin-width} \sum_{j=1}^M (P_l)_j^{(i)} * t_j^{(l)} + bias_l \rfloor$

$N_i^{(l)} = \frac{\text{Total data points with hash index } h_i^{(l)}}{N} \quad \forall i \in \{1, \dots, N\}$

$score_i = -2 \sum_{l=1}^L \log N_i^{(l)} \quad \forall i \in \{1, \dots, N\}$

3.3 Outlier score on unseen data

The FiRE family of algorithms assigns scores to every data sample or point, by dividing the whole space into bins. FiRE algorithms approximate the data distribution based on each bin's population density. This information can be used to assign scores to unseen points as well.

Let S' contains N' points drawn independently and identically from a distribution D over X . Points $x_i \in S' \forall i \in \{1, \dots, N'\}$ are then projected onto $m^{(l)} \forall l \in \{1, \dots, L\}$. Say, P_l denotes this projected set. Then, (3.1) is used to place all unseen data points into bins, say $hu_i^{(l)}$ for point i . Probabilistic neighborhood $Nu_i^{(l)}$ in this scenario is defined as

$$Nu_i^{(l)} = \frac{1 + \text{Total data points with hash index } hu_i^{(l)} \text{ in } h^{(l)}}{1 + N} \quad (3.2)$$

In (3.2) N denotes the total number of training instances. When a point falls into an empty bin, it's probabilistic neighborhood is $1/(N+1)$. FiRE.1 uses (2.4) to assign scores based on these neighborhood values to every point. Algorithm 3 describes FiRE.1's procedure for assigning scores to unseen samples. The heatmap in figure 3.2 shows a heatmap depicting scores for regions that have no training samples.

Algorithm 3 Outlier Score on unseen data.

Input: Unseen data points $(x^{(1)}, x^{(2)}, \dots, x^{(N')})$, $x^{(i)} \in S', S' \subseteq \mathbb{R}^d$

$L \leftarrow$ Number of projectors

$N \leftarrow$ Total number of training instances

$bin-width \leftarrow$ Width of each bin

$h \leftarrow L \times N$ size array for seen hash indexes.

$m \leftarrow L \times M$ size array for dimensions.

$t \leftarrow L \times M$ size array for weights.

$bias \leftarrow L$ size array for bias.

Run:

for $l \in \{1, \dots, L\}$

$P_l \leftarrow$ Project data from S' onto $m^{(l)}$.

$hu_i^{(l)} = \lfloor \frac{1}{bin-width} \sum_{j=1}^{j=M} (P_l)_j^{(i)} * t_j^{(l)} + bias_l \rfloor$

$Nu_i^{(l)} = \frac{1 + \text{Total data points with hash index } hu_i^{(l)} \text{ in } h^{(l)}}{1 + N} \forall i \in \{1, \dots, N'\}$

$score_i = -2 \sum_{l=1}^L \log Nu_i^{(l)} \forall i \in \{1, \dots, N'\}$

3.3.1 Local vs Global outliers

We propose an "outlierness" criterion *o-score* to determine the type of outliers present in a dataset. Let S denote a given set of data points, where O denotes points marked as outliers and I denotes points marked as inliers. For every $o \in O$, *o-score* is defined as.

$$o\text{-score}(o) = \frac{\min_{i \in I}(\text{dist}(o, i))}{\max_{i \in I}(\text{dist}(o, i))} \quad (3.3)$$

For global outliers, both minimum and maximum distances to inliers are comparable. However, for local outliers, the minimum value is small, because the context is local. Hence, global outliers have higher values of *o-score* when compared with local outliers, as shown in Figure 3.1(e). The existence of noise may lead to a spurious minimum and maximum distance values. Therefore, we average ϕ smallest (largest) distances between o and inliers for the minimum (maximum) distance.

3.4 Run time complexity

Methods such as k NN [101], ODIN [54], LOF [13], Simplified-LOF [111], INFLO [64], LoOP [78], LDF [83], LIC [141], DB-outlier score [73], and KDEOS [110] require $O(N^2)$ running time to identify k nearest neighbors. This may be further reduced to $O(N \log N)$ if the dataset is indexed. k NNW [4] has an overall complexity of $O(N \log N)$. On the other hand, COF [120], LDOF [144], and FastABOD [80] require an additional $O(k^2)$ computations per point and therefore incur an overall cost in $O(N \log N + N \times k^2)$. SOD has an overall complexity of $O(d \times N^2)$. This can also be reduced to $O(d \times N \log N)$ if an index structure is used to find NNs. HBOS [45] has $O(N)$ complexity for fixed bin width and $O(N \log N)$ for dynamic bin widths. However, PyOD [147] supports the implementation of HBOS with fixed bin width and hence, it has $O(N)$ time complexity.

FiRE and FiRE.1 require only $O(N)$ running time. Both FiRE and FiRE.1 perform only two passes over the entire dataset. In the first pass, all data points are hashed individually to their respective bins in $O(N)$ operations. The overall time for initializing a weight matrix for hashing is determined by $L \times M$. The hashing of a point to a bin for a given projector involves dot product with the weight vector, and subsequent quantization into one of the bins. The overall time for hashing a point is $L \times M$. Thus,

Table 3.1: Run-time complexities of algorithms is compared. These complexities are presented with respect to the number of samples only.

Algorithm	Complexity	Remarks
FiRE [67] FiRE.1 [20]	$O(N)$	
kNN [101] ODIN [54] LOF [13] Simplified-LOF [111] INFLO [64] LoOP [78] LDF [83] LIC [141] DB-outlier score [73] KDEOS [110]	$O(N^2)$, $O(N \log N)$	Tree/index based approaches can be used to speed-up the nearest neighbor searches.
kNNW [4]	$O(N \log N)$	
COF [120] LDOF [144] Fast-ABOD [144]	$O(N \log N + N \times k^2)$	For every sample an extra computation of $O(k^2)$ is performed, where k is the number of nearest neighbors needs to be evaluated.
SOD [79]	$O(d \times N^2)$ $O(d \times N \log N)$	Here d is data dimension used for subspace creation. Reduction in time can be achieved by indexing.
HBOS [45]	$O(N)$	With fixed bin width (PyOD [147] implements this version)
	$O(N \log N)$	With dynamic bin width.

the overall complexity of the first pass is $O(CN)$, where the constant C is $L \times M$. In the second pass, the neighborhood information is extracted for each entity depending on the accumulation of data points in bins. Therefore, this step is also linear in the sample size. Thus, the overall complexities of FiRE and FiRE.1 are $O(N)$. Table 3.1 summarizes the run-time complexities of different algorithms.

3.5 Experimental setup

3.5.1 Description of datasets

The effectiveness of outlier detection approaches needs to be evaluated across benchmark datasets with known nature of outlierness. Campos and colleagues [17] created a publicly available database of approximately 1000 datasets (including all variants), derived from 23 datasets from UCI repository [31]. For every dataset, two different versions: unnormalized, and attribute-wise normalization, have been considered. Further, for a dataset consisting of duplicates, the corresponding version without duplicates is also generated. Also, different sub-sampled versions are generated from a given dataset, with different percentages of outliers. They argue that random subsampling may have a different impact on the resultant outliers, and hence, 10 different versions were generated. The database consists of diverse datasets ranging from 5 - 1,555, dataset size varying from 80 to $\sim 60,000$, and outlier percentage from 2% to $\sim 40\%$.

3.5.2 Metrics for comparing outlier detection methods

The literature is replete with several well-known performance metrics: *Precision at n* ($P@n$) measures how many points are marked as top n outliers are true outliers. The highest value is 1 when all top n points are true outliers. $P@n$ is sensitive to the value of n . For all experiments, total outliers in a dataset are used as the value of n .

$$P@n = \frac{|\{o \in O \mid \text{rank}(o) \leq n\}|}{n} \quad (3.4)$$

It must be noted that for datasets with few outliers, $P@n$ may be low. Hence, when methods are compared across datasets with different proportions of outliers, $P@n$ is adjusted for chance and is referred to as *Adjusted $P@n$* [17].

$$\text{Adjusted } P@n = \frac{P@n - |O|/N}{1 - |O|/N} \quad (3.5)$$

Average Precision (AP) captures the values of *Precision* with increasing values of *Recall*. In other words, the average of values of *Precision* when *Recall* varies between $1/|O|$ and 1. *AP* is equivalent to area under the *Precision-Recall* curve.

$$AP = \frac{1}{|O|} \sum_{o \in O} P@rank(o) \quad (3.6)$$

Similarly AP must be adjusted for chance when methods are compared across datasets with differing outlier proportions [17].

$$Adjusted\ AP = \frac{AP - |O|/N}{1 - |O|/N} \quad (3.7)$$

Receiver Operator Characteristics Area Under the Curve (ROC AUC) measures how well a method distinguishes between inliers and outliers at different thresholds. The higher the value of AUC , the better the method's performance. $ROC\ AUC$ is insensitive to outlier percentage.

$$ROC\ AUC = \text{mean}_{o \in O, i \in I} \begin{cases} 1 & \text{if } score(o) > score(i) \\ 1/2 & \text{if } score(o) = score(i) \\ 0 & \text{if } score(o) < score(i) \end{cases} \quad (3.8)$$

Adjusted P@n, *Adjusted AP*, and *ROC AUC* are the most suitable metrics for comparing methods across datasets with different outlier proportions. For skewed datasets, $P@n$, *Adjusted P@n*, AP , or *Adjusted AP* are more suitable than $ROC\ AUC$ [28]. AP approximates the area under the *Precision-Recall* curve, while $ROC\ AUC$ measures the area under the *True Positive Rate (TPR)*-*False Positive Rate (FPR)* curve. *Recall* (3.12) is same as *TPR* (3.9). If the size of the negative class significantly exceeds the positive one, then even large changes in false positives (FP) are not captured by FPR , which is used in ROC . This is because FPR , compares false positives with true negatives (TN) (3.10). On the other side, *Precision* compares false positives with true positives (3.11). Since true positives are comparable to false positives, changes in false positives are easily captured by *Precision*.

$$True\ Positive\ Rate\ (TPR) = \frac{TP}{TP + FN} \quad (3.9)$$

$$\text{False Positive Rate (FPR)} = \frac{FP}{FP + TN} \quad (3.10)$$

$$\text{Precision} = \frac{TP}{FP + TP} \quad (3.11)$$

$$\text{Recall} = \frac{TP}{TP + FN} \quad (3.12)$$

$P@n$ also differs from AP . As $Recall$ varies, $Precision$ does not change linearly. Hence, if a high $Recall$ is desired for an outlier class, then $Precision$ may drop. In contrast, $P@n$ finds $Precision$ only for a given threshold n . A high value of $P@n$ indicates, that at least some of the highest scores are assigned to true outliers. In other words, every evaluation measure serves a different purpose, and hence, a comparison between methods using a single metric may not always be appropriate [28].

3.6 Performance comparison of methods on a repository of almost 1000 datasets

3.6.1 Tuning of hyperparameters

Eighteen methods were compared in our study. Campos and colleagues [17] reported the performance of 12 methods using the ELKI framework [109]. The methods used in this study are kNN , $kNNW$, LOF, Simplified-LOF, KDEOS, COF, LDOF, INFLO, LoOP, LDF, FastABOD, and ODIN. For all these methods, the value of k was tuned in the range 1 to 100. FastABOD, LDF, and KDEOS have additional hyperparameters. For FastABOD, a polynomial kernel of degree 2 was used. A constant value of 1 was used for kernel bandwidth multiplier h for both KDEOS and LDF. In addition to this, LDF also needs a constant c ($c = 0.1$). These previously reported results were compared with additional methods. Predictions of DB-outlier score, LIC, and SOD were also computed using the ELKI framework. LIC was tuned by trying different values of k ranging between 1 and 100. However, for SOD, k was varied between 2 and 100 (so that there are at least 2 NNs to choose from to define the reference set). In addition to this, for SOD,

we adhered to $\alpha = 0.8$, as suggested in Kriegel *et al.* [79]. For the DB-outlier score, the *distance* was varied between 0.1 and 0.8, with a step size of 0.01. For HBOS, the PyOD toolkit [147] was used. PyOD implementation supports the construction of histograms with fixed bins. For HBOS, the numbers of bins varied from 1 to 100. For FiRE.1, the value of L was fixed at 100, while in FiRE, the value of L was selected from $\{50, 100, \dots, 500\}$. For both FiRE and FiRE.1 the value of M was selected from $\{\lceil \log d \rceil, \lceil \sqrt{d} \rceil, \lceil \frac{d}{2} \rceil, d, \lceil 1.5 \times d \rceil\}$. In addition to this, FiRE.1 also needs to be tuned for *bin-width*. The value of *bin-width* was tuned over $\{10, 9, 8, 7, 6, 5, 4, 3, 2, 1, 0.1, 1e-2, 1e-3, 1e-4, 1e-5, 1e-6\}$.

3.6.2 Comparison of methods using Friedman ranking

Friedman ranking is a non-parametric statistical technique that measures the performance of a set of methods on multiple datasets. Friedman ranking was computed for methods on all evaluation measures. For a given evaluation measure, methods were ranked from 1 to Φ for a given dataset, where Φ is the total number of methods that could scale for the given dataset. The increasing values of ranks were assigned to methods with decreasing values of measure. Thus, the method with the highest value of the measure (the best performance) has the lowest rank. The ties between methods with the same values of a certain measure were broken by replacing them with an average value of successive ranks. For a given evaluation measure, we reported the average rank across all datasets (Figure 3.3). Among 18 methods, FiRE.1, FiRE, HBOS, and SOD have outstanding performances when compared with others. However, SOD could not scale for all datasets due to higher running time complexity. SOD also requires $O(N^2)$ memory for every dimension. For every sample p , it calculates distances between points in $R(p)$ and it's mean. FiRE.1 consistently yielded the best performance on all considered evaluation criteria. FiRE.1 exhibited a significant margin w.r.t. the remaining methods in terms of the calculated $P@n$ and *Adjusted $P@n$* , which indicates that FiRE.1 reports less false positive than the rest of the methods.

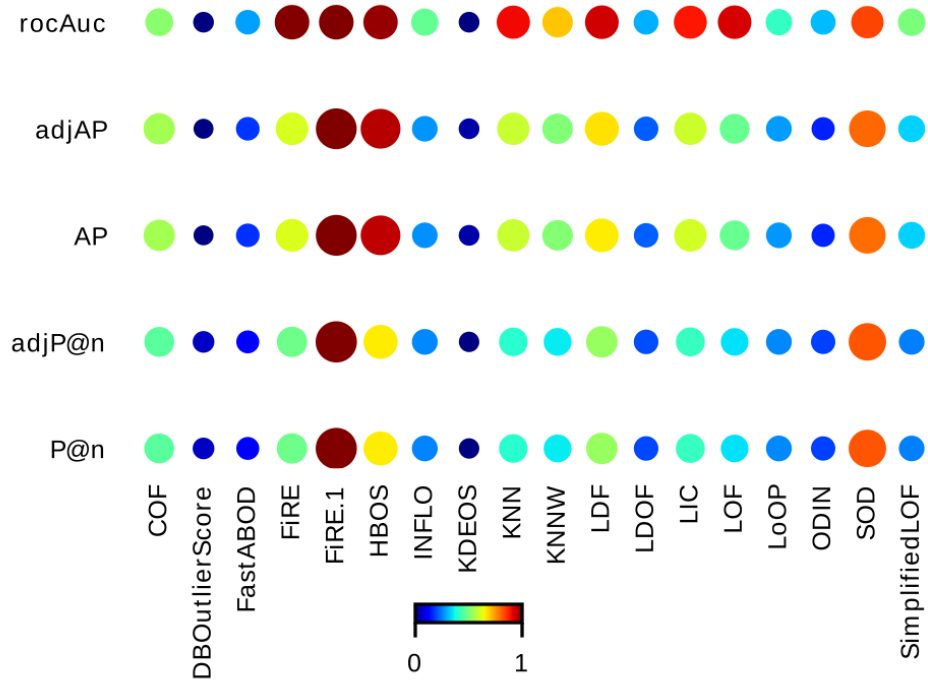


Figure 3.3: Performance comparison of 18 outlier detection methods on ~ 1000 datasets. The performance of all methods was evaluated on 5 evaluation metrics. Friedman ranking determined for every method for each metric. The method with the smallest Friedman rank performs the best on a given measure. The color intensity in a heatmap depicts the inverse of the Friedman ranking.

3.6.3 Comparison of linear complexity methods from the perspective of outlierness type

The fitness of the linear time algorithms viz. FiRE, FiRE.1 and HBOS was evaluated on varied data types, clustered based on the abundance of local and global outliers. For data grouping, we used the *o-score* with $\phi = 10$ (section 3.3.1). For a given dataset, an *o-score* is assigned to every point marked as an outlier. A dataset with large number of local (global) outliers is assigned a low (high) *o-score*. For each dataset, a univariate histogram with 20 bins is constructed using the outliers' *o-score*. The resultant 21 bin edges are used as features for every dataset. The matrix of size $total_datasets \times 21$ is then clustered into 5 different groups using hierarchical clustering (*SciPy* [69] function `scipy.cluster.hierarchy.cut_tree`) as shown in Figure 3.4. A cluster was composed of datasets with similar *o-score*. The count of datasets varied across clusters. Cluster#2 was the largest with $\sim 59\%$ of the total datasets. Figure 3.4 shows varying *o-score* across cluster#1 to cluster#4 in an ascending order. Cluster#5 consists of datasets with wide range range of *o-score*.

For each cluster, the methods were compared against each other and ranked for every evaluation measure. The performance of a method varies with clusters, as shown in Table 3.2. For clusters #1 and #2, FiRE.1 has the smallest Friedman rank for nearly all evaluation measures. Clusters #1 and #2 comprise of datasets with the smallest *o-score*, which are rich with local outliers. On the other end, cluster#4 is composed of datasets with the largest *o-scores*. FiRE has the smallest Friedman rank. HBOS has the smallest Friedman ranking for cluster#3, which consists of 31 datasets; this cluster mainly consists of non-duplicate and normalized versions of the Hepatitis dataset. In cluster#5, FiRE.1 outperforms others when compared using $P@n$, *Adjusted P@n*, and *ROC AUC*. However, the performance of HBOS is better for the *AP* and *Adjusted AP* metrics. Clearly, it is imperative to evaluate the performance of a method on a given dataset from the context of different evaluation measures. The overall performance of FiRE.1 is superior when averaged across all clusters, closely followed by HBOS in terms of *AP* and *Adjusted AP*.

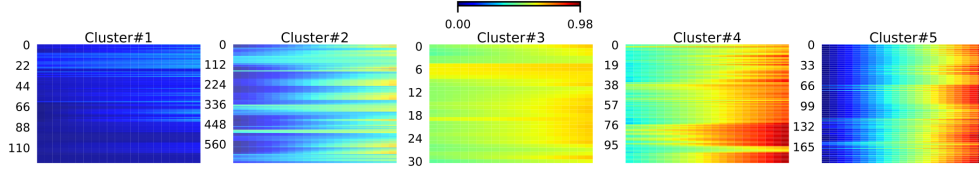


Figure 3.4: Performance comparison of linear time complexity outlier detection methods - FiRE.1, FiRE, and HBOS based on o -score. The datasets are grouped into 5 different clusters using hierarchical clustering. Cluster#1 consists of 127 (11.2% of the entire collection of datasets), cluster#2 has 667 (59.1%), cluster#3 has 31 (2.7%), cluster#4 has 113 (10%), and cluster#5 has 191 (16.9%) datasets. Every row in the heatmap represents a dataset. The o -score of a given dataset is distributed in 20 bins of a histogram. The bin edges are arranged in columns along the corresponding row of the dataset. The distribution of o -score varies across clusters.

Table 3.2: The performance of FiRE.1 [53], FiRE [67], and HBOS [45] is evaluated on 5 different clusters. A cluster consists of datasets with similar distributions of o -score. Different clusters consist of a different count of datasets. For every cluster, the performances have been compared from the context of all evaluation measures and graded using Friedman ranking. The lowest value of Friedman ranking across methods for a given measure is boldfaced.

Algorithm	Cluster ID	Cluster size	<i>Adjusted AP</i>	<i>Adjusted P@n</i>	<i>AP</i>	<i>P@n</i>	<i>ROC-AUC</i>
FiRE.1	1	127	0.546	0.506	0.552	0.504	0.625
FiRE			0.888	0.882	0.880	0.877	0.733
HBOS			0.708	0.764	0.711	0.758	0.683
FiRE.1	2	667	0.659	0.621	0.655	0.623	0.726
FiRE			0.682	0.740	0.683	0.740	0.649
HBOS			0.694	0.741	0.696	0.742	0.709
FiRE.1	3	31	0.699	0.830	0.699	0.830	0.610
FiRE			0.911	0.823	0.905	0.823	0.876
HBOS			0.526	0.754	0.518	0.754	0.624
FiRE.1	4	113	0.796	0.761	0.799	0.768	0.694
FiRE			0.613	0.687	0.617	0.692	0.612
HBOS			0.640	0.812	0.647	0.812	0.757
FiRE.1	5	191	0.636	0.571	0.641	0.574	0.595
FiRE			0.826	0.811	0.828	0.811	0.803
HBOS			0.556	0.638	0.557	0.637	0.639
FiRE.1	overall	1129	0.657	0.619	0.656	0.621	0.686
FiRE			0.729	0.765	0.729	0.765	0.687
HBOS			0.662	0.734	0.664	0.733	0.697

3.6.4 Performance comparison of linear-time methods on large datasets

The performances of methods have been compared on additional datasets to illustrate their wide applicability on extremely large database sizes. *Cod-RNA* [123] is a genome sequenced data that consists of non-coding RNAs (ncRNAs) as an outlier class. *Protein-homology* [19] was used for the KDD-Cup 2004. It was used to identify proteins that are homologous to a native sequence. Non-homologous sequences were labeled as outliers. *Poker* [20] dataset from UCI repository [31] categorizes a set of 5 cards in hands from 4 different suits into one of the 10 categories. Out of those categories, 8 are rare and represent a minor fraction of the data. *RCV1* [84] consists of newswire stories produced by Reuters and is used mainly for text categorization. It is a multi-label dataset and consists of 103 different labels. The top 10 labels with the highest number of sample count represent the inlier category, and samples corresponding to bottom 30 labels are outliers (similar to processing steps in Huang *et al* [59]). An inlier category may cover the entire dataset. Thus, when the samples are categorized, an outlier category takes precedence over an inlier one. Table 3.3 presents some additional statistics about the datasets such as sample size, dimensions, and outlier percentage.

For large datasets, we could only evaluate the performance of the linear time algorithms. Specifics about the parameter tuning is furnished in section 3.6.1. Figure 3.5 shows the distribution of outliers' *o-score* in a dataset. *Poker*, and *Cod-RNA* mainly consist of local outliers, while *Protein-homology*, and *RCV1* consist of a mixture of local and global outliers.

Table 3.4 captures metrics depicting the performances of FiRE, FiRE.1, and HBOS on these datasets for all evaluation measures. FiRE.1 offers the best performance on *Cod-RNA*, and *Poker* datasets, that mainly consist of local outliers (as shown in Figure 3.5). On *RCV1*, FiRE and FiRE.1 performed competitively. HBOS yielded the best performance on *Protein-homology* dataset, followed closely by FiRE.1. Both *RCV1* and *Protein-homology* consist of a mixture of local and global outliers.

Table 3.3: Summary of the large datasets

Dataset	Samples	Features	Outliers(%)
<i>Cod-RNA</i> [123]	488565	8	33.33%
<i>Protein-homology</i> [19]	145751	74	0.89%
<i>Poker</i> [20]	1025010	10	7.6%
<i>RCV1</i> [84]	804414	1000	4.3%

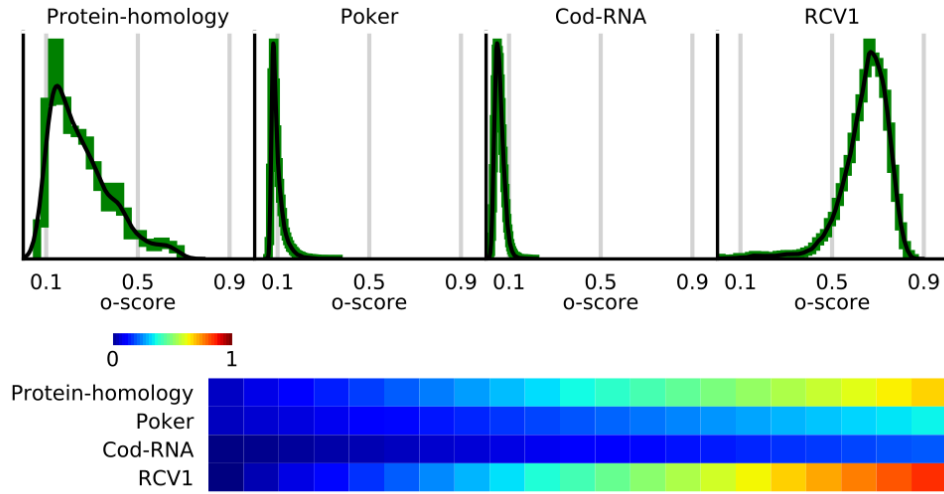


Figure 3.5: Density plot and heatmap illustrating the distribution of *o-score* for 4 different large size datasets. The density plot shows the frequency distribution of *o-score* for outliers. Every row in the heatmap represents a dataset. The *o-score* of a given dataset is distributed in 20 bins of a histogram. The bin edges are arranged in columns along the corresponding row of the dataset.

Table 3.4: The performances of FiRE.1 [53], FiRE [67], and HBOS [45] are compared on 4 large datasets. The values of the following evaluation measures are reported: *Adjusted AP*, *Adjusted P@n*, *AP*, *P@n*, and *ROC AUC*. A method with the highest value of evaluation measure for a given dataset is boldfaced.

Dataset	Algorithm	<i>Adjusted AP</i>	<i>Adjusted P@n</i>	<i>AP</i>	<i>P@n</i>	<i>ROC-AUC</i>
Cod-RNA [123]	FiRE.1	0.35	0.3701	0.5667	0.58	0.684
	FiRE	0.0994	0.2089	0.3996	0.4726	0.58499
	HBOS	0.0955	0.1144	0.397	0.4096	0.5548
Protein-homology [19]	FiRE.1	0.6787	0.659	0.6816	0.662	0.8823
	FiRE	0.013	0.0112	0.0219	0.02	0.753
	HBOS	0.7147	0.6862	0.7173	0.689	0.9384
Poker [20]	FiRE.1	0.7219	0.6419	0.7431	0.6692	0.9355
	FiRE	0.0438	0.0814	0.1168	0.1515	0.486
	HBOS	0.0434	0.1199	0.1164	0.1871	0.5303
RCV1 [84]	FiRE.1	0.0096	0.024	0.0519	0.0657	0.5792
	FiRE	0.0133	0.0239	0.0555	0.0656	0.6068
	HBOS	0.0108	0.0154	0.0531	0.05758	0.5819

3.7 Conclusions

Despite the existence of several methods for outlier detection, only a few scale well to large datasets in high dimensions. Most reported methods require $O(N^2)$ operations to identify k nearest neighbors for every point, or $O(N^2)$ memory to calculate the distances between data points. Some reported approaches compromise on feature coverage to keep the computational complexity low. FiRE and FiRE.1 address both these concerns. Both FiRE versions have a run time complexity of $O(N)$. They take into account the entire spectrum of dimensions by screening a large number of feature subsets. HBOS has $O(N)$ complexity as well for fixed bin widths. However, unlike FiRE, it assumes independence between features.

FiRE was designed to find global outliers in the data generated by a specific technology in molecular biology. Local outliers are generally considered as artifacts or noise in such datasets. Keeping this in mind, FiRE was designed using the Sketching process. The granularity of the space in sketching is dependent on the size of the sub-space (or the number of features). Hence, to achieve the required granularity to find local outliers in datasets with fewer features, FiRE may need to repeat features to split the space into finer regions. This process will also increase the required computational cost. FiRE.1

proposes a solution to this problem. FiRE.1 works in the sub-space (or original space) and quantizes the projection in a random direction as opposed to the sketching, which binarizes the features by random thresholds. The quantization-width provides explicit control over the size of bins, making it easier to tune the FiRE.1 to detect local outliers. Since FiRE.1 works in the sub-space (or original space), its computational cost is also optimal.

Experiments on about 1000 datasets show, that the performance of different methods may vary depending on the choice of evaluation measure. We used Friedman ranking to overcome this ambiguity. The overall Friedman ranking of individual methods shows that FiRE.1 outperforms others for all evaluation measures. Our analysis also demonstrates that a method’s performance is linked to the abundance of local and global outliers in specific data. While FiRE outperforms existing best-practice methods on datasets rich with global outliers, FiRE.1 performs consistently well on all types of datasets and exceptionally well on datasets with abundant local outliers. The performance on large datasets also reinforces this.

Chapter 4

Enhash: A Fast Streaming Algorithm for Concept Drift Detection^{*}

4.1 Introduction

A data stream environment is often characterized by large volumes of data that flow rapidly and continuously. These are processed in an *online* fashion to accommodate data that cannot reside in main memory. A streaming data environment is commonly used for tasks such as making recommendations for users on streaming platforms [119], and real-time analysis inside IoT devices [5]. In such a stream, the underlying data distribution may change, and this phenomenon is referred to as *concept drift*. Formally, the posterior probability of a sample’s class changes with time. Consequently, the method must also be able to adapt to the new distribution. To adapt to a new *concept*, the method may require supplemental or replacement learning. Tuning a model with new information is termed as supplemental learning. Replacement learning refers to the case when the model’s old information becomes irrelevant, and is replaced by new information. A shift in the likelihood of observing a data point x within a particular class when class

^{*}The work presented in this chapter has been published as a research paper titled “*Enhash: A fast streaming algorithm for concept drift detection*” in ESANN proceedings (2021).

boundaries are altered, is called *real concept drift*. *Concept drift* without an overlap of true class boundaries, or an incomplete representation of the actual environment, is referred to as *virtual concept drift*. In *virtual concept drift*, one requires supplemental learning, while *real concept drift* requires replacement learning [41]. The other common way to categorize *concept drift* is determined by the speed with which changes occur [29]. Hence, drift may be *incremental*, *abrupt* or *gradual*. A *reoccurring drift* is one that emerges repeatedly. Thus, in order to handle *concept drift*, a model must be adaptive to non-stationary environments.

Several methods have been recently proposed to handle *concept drift* in a streaming environment. The most popular of these are ensemble learners [10, 33, 48, 74, 75, 99, 127, 129]. As the data stream evolves, an ensemble method selectively retains a few learners to maintain prior knowledge while discarding and adding new learners to learn new knowledge. Thus, an ensemble method is quite flexible, and maintains the *stability-plasticity* balance [85] i.e. retaining the previous knowledge (*stability*) and learning new concepts (*plasticity*).

We propose *Enhash*, an ensemble learner that employs projection hash [60] to handle *concept drift*. For incoming samples, it generates a hash code such that similar samples tend to hash into the same bucket. A gradual forgetting factor weights the contents of a bucket. Thus, the contents of a bucket are relevant as long as the incoming stream belongs to the *concept* represented by them.

4.2 The proposed method: Enhash

Several recent methods employ hashing for online learning and outlier detection [67, 104]. We propose *Enhash*, an ensemble learner, that employs hashing for *concept drift* detection. Let $x_t \in \mathbb{R}^d$ represent a sample from a data stream S at time step t and let $y \in \{1, 2, \dots, C\}$ represent its corresponding *concept*, where C is the total number of *concepts*. Further, let us assume a family of hash functions H such that each $h_l \in H$ maps x_t to an integer value. The hash code $h_l(x_t)$ is assigned to x_t by hash function h_l . A bucket is a set of samples with the same hash code; both these terms are used interchangeably. The total number of samples in bucket $h_l(x_t)$ is denoted by $N_{h_l(x_t)}$. Further assume that N samples have been seen and hashed from the stream so far, of

which N_c samples belong to the *concept class* c such that $\sum_{c=1}^{C=C} N_c = N$. Based on the evidence from the data stream seen so far, the probability of bucket $h_l(x_{t+1})$ is given by

$$p(h_l(x_{t+1})) = \frac{N_{h_l(x_{t+1})}}{N} \quad (4.1)$$

and prior for class c is given by $p(c) = N_c/N$. Assuming, $(N_{h_l(x_{t+1})})_c$ represents the samples of *concept* c in bucket $h_l(x_{t+1})$. Hence, the likelihood of x_{t+1} belonging to *concept* c in bucket $h_l(x_{t+1})$ is given by

$$p(h_l(x_{t+1})|c) = \frac{(N_{h_l(x_{t+1})})_c}{N_c} \quad (4.2)$$

The probability of x_{t+1} belonging to class c is given by

$$p(c|h_l(x_{t+1})) = \frac{p(h_l(x_{t+1})|c)p(c)}{p(h_l(x_{t+1}))} = \frac{(N_{h_l(x_{t+1})})_c}{N_{h_l(x_{t+1})}} \quad (4.3)$$

Equation (4.3) is simply the normalization of counts in bucket $h_l(x_{t+1})$.

To predict the *concept class* of x_{t+1} , an ensemble of L such hash functions can be employed and the weight for each *concept class* is computed as

$$\hat{p}_c = \sum_{l=1}^{l=L} \log \left(1 + p(c|h_l(x_{t+1})) \right) \quad (4.4)$$

and the *concept class* is predicted as

$$\hat{y} = \arg \max_{c \in \{1, \dots, C\}} \hat{p}_c \quad (4.5)$$

To accommodate an incoming sample of class c , the bucket is updated as

$$(N_{h_l(x_{t+1})})_c = 1 + (N_{h_l(x_{t+1})})_c \quad \forall c \in \{1, \dots, C\} \quad (4.6)$$

Enhash utilizes a simple strategy as described above to build an ensemble learner for *concept drift* detection.

In Enhash, the projection hash family is selected as a base learner. Here, a hash

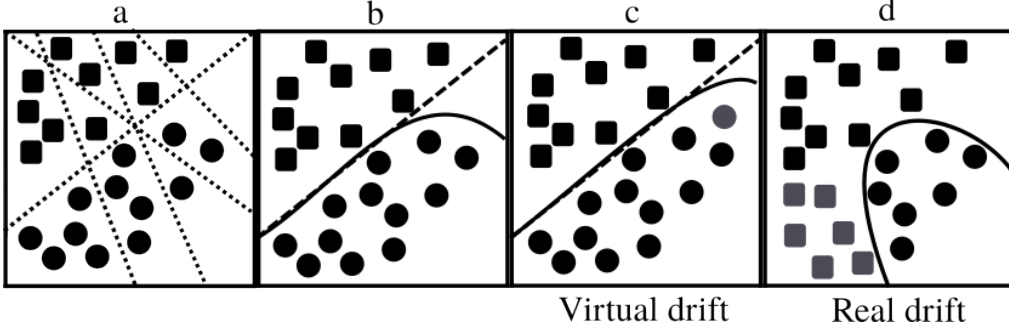


Figure 4.1: Enhash accommodates both virtual and real drift.

function involves the dot product of hyperplane $w^{(l)}$ and sample x_t . It is defined as

$$h_l(x_t) = \lfloor \frac{1}{bin-width} \left(\sum_{j=1}^{j=d} (w_j^{(l)} * (x_t)_j) + bias^{(l)} \right) \rfloor \quad (4.7)$$

where, $bin-width$ is quantization width, $w_j^{(l)}$ and $bias^{(l)}$ can be sampled from any desired distribution. In our implementation, $w_j^{(l)} \sim N(0, 1)$ and $bias^{(l)} \sim [-bin-width, bin-width]$.

Effectively, each h_l (4.7) divides the space into equally spaced unbounded regions of size $bin-width$ (earlier referred to as bucket). Equation (4.3) computes the probability of each *concept class* in a region. An ensemble of hash functions makes all regions bounded. The weight of a *concept class* in the bounded region is computed using (4.4). An absolute value of *concept class* is assigned to each region in (4.5). Figure 4.1a shows the arrangement of randomly generated hyperplanes. The solid line in Figure 4.1b shows the inferred decision boundary (learned distribution) after an absolute assignment of *concept class* to every bounded region. The dashed line in Figure 4.1b depicts the true decision boundary (true distribution).

Assume that Figure 4.1b shows the current stage of learner at time t . At time $t+1$, a new sample x_{t+1} arrives (gray sample in Figure 4.1c). After updating the bucket (4.6), the learned distribution shifts and moves towards the true distribution. Hence, Enhash accommodates virtual drift present in the data stream.

Figure 4.1d depicts the real drift when the true distribution evolves. This requires forgetting some of the previously learned information. Suppose that sample $x_{t+\Delta t}$ hashes to bucket $h_l(x_{t+\Delta t})$ at time say, $t + \Delta t$. Assume that previously, x_t from a different

concept, was hashed into this bucket. In order to accommodate forgetting, Enhash employs a decay factor multiplier to $p(c|h_l(x_{t+\Delta t}))$ (4.4) while weighting a bounded region.

$$\hat{p}_c = \sum_{l=1}^{l=L} \log \left(1 + 2^{-\lambda \Delta t} p(c|h_l(x_{t+\Delta t})) \right) \quad (4.8)$$

where λ is the decay rate. The update rule for the bucket (4.5) is also changed to reflect the new *concept class* as follows

$$(N_{h_l(x_{t+1})})_c = 1 + 2^{-\lambda \Delta t} (N_{h_l(x_t)})_c \quad (4.9)$$

Setting $\lambda = 0$ will reduce these equations to the base case.

In order to break ties in $p(c|h_l(x_t))$, the class weight in the region is also weighted by the distance of the sample x_t from the mean of class samples in bucket $h_l(x_t)$, i.e. $\text{mean}_{h_l(x_t)}^c$

$$\text{dist}_c(x_t) = \sqrt{\sum_{i=1}^{i=d} \left((x_t)_i - (\text{mean}_{h_l(x_t)}^c)_i \right)^2} \quad (4.10)$$

$$\hat{p}_c = \sum_{l=1}^{l=L} \log \left(1 + \frac{2^{-\lambda \Delta t} p(c|h_l(x_t))}{\text{dist}_c(x_t)} \right) \quad (4.11)$$

All remaining ties are broken arbitrarily.

4.2.1 Implementation details

Algorithm 4 describes Enhash's pseudo-code. We refer to an instance of the ensemble as an estimator. The parameter *bin-width* determines the granularity of the buckets, and λ represents the rate of decay that accounts for gradual forgetting [71]. Every estimator l generates a hash code for incoming stream samples and hashes them into bucket $b^{(l)}$. The hash code for a sample x is compute using (4.7). The timestamp when a sample of class y was last hashed into a bucket $b^{(l)}$ is stored in $\text{tstamp}^{(l)}[b^{(l)}][y]$. $\text{tstamp}^{(l)}$ is an infinitely indexable 2D-array. An infinitely indexable ND-array is a data structure

that has N dimensions and can store values at any arbitrary combinations of indexes in those dimensions. In practice, an infinitely indexable ND-array can be created using maps or dictionaries. The recent access time of the hash code $b^{(l)}$ can be retrieved by selecting the maximum value in $tstamp^{(l)}[b^{(l)}]$. The count of samples in bucket $b^{(l)}$ is stored in another infinitely indexable 2D-array $counts^{(l)}$ at an index $counts^{(l)}[b^{(l)}]$. The information required to break ties during prediction is stored in $sCounts^{(l)}$ and $sAcc^{(l)}$. Variable $sCounts^{(l)}$, an infinitely indexable 2D-array, keeps track of the number of samples from every class y falling into the bucket $b^{(l)}$. $sAcc^{(l)}$, an infinitely indexable 3D-array, stores the class-wise vector sum of all the samples falling into the bucket $b^{(l)}$. The last dimension in this array belongs to the features in the dataset.

Enhash has two phases. In the first one, Enhash predicts the class of a new sample. Assuming that sample x falls into bucket $b^{(l)}$, its distance from all the cluster centers in the bucket is computed (steps 18 and 19). The variable $cweights$ accumulates the prediction for a sample x via each estimator. This variable is also an infinitely indexable array so that it can accommodate unseen class labels. To get the prediction for sample x from an estimator l , a decayed value of count (weighted by distance) is computed (step 21). The decay factor $2^{-\lambda\Delta t_1}$, depends upon the decay parameter λ and the difference of the current time and the last access time of bucket $b^{(l)}$. The decay factor determines whether the previous value in $counts^{(l)}[b^{(l)}]$ is relevant or not, and hence, introducing the forgetting effect in the algorithm. In effect, if the difference in the time is large, then decay is almost zero, and this emulates local replacement in the bucket $b^{(l)}$ [18]. On the other hand, λ reduces the effect of samples (possibly, of the same *concept*) hashing into a bucket. The higher is the value of λ , then more is the rate of decay. Collectively, λ , and time difference play an important role in drift detection. The log-transformed value of the prediction is added to $cweights$. A pseudo-count of 1 is added during log-transformation to handle 0 or near-zero values in prediction. After accumulating predictions from every estimator, a class with maximum weight is designated as the class of sample x (step 30).

In the second phase, the variables are updated to accommodate recent changes in the *concept*. Assume that a recent sample belongs to class y . Hence, the value in $tstamp[b^{(l)}][y]$ is set to the current timestamp. Further, to update the effective count in

bucket for class y in $counts^{(l)}[b^{(l)}][y]$, the present value is decayed by the difference of the current time and the last seen time of sample from class y and then incremented by 1 (steps 24- 25). This introduces the forgetting phenomenon during updates and also handles spurious changes. For example, if a bucket was accustomed to seeing samples from a particular class and the sudden arrival of a sample from another class that had not been seen by the bucket for a long time, it would not alter the bucket's prediction abruptly. However, after seeing a few samples from the new class, the bucket's confidence will grow gradually towards the recent trends. The value in $counts^{(l)}[b^{(l)}]$ is normalized for numerical stability. Finally, $sCounts^{(l)}[b^{(l)}][y]$ is incremented by 1 and a new sample x is added in $sAcc^{(l)}[b^{(l)}][y]$.

In essence, samples with a similar *concept* are most likely to have the same hash code and hence, share the bucket. For an evolving stream, thus, different buckets are populated. The weight associated with the bucket is gradually incremented when samples of the same *concept* arrive. The contents of a bucket are more relevant when the *concept* reoccurs in the near future than in a faraway future.

Formally, the temporal nature of the posterior distribution of a sample x belonging to a class y is modeled as the Bayes posterior probability $P(y|x) = P(y)P(x|y)/P(x)$. Let n and n_y denote the count of total samples and samples of a class y , respectively. In the proposed method, for a given estimator l , $P(y) = n_y/n$, $P(x|y) = counts^{(l)}[b^{(l)}][y]/n_y$, and $P(x) = \sum_j (counts^{(l)}[b^{(l)}][j])/n$.

Thus, $P(y|x) = counts^{(l)}[b^{(l)}][y] / \sum_j (counts^{(l)}[b^{(l)}][j])$ and hence, information in $counts^{(l)}[b^{(l)}][y]$ accounts for *concept drift*. For virtual drift, the contents of $b^{(l)}$ may only be supplemented with the additional information from the distribution. For real drift, however, the previous contents of $b^{(l)}$ may be discarded via the decay factor.

4.2.2 Time complexity analysis

There are three important steps in Algorithm 4, namely, the computation of hash function (step 17), prediction of class (steps 18-22), and update of model parameters (steps 23-28). In Enhash, the hash function computation is the dot product of a sample with weight parameters (4.7). Let the time required to compute the hash function be given by $\psi(d) = \mathcal{O}(d)$. The prediction of a sample's class involves the

Algorithm 4 Enhash

```
1: Input: Data stream  $S$ 
2:    $L \leftarrow$  Number of estimators
3:    $bin-width \leftarrow$  Width of bucket
4:    $\lambda \leftarrow$  Rate of decay
5: Initialize:  $t \leftarrow 0$ 
6:   For every estimator  $l \in \{1, \dots, L\}$ 
7:      $counts^{(l)} \leftarrow$  infinitely indexable 2D-array
8:      $tstamp^{(l)} \leftarrow$  infinitely indexable 2D-array
9:      $sCounts^{(l)} \leftarrow$  infinitely indexable 2D-array
10:     $sAcc^{(l)} \leftarrow$  infinitely indexable 3D-array
11: Run:
12: while  $HasNext(S)$  do
13:    $(x, y) \leftarrow next(S)$ 
14:    $t \leftarrow t + 1$ 
15:    $cweights \leftarrow$  array initialized with 0s
16:   for  $l \in \{1, \dots, L\}$  do
17:     $b^{(l)} =$  generate hash code using (4.7) for estimator  $l$ 
18:     $sMean = \frac{sAcc^{(l)}[b^{(l)}]}{sCounts^{(l)}[b^{(l)}]}$ 
19:     $dist = \sqrt{\sum ((sMean - x)^2)}$ 
20:     $\Delta t_1 = t - \max_j (tstamp^{(l)}[b^{(l)}][j])$ 
21:     $v = 2^{-\lambda \times \Delta t_1} \times \frac{counts^{(l)}[b^{(l)}]}{dist}$ 
22:     $cweights = cweights + \log(1 + v)$ 
23:     $\Delta t_2 = t - tstamp^{(l)}[b^{(l)}][y]$ 
24:     $counts^{(l)}[b^{(l)}][y] = 1 + (2^{-\lambda \times \Delta t_2} \times counts^{(l)}[b^{(l)}][y])$ 
25:     $counts^{(l)}[b^{(l)}] = \frac{counts^{(l)}[b^{(l)}]}{\sum_j (counts^{(l)}[b^{(l)}][j])}$ 
26:     $tstamp^{(l)}[b^{(l)}][y] = t$ 
27:     $sCounts^{(l)}[b^{(l)}][y] = 1 + sCounts^{(l)}[b^{(l)}][y]$ 
28:     $sAcc^{(l)}[b^{(l)}][y] = x + sAcc^{(l)}[b^{(l)}][y]$ 
29:   end for
30:    $\hat{y} \leftarrow \arg \max(cweights)$ 
31: end while
```

computation of distances from cluster centers in the bucket (4.10). Assuming that, Enhash has observed C concept classes so far; then, the time required for prediction is given by $\phi(d, C) = \mathcal{O}(d * C)$. Model update involves updating the bucket's timestamp, the effective count of the *concept class* in the bucket, the total samples hashed into the bucket, and accumulation of samples. Effective counts are also normalized in the update step which depends upon C . Let the time required to update model parameter be denoted by $\zeta(d, C) = \mathcal{O}(d + C)$. An estimator takes time $\mathcal{O}(\psi(d) + \phi(d, C) + \zeta(d, C)) = \mathcal{O}(d + d * C + d + C) = \mathcal{O}(d * C)$. These steps are repeated by all L estimators, and hence, the total time complexity of Enhash, for an arbitrary dataset and hyper-parameters settings, is given by $\mathcal{O}(L * d * C)$.

Table 4.1: Time complexities of algorithms is compared. This table presents the complexity to process the N samples from a stream. The base estimators are as per the default parameters of the corresponding classes in `scikit-multiflow` package. In the table N represents number of samples, d represents number of dimensions, L represents number of estimators, C represents the number of classes, w is the window size, k is the number of trials coming from Poisson distribution, and s is the oversampling rate. To be noted, these are the simplified estimates of the time complexity.

Algorithm	Complexity	Remarks
Enhash [66]	$\mathcal{O}(L * d * N * C)$	
DWM [74]	$\mathcal{O}(L * d * (N + C))$	The base classifier is Naive Bayes' Classifier.
Learn ⁺⁺ .NSE [33]	$\mathcal{O}(L * (\log N + N * d * \log N))$	The base classifier is decision tree. The best case complexity for training and testing is assumed in this estimate.
Learn ⁺⁺ [99]	$\mathcal{O}(L * (\log N + N * d * \log N))$	The base classifier is decision tree. The best case complexity for training and testing is assumed in this estimate.
LB [10]	$\mathcal{O}(L * N * k * \log N)$	The base classifier is <code>KNNClassifier</code> from <code>scikit-multiflow</code> package.
OB [9, 96]	$\mathcal{O}(L * N * k * (\log N + \log w))$	The base classifier is <code>KNNAdwinClassifier</code> from <code>scikit-multiflow</code> package.
OSMOTEB [127]	$\mathcal{O}(L * N * k * s * (\log N + \log w))$	The base classifier is <code>KNNAdwinClassifier</code> from <code>scikit-multiflow</code> package.
AWE [129]	$\mathcal{O}(L * d * (N + C))$	The base classifier is Naive Bayes' classifier.
AEE [75]	$\mathcal{O}(L * d * (N + C))$	The base classifier is Naive Bayes' classifier.
ARF [48]	$\mathcal{O}(L(\log N + N * d * \log N))$	The best case complexity for training and testing is assumed in this estimate.

Thus, for a fixed setting of hyper-parameter L , the time complexity of Enhash to process a newly arrived sample for an arbitrary dataset is given by $\mathcal{O}(d * C)$. However, it can be argued that for a fixed dataset, the dimension of data d and number of concept

classes C are fixed. Hence, Enhash will effectively take only a constant time, $\mathcal{O}(1)$, in the processing of a new sample. The comparison, in terms of time taken in processing N samples from stream, with other algorithms is presented in Table 4.1.

4.3 Experimental Setup

Enhash’s performance on *concept drift* detection was compared with some widely used ensemble learners. These include Learn++ [99], Learn⁺⁺.NSE [33], Accuracy-Weighted Ensemble (AWE) [129], Additive Expert Ensemble (AEE) [75], DWM [74], Online Bagging-ADWIN (OB) [9, 96], Leveraging Bagging [10], Online SMOTE Bagging (OS-MOTEB) [127], and ARF [48]. The implementation of these methods is available in `scikit-multiflow python` package [95]. A fixed value of *estimators* was used for all the methods. For methods such as Accuracy-Weighted Ensemble, Learn⁺⁺.NSE, Learn++, Leveraging Bagging, and Online Bagging-ADWIN, the maximum size of window was set $\min(5000, 0.1 * n)$, where n is the total number of samples. For the rest of the parameters, the default value was used for all the methods.

4.3.1 Evaluation metrics for performance comparison

We evaluated all the experiments in terms of time, memory consumption, and classifiers’ performance. The memory consumption is measured in terms of RAM-hours [11]. Every GB of RAM employed for an hour defines one RAM-hour. The performance of a classifier is measured in terms of accuracy/error, Kappa M, and Kappa Temporal [8]. Kappa M, and Kappa Temporal handle imbalanced data streams, and data streams that have temporal dependencies, respectively. We evaluated the classifiers’ performance using the Interleaved Test-Train strategy [88]. This strategy is commonly employed for incremental learning since every sample is used as a test and a training point as it arrives.

4.3.2 Description of datasets

We used 6 artificial/synthetic (Samples x Features)- transientChessboard (200000 x 2), rotatingHyperplane (200000 x 10), mixedDrift (600000 x 2), movingSquares (200000 x

Table 4.2: Description of datasets.

Synthetic datasets	Samples x Features	Classes	Drift	Real datasets	Samples x Features	Classes
transientChessboard	200,000 x 2	8	Virtual	airlines	539,383 x 7	2
rotatingHyperplane	200,000 x 10	2	Abrupt	elec2	45,312 x 8	2
mixedDrift	600,000 x 2	15	Incremental, Abrupt, and Virtual	NEweather	18,159 x 8	2
movingSquares	200,000 x 2	4	Incremental	outdoorStream	4,000 x 21	40
interchangingRBF	200,000 x 2	15	Abrupt			
interRBF20D	201,000 x 20	15	Abrupt			

2), interchangingRBF (200000 x 2), interRBF20D (201000 x 20), and 4 real datasets- airlines (539383 x 7), elec2 (45312 x 8), NEweather (18159 x 8), outdoorStream (4000 x 21) for all experiments. The datasets are available on <https://github.com/vlosing/driftDatasets>. The synthetic datasets simulate drifts such as abrupt, incremental, and virtual. The real datasets have been used in the literature to benchmark *concept drift* classifiers. The count of samples varies from 4000 (in outdoorStream) to 600,000 (in mixedDrift). Also, outdoorStream has the maximum number of classes, i.e., 40. The summary of the description of datasets is available in Table 4.2.

4.3.3 System details

All experiments were performed on a workstation with 40 cores using Intel Xeon E7-4800 (Haswell-EX/Brickland Platform) CPUs with a clock speed of 1.9 GHz, 1024 GB DDR4-1866/2133 ECC RAM and Ubuntu 14.04.5 LTS operating system with the 4.4.0-38-generic kernel.

4.4 Tuning of parameters for Enhash

The hyperparameters that govern the performance of Enhash constitute L (number of estimators), and *bin-width* (quantization parameter). Even though the decay rate λ is also one of the hyperparameters, its value does not require much tuning, and usually, $\lambda = 0.015$ is preferred [104]. However, making $\lambda = 0$ is equivalent to removing the forgetting phenomenon and hence, worsens the performance (discussed further in Section 4.6).

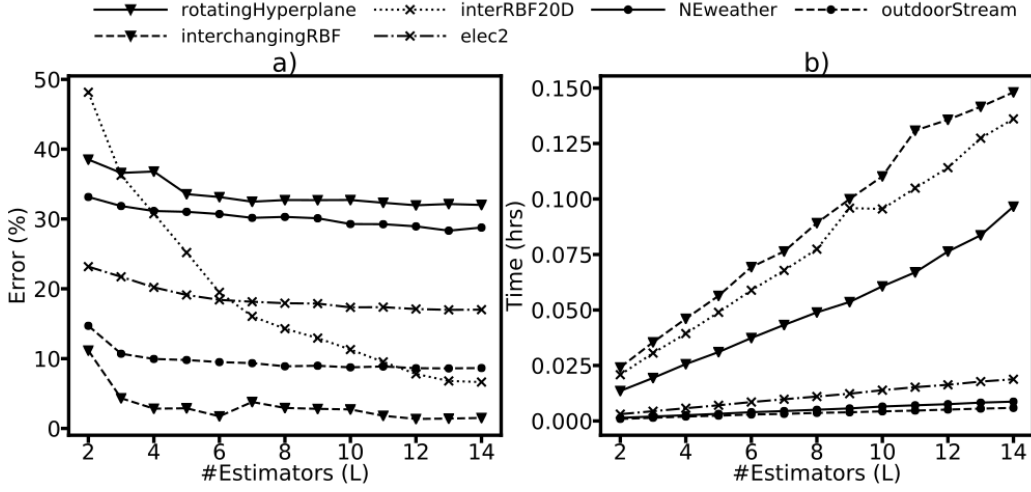


Figure 4.2: Tuning of L . For both synthetic and real datasets, we show a trend in performance metrics, Error (%), and Time(hrs) for an increase in values of L . The value of L varies from $[2, 14]$. For a given value of L , the running time is measured across all the samples for all the estimators in a configuration. The value of error is evaluated across all the samples for a given value of L .

4.4.1 Constraints to tune L

In Figure 4.2, it is shown empirically that with an increase in the value of L , the performance of Enhash eventually saturates. The time taken by Enhash also increases with L . This may be attributed to the fact that for every sample arriving at time t , the insertion involves calculating the hash code of the sample for every estimator l . It should be emphasized that, as shown empirically in Figure 4.2, only a few estimators are needed to achieve optimum performance. Further, the increase in time due to an increase in L can be reduced through a parallel implementation of Enhash. In that case, evaluation of a hash code for a sample for each l can be done independently of others. Consequently, a moderate value of $L = 10$ is used to perform all the experiments.

4.4.2 Constraints to tune *bin-width*

The parameter *bin-width* divides the space into equally spaced unbounded regions of size *bin-width*. The smaller is the value of *bin-width*, the more granular is the division of space. In other words, for smaller values of *bin-width*, the possible values of different hash codes (or buckets) increase rapidly. In the worst case, every sample may fall into

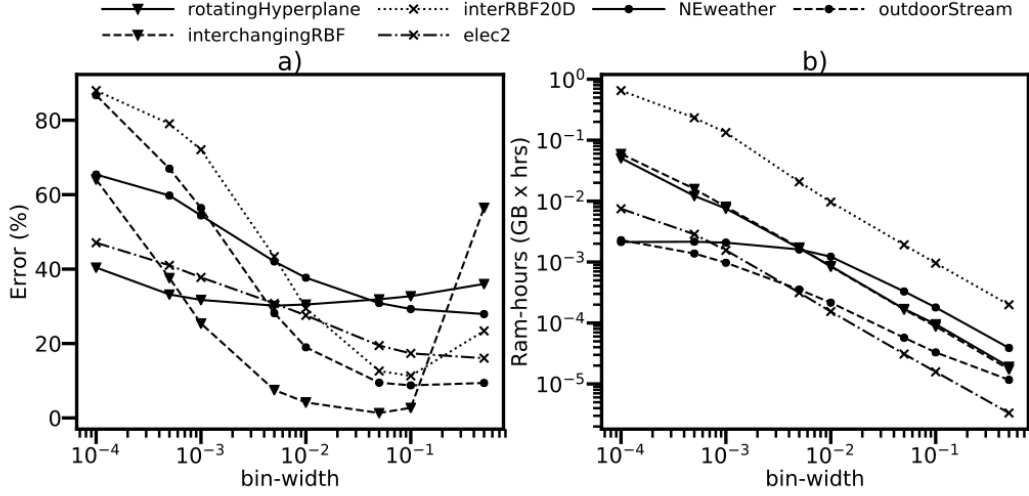


Figure 4.3: Tuning of *bin-width*. For both synthetic and real datasets, we show a trend in performance metrics, Error (%), and Ram-hours for different values of *bin-width*. The value of *bin-width* varies in $[0.0001, 0.0005, 0.001, 0.005, 0.01, 0.05, 0.1, 0.5]$. a) The value of error is evaluated across all the samples for a given value of *bin-width*. The values of *bin-width* on x-axis are on logarithmic scale. b) Ram-hours are calculated across all the samples for all the estimators for a given configuration. The values of *bin-width* on x-axis and Ram-hours on y-axis, both are on log scale.

a different bucket. Thus, the overall cost to store the contents of all buckets for every estimator grows exponentially. Figure 4.3 shows empirically the effect of *bin-width* on memory consumption. The figure highlights that for small values of *bin-width*, the overall memory requirement is extremely high. Also, the prediction of the *concept* for the sample may be arbitrary for extremely small values of *bin-width* since there is no neighborhood information in the bucket. As a result, for every new sample, a new *concept* may be falsely predicted. On the other extreme, for large values of *bin-width*, samples from different classes may lead to frequent collision. As a result of this, the *concept* of an arriving sample may not be predicted correctly due to confusion in the bucket. Thus, in general, an intermediate range of values for $\text{bin-width} \in \{0.01, 0.1\}$ is more suitable for all datasets.

4.5 Experimental Results

For all methods, the number of *estimators* is considered as 10. In addition for En-hash, *bin-width* was set to $\{0.1, 0.01\}$ and λ was set to 0.015. Tables 4.3, 4.4, and 4.5

Table 4.3: Error (in %) is reported to compare the performance of Enhash [66] with other methods. For a given dataset, the method with the least error is in boldface. Due to implementation constraint, Learn⁺⁺.NSE could not run for the outdoorStream dataset.

Dataset	DWM [74]	Learn ⁺⁺ .NSE [33]	Learn++ [99]	LB [10]	OB [9, 96]	OSMO- -TEB [127]	AWE [129]	AEE [75]	ARF [48]	Enhash [66]
transientChessboard	49.89	3.67	2.75	13.13	29.62	24.28	89.78	85.37	27.56	18.84
rotatingHyperplane	10.11	24.13	19.36	24.65	15.08	19.75	16.27	18.10	16.40	32.72
mixedDrift	65.77	39.46	49.67	16.71	23.63	20.30	77.79	81.17	19.79	12.88
movingSquares	29.03	68.74	67.84	55.69	65.42	61.12	67.51	67.23	58.54	13.29
interchangingRBF	7.02	75.43	82.79	4.61	37.67	22.05	83.49	82.58	3.22	2.72
interRBF20D	7.62	76.36	81.59	5.62	37.02	21.00	84.90	82.35	2.39	11.30
airlines	37.42	42.92	37.53	43.36	39.23	40.66	38.49	39.17	33.09	41.66
elec2	20.62	34.63	31.40	18.64	23.26	24.60	39.64	26.71	11.59	17.34
NEweather	29.52	29.20	24.63	27.20	20.84	22.74	30.72	30.78	21.43	29.27
outdoorStream	57.62	-	60.88	9.33	34.15	21.25	78.55	42.45	26.12	8.75

Table 4.4: KappaM is tabulated to compare the performances of the methods. For a given dataset, the method with the highest value of KappaM is in boldface.

Dataset	DWM [74]	Learn ⁺⁺ .NSE [33]	Learn++ [99]	LB [10]	OB [9, 96]	OSMO- -TEB [127]	AWE [129]	AEE [75]	ARF [48]	Enhash [66]
transientChessboard	0.43	0.96	0.97	0.85	0.66	0.72	-0.03	0.02	0.68	0.78
rotatingHyperplane	0.80	0.52	0.61	0.51	0.70	0.60	0.67	0.64	0.67	0.35
mixedDrift	0.23	0.54	0.42	0.80	0.72	0.76	0.09	0.05	0.77	0.85
movingSquares	0.61	0.08	0.10	0.26	0.13	0.19	0.10	0.10	0.22	0.84
interchangingRBF	0.92	0.18	0.10	0.95	0.59	0.76	0.09	0.10	0.96	0.97
interRBF20D	0.92	0.17	0.11	0.94	0.60	0.77	0.08	0.10	0.97	0.88
airlines	0.16	0.04	0.16	0.03	0.12	0.09	0.14	0.12	0.26	0.06
elec2	0.51	0.18	0.26	0.56	0.45	0.42	0.07	0.37	0.73	0.59
NEweather	0.06	0.07	0.22	0.13	0.34	0.28	0.02	0.02	0.32	0.07
outdoorStream	0.41	-	0.37	0.90	0.65	0.78	0.19	0.56	0.73	0.91

compare the performance of the methods in terms of error, KappaM, and KappaT respectively using Interleaved Test-Train strategy. For these measures, the performance of the proposed method was superior to Accuracy-Weighted Ensemble (AWE), and Additive Expert Ensemble (AEE) on 8 datasets, DWM, Learn⁺⁺.NSE, Online SMOTE Bagging (OSMOTEB), and Online Bagging-ADWIN (OB) on 7 datasets, Learn++, and Leveraging Bagging (LB) on 6 datasets, and ARF on 5 datasets. The performance of Enhash supersedes all other methods for 4 datasets - mixedDrift, movingSquares, interchangingRBF, and outdoorStream.

Other evaluation criteria are speed (Table 4.6) and RAM-hours (Table 4.7). Table 4.6 reports the overall time (in hrs) taken by each method for a given dataset. For a majority of the datasets, Enhash takes the least time. For instance, it took only 0.339 hrs for the mixedDrift dataset, followed by Learn⁺⁺.NSE, which took 0.627 hrs. Notably,

Table 4.5: KappaT is reported to compare the performances of the methods. The highest value of KappaT in each row is highlighted.

Dataset	DWM [74]	Learn ⁺⁺ .NSE [33]	Learn++ [99]	LB [10]	OB [9, 96]	OSMO- -TEB [127]	AWE [129]	AEE [75]	ARF [48]	Enhash [66]
transientChessboard	-0.17	0.91	0.94	0.69	0.30	0.43	-1.11	-1.00	0.35	0.56
rotatingHyperplane	0.80	0.52	0.61	0.50	0.70	0.60	0.67	0.64	0.67	0.34
mixedDrift	0.28	0.57	0.46	0.82	0.74	0.78	0.15	0.11	0.78	0.86
movingSquares	0.71	0.31	0.32	0.44	0.35	0.39	0.32	0.33	0.41	0.88
interchangingRBF	0.92	0.19	0.11	0.95	0.60	0.76	0.11	0.12	0.97	0.97
interRBF20D	0.92	0.18	0.13	0.94	0.60	0.78	0.09	0.12	0.97	0.88
airlines	0.11	-0.02	0.11	-0.03	0.06	0.03	0.08	0.07	0.21	0.01
elec2	-0.41	-1.36	-1.14	-0.27	-0.59	-0.68	-1.70	-0.82	0.21	-0.18
NEweather	0.08	0.09	0.23	0.15	0.35	0.29	0.04	0.04	0.33	0.08
outdoorStream	-4.90	-	-5.23	0.05	-2.49	-1.17	-7.04	-3.34	-1.67	0.10

Table 4.6: The running time of different methods is compared using Time (in hrs). The method with the fastest speed is highlighted for every dataset.

Dataset	DWM [74]	Learn ⁺⁺ .NSE [33]	Learn++ [99]	LB [10]	OB [9, 96]	OSMO- -TEB [127]	AWE [129]	AEE [75]	ARF [48]	Enhash [66]
transientChessboard	0.169	0.287	0.477	8.374	0.983	13.623	0.181	0.570	0.481	0.099
rotatingHyperplane	0.205	0.199	0.851	14.022	6.960	114.615	0.198	0.660	1.318	0.067
mixedDrift	0.757	0.627	2.726	26.686	7.916	185.500	1.673	17.149	1.875	0.339
movingSquares	0.055	0.179	0.790	9.368	5.936	28.028	0.142	0.567	7.308	0.068
interchangingRBF	0.038	0.185	0.972	8.298	1.444	7.424	0.376	1.048	0.499	0.132
interRBF20D	0.276	0.166	0.801	19.167	1.507	7.604	2.091	3.200	3.080	0.106
airlines	0.469	0.571	2.180	37.910	15.151	403.378	0.744	21.669	3.796	0.182
elec2	0.037	0.020	0.160	7.575	1.777	14.511	0.016	0.059	0.181	0.015
NEweather	0.021	0.008	0.068	0.590	0.183	1.326	0.013	0.020	0.083	0.006
outdoorStream	0.055	-	0.014	0.069	0.127	0.162	0.047	0.129	0.071	0.004

Table 4.7: The memory consumption is measured in terms of RAM-hours. The method with the least value of RAM-hours is highlighted for every dataset.

Dataset	DWM [74]	Learn ⁺⁺ .NSE [33]	Learn++ [99]	LB [10]	OB [9, 96]	OSMO- -TEB [127]	AWE [129]	AEE [75]	ARF [48]	Enhash [66]
transientChessboard	1.5e-5	8.1e-5	3.3e-5	8.0e-2	3.3e-4	5.5e-1	2.3e-4	5.5e-5	1.2e-3	4.4e-4
rotatingHyperplane	3.3e-5	5.6e-5	5.7e-5	3.5e-1	1.7e-1	4.6e+1	5.8e-4	1.1e-4	3.4e-2	7.8e-5
mixedDrift	1.2e-4	4.9e-4	3.1e-4	2.6e-1	2.9e-2	3.9e+1	2.5e-3	2.9e-3	1.3e-2	5.3e-3
movingSquares	1.2e-6	4.9e-5	5.8e-5	9.0e-2	5.5e-2	2.3e+0	1.6e-4	3.3e-5	3.1e+0	1.2e-5
interchangingRBF	7.1e-7	5.2e-5	1.1e-4	8.2e-2	7.9e-4	2.4e-1	5.6e-4	1.8e-4	9.3e-4	9.9e-5
interRBF20D	3.9e-5	1.7e-4	6.4e-4	7.8e-1	2.7e-3	1.1e+0	1.8e-2	4.5e-3	2.6e-3	1.0e-3
airlines	5.5e-5	1.3e-3	3.4e-3	7.3e-1	2.7e-1	3.0e+2	1.7e-3	2.6e-3	1.5e-1	1.6e-1
elec2	4.9e-6	3.7e-6	1.1e-5	1.4e-1	3.3e-2	1.3e+0	3.2e-5	8.0e-6	1.5e-3	1.8e-5
NEweather	2.7e-6	7.0e-7	4.6e-6	4.6e-3	1.4e-3	3.1e-2	1.2e-5	2.6e-6	1.2e-3	1.7e-4
outdoorStream	1.5e-4	-	2.0e-6	2.6e-4	1.9e-3	6.0e-3	1.4e-4	4.5e-4	1.0e-4	3.4e-5

OSMOTEB took more than 185 hrs.

In terms of speed, DWM, Learn⁺⁺.NSE, and Learn++ are comparable to Enhash. In terms of accuracy, however, Enhash supersedes the individual methods on the majority of the datasets. Our findings were consistent across all commonly used evaluation metrics namely error, KappaM, and KappaT. For instance, DWM requires 0.038 hrs on the interchangingRBF dataset as compared to 0.132 hrs needed by Enhash. However, the error of Enhash is 2.72%, while DWM has an error of 7.02%.

The overall closest competitors of Enhash in terms of evaluation measures error, KappaM, and KappaT are ARF, LB, and OB. Enhash’s speed and RAM-hours’ requirement are almost insignificant when compared with other methods. For instance, on the movingSquares dataset, Enhash needed only $1.2\text{e}-5$ RAM-hours, while ARF, LB, and OB required 3.1, $9.0\text{e}-2$, and $5.5\text{e}-2$ RAM-hours, respectively. Similarly, on the movingSquares dataset, Enhash completed the overall processing in 0.068 hrs, while ARF, LB, and OB took 7.308, 9.368, and 5.936 hrs, respectively.

OSMOTE is the slowest when compared with all other methods. For the airlines dataset, OSMOTE took more than 403 hrs, while Enhash required only the minimum amount of time of 0.182 hrs.

The remaining methods, AWE, and AEE have inadequate performances as compared to Enhash. On the transientChessboard dataset, the error values are as high as 89.78% and 85.37% for AWE and AEE, respectively.

In summary, DWM has relatively poor performance in detecting virtual drifts but fairs well in abrupt and incremental drifts. Learn++ is exceptionally well in detecting virtual drift but severely under-performs in abrupt and incremental drifts. LB and ARF suffer in detecting incremental drifts. However, LB and ARF have an overall satisfactory performance. Enhash performs relatively well on all datasets. Enhash has a superior performance on a dataset consisting of three different kinds of drifts, namely incremental, virtual, and abrupt drifts. Although Enhash falls short in detecting abrupt drifts, but the performance gap is not very significant.

Table 4.8: Ablation study of Enhash. The performance of Enhash is compared with its two different variants- 1. Enhash with $\lambda = 0$ (referred to as Enhash-lambda0), and 2. Enhash when ties in *concept class* assignments are not broken by considering the distance of an incoming sample from the mean of classes in the bucket (referred to as Enhash-noWeights).

Dataset	Enhash	Enhash-lambda0	Enhash-noWeights
transientChessboard	18.84	19.57	30.58
rotatingHyperplane	30.49	32.26	36.69
mixedDrift	12.88	13.13	16.45
movingSquares	11.76	11.68	11.66
interchangingRBF	2.72	2.82	3.58
interRBF20D	11.30	11.75	12.98
airlines	41.66	41.36	43.03
elec2	17.34	17.28	17.65
NEweather	29.27	30.17	32.19
outdoorStream	8.75	8.75	9.55

4.6 Ablation study

Enhash is built by modifying (4.5) and (4.6). The two major changes in Enhash from these are the inclusion of a forgetting factor and a heuristic for tie braking mechanism to reduce the false positives. In this section, we assess the impact of these changes, which make Enhash suitable for the *concept drift* detection.

Table 4.8 compares the performances of Enhash with its two variants - Enhash-lambda0 and Enhash-noWeights. Enhash-lambda0 refers to the variant when $\lambda = 0$ or equivalently, the forgetting phenomenon is not accounted. Enhash-noWeights refers to the variant of Enhash when ties in the assignment of *concept class* are broken randomly. In other words, the distance (4.10) of an incoming sample from the mean of the classes in the bucket is not used to determine the class in case of ties. The values of the other hyperparameters are the same as that in Section 4.5. Table 4.8 shows that the performance of Enhash is much superior to its both variants for the majority of the datasets. The sub-optimal results of Enhash-noWeights may be attributed to the fact that when the same count of samples from different classes is present in the same bucket, the class for an incoming sample gets assigned randomly.

4.7 Conclusions

We conclude that Enhash supersedes other methods in terms of speed since the algorithm effectively requires only $\mathcal{O}(1)$ running time for each sample on a given estimator. In addition, the performance of Enhash in terms of error, KappaM, and KappaT is better or comparable to others for majority datasets. These datasets constitute abrupt, gradual, virtual, and reoccurring drift phenomena. The closest competitor of Enhash in terms of performance is the Adaptive Random Forest. Notably, Enhash requires, on an average 10 times lesser RAM-hours than that of Adaptive Random Forest.

Chapter 5

Conclusions and Future Work

5.1 Conclusions

This thesis is motivated by the observation that rare events are not always noise but often represent significant events. The detection of rare events poses several challenges in terms of speed and performance. We designed multiple hashing-based rare events and outlier detection algorithms to overcome these challenges. In this regard, Chapter 1 contains introductory remarks and a survey of some background literature. Chapter 2 proposed FiRE, an algorithm for identifying rare events. The application of FiRE to rare cell type identification in single-cell RNA data was presented. The FiRE algorithm is an ultra-fast linear time rare event detection algorithm that can scale up to large databases. The simulation study with a minor cell cluster highlighted the efficiency of FiRE in the detection of rare cells. In another study, FiRE could identify dendritic cell subtypes amongst thousands of single cells. However, there are a few limitations of FiRE. Firstly, FiRE does not discriminate between outliers and cells representing minor cell types. The outliers, if any, are submerged into the minor cell clusters. To flag outlier cells, one may use hierarchical or density-based clustering techniques along with FiRE. Secondly, the number of possible bins that can be created in FiRE is limited by the number of dimensions used to create hashes. This limitation arises from the use of sketching as the base hash function in FiRE. Although sketching makes the FiRE robust to noises, it impedes its adoption for various cases where dimensions are less. As

a solution, one may tune hyperparameters by creating more estimators or use super-spacing to increase the dimensionality of data. Note that the biological datasets do not have such issues as they tend to have large dimensions and may work well with the proposed values of hyperparameters. However, to address this issue, we proposed FiRE.1 in Chapter 3, which solves the dimension issue by replacing sketching with projection hash and introducing a new hyperparameter for quantization. This hyper-parameter reduces the hashing dependency from the number of dimensions and also extends the functionality of FiRE.1 to identify local outliers as well; thus, FiRE.1 can efficiently identify both local and global outliers. FiRE.1 was extensively compared with relevant state-of-the-art algorithms. In this chapter, a supervised scoring mechanism was also proposed that can be used to characterize datasets based on their outlier composition. About ~ 1000 datasets were characterized and categorized to compare the performance of FiRE.1 with other relevant linear-time outlier detection algorithms. Although the quantization and projection hashing make FiRE.1 more suitable for outlier detection, they make FiRE.1 prone to noise. A too-low quantization value tends to mark every sample as an outlier, and a large quantization value converts the algorithm to a global outlier detection algorithm. Thus a proper selection of quantization values is needed. These issues may be solved using more sophisticated hashing algorithms such as spectral hashing [136], spherical hashing [56], semi-supervised hashing [131, 132], etc., or building new heuristics to estimate such parameters.

The algorithms discussed so far assumed that the entire dataset is available all the time, and the distribution of the dataset remains unchanged. However, this is not always the case. The learned distribution may change with time, and in resource-constrained environments such as IoT devices, there is not enough space to accommodate the entire dataset. To overcome these challenges, Chapter 4 extended the FiRE family to non-stationary environments and proposed Enhash, an algorithm that adapts to a changing environment and identifies concept drift. Enhash incorporates a gradual forgetting of past phenomena and incrementally updates the model in response to new events to identify and adapt to concept drift. All of the above algorithms exploit the concept of hashing to their advantage, resulting in fast algorithms.

5.2 Future Work

In summary, the thesis proposes a family of FiRE algorithms that work well in tabular and streaming data. However, temporal continuity is also important, where time forms the contextual variable. Some of the prevalent examples of anomaly detection in time-series domain are electrocardiogram (ECG) signals, intrusion detection, patient-health monitoring, sudden drift in customer behavior, vibration monitoring system for machines, etc. We briefly discuss the performance of FiRE when adapted for time-series.

5.2.1 Identification of anomalies in time-series data

Outlier detection plays an important role in time series data, where temporal continuity is paramount [14, 39]. Unusual changes in temporal patterns in data are used to model outliers. In effect, time forms the contextual variable on the basis of which analysis is performed. Data arrives sequentially, and must be processed in an online fashion. The statistics of a system may also change with time, referred to as concept drift, which was discussed in the previous chapter. Anomalous behaviour needs to be detected as soon as possible [26, 52], and latency may be unacceptable. In some applications, computational and storage resources may be limited, and anomaly detection in such a scenario is doubly challenging.

A significant amount of work has been done to identify time series outliers. They consist of statistical techniques [6, 34, 103] such as Hidden Markov Models [38], Auto-Regressive Moving Average (ARMA), Auto-Regressive Integrated Moving Average (ARIMA) [32], Vector Auto-Regression Moving Average (VARMA) [102], etc. Recurrent Neural Networks (RNNs) [91], Long Short-Term Memory (LSTM) [57] also have the ability to process data sequentially and model dependencies through time. Some other commonly used algorithms for identifying outliers in time-series are Bayesian Online Changepoint detection [1], EXPoSE [108], and Multinomial Relative Entropy [128].

The NAB corpus [2] consists of about 58 labelled data streams from various sources. The sources range from a variety of domains including social media, industrial production, cpu utilization, etc. The characteristics of data streams vary in terms of periodicity, number of outliers, concept drift, etc. We show empirically the performance of FiRE adapted for time-series with different data streams. For every stream, we define a proba-

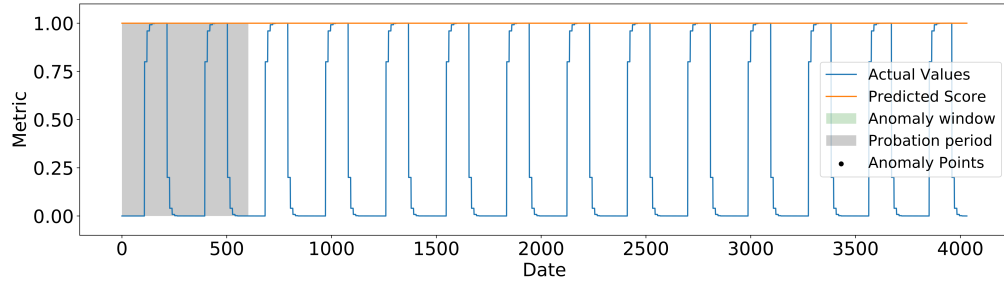


Figure 5.1: The data stream is periodic, has no fluctuation in observed values across different time periods and there is no anomaly.

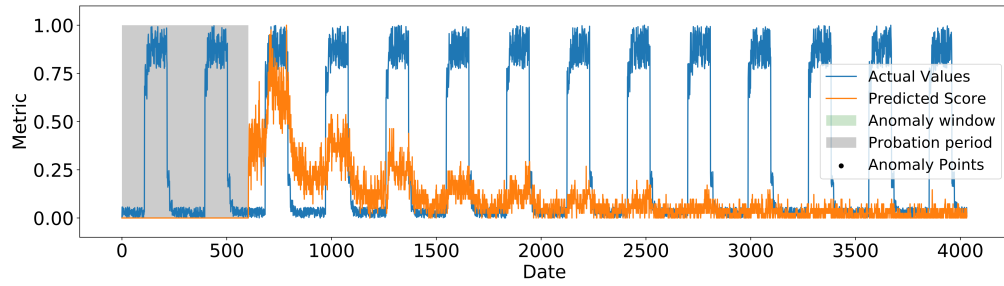


Figure 5.2: A periodic data stream with minor fluctuations and no anomaly.

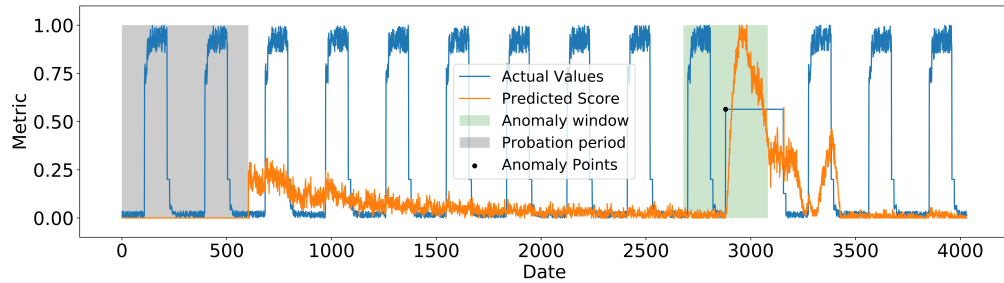


Figure 5.3: A periodic time-series with an anomaly.

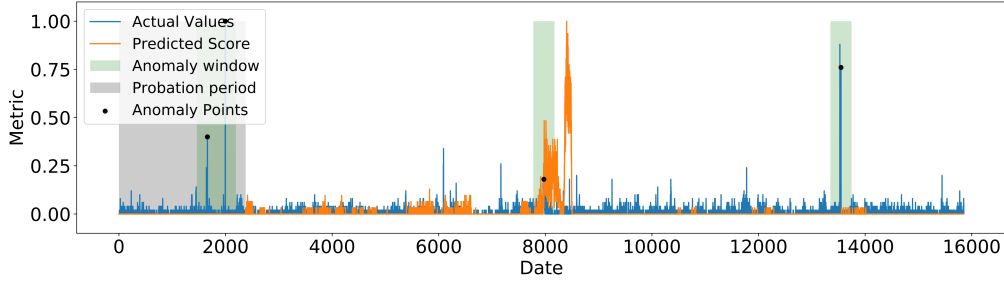


Figure 5.4: The presence of an anomaly in an aperiodic time-series.

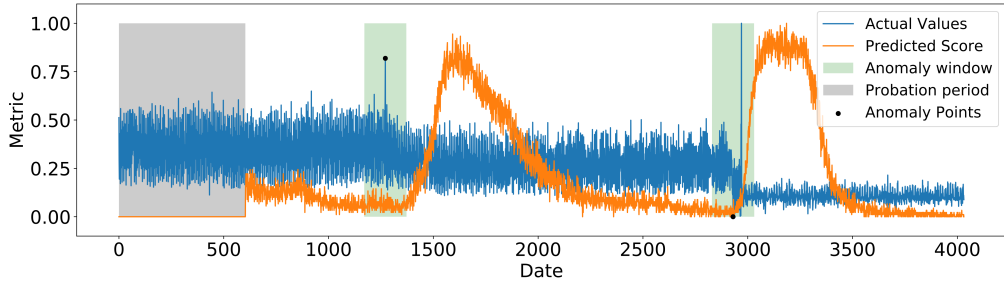


Figure 5.5: A data stream with a concept drift.

tion period to fit the model. The initial 15% of the entire records defines the probation period. Figure 5.1 shows the performance of FiRE when the stream is periodic, has no fluctuation in observed values for different periods and there is no anomaly. When the model is used to predict for the remaining stream, the FiRE-score is a constant and in correspondence with the fact that there is no anomaly. Figure 5.2 represents a periodic data stream with minor fluctuations in observed values but there is no anomaly. We observe that FiRE is particularly sensitive to minor fluctuations, and hence, after the probation period completes, minor fluctuations in the observed values lead to high values of FiRE-score. Once FiRE adapts, after some iterations, FiRE-scores eventually reduce. Figure 5.3 shows FiRE's behaviour, when the periodic time-series has an anomaly. A high peak in FiRE-score is observed with a slight delay w.r.t. the point of anomaly. FiRE uses a window-based technique to hash the incoming records. As a result, it takes some time for the effect to show up and the effect remains for the size of the window. Figure 5.4 represents an aperiodic time-series. FiRE is not able to identify all outliers. Figure 5.5 shows a data stream with a concept drift. At the point of drift, FiRE-score has a high peak, and adapts eventually.

In effect, FiRE can provide a fast and scalable solution to detect outliers where

temporal continuity is important. However, there are certain limitations in the current approach and it needs some update to incorporate temporal continuity more effectively. These are some challenges that researchers may endeavour to address in the future.

Bibliography

- [1] Ryan Prescott Adams and David JC MacKay. Bayesian online changepoint detection. *arXiv preprint arXiv:0710.3742*, 2007.
- [2] Subutai Ahmad, Alexander Lavin, Scott Purdy, and Zuha Agha. Unsupervised real-time anomaly detection for streaming data. *Neurocomputing*, 262:134–147, 2017.
- [3] J.D. Altman, P.A.H. Moss, P.J.R. Goulder, D.H. Barouch, M.G. McHeyzer-Williams, J.I. Bell, A.J. McMichael, and M.M. Davis. Phenotypic analysis of antigen-specific t lymphocytes. *Science*, 274(5284):94–96, 1996.
- [4] Fabrizio Angiulli and Clara Pizzuti. Fast outlier detection in high dimensional spaces. In *European Conference on Principles of Data Mining and Knowledge Discovery*, pages 15–27. Springer, 2002.
- [5] Luigi Atzori, Antonio Iera, and Giacomo Morabito. The internet of things: A survey. *Computer networks*, 54(15):2787–2805, 2010.
- [6] Vic Barnett and Toby Lewis. Outliers in statistical data. *osd*, 1984.
- [7] Erik Bernhardsson. *Annoy: Approximate Nearest Neighbors in C++/Python*, 2018. Python package version 1.13.0.
- [8] Albert Bifet, Gianmarco de Francisci Morales, Jesse Read, Geoff Holmes, and Bernhard Pfahringer. Efficient online evaluation of big data stream classifiers. In *Proceedings of the 21th ACM SIGKDD international conference on knowledge discovery and data mining*, pages 59–68. ACM, 2015.
- [9] Albert Bifet and Ricard Gavaldà. Learning from time-changing data with adaptive windowing. In *Proceedings of the 2007 SIAM international conference on data mining*, pages 443–448. SIAM, 2007.
- [10] Albert Bifet, Geoff Holmes, and Bernhard Pfahringer. Leveraging bagging for evolving data streams. In *Joint European conference on machine learning and knowledge discovery in databases*, pages 135–150. Springer, 2010.
- [11] Albert Bifet, Geoff Holmes, Bernhard Pfahringer, and Eibe Frank. Fast perceptron decision tree learning from evolving data streams. In *Pacific-Asia conference on knowledge discovery and data mining*, pages 299–310. Springer, 2010.
- [12] Leo Breiman. Random forests. *Machine learning*, 45(1):5–32, 2001.
- [13] Markus M. Breunig, Hans-Peter Kriegel, Raymond T. Ng, and Jörg Sander. Lof:

Identifying density-based local outliers. *SIGMOD Rec.*, 29(2):93–104, May 2000.

- [14] J Peter Burman and Mark C Otto. Census bureau research project: Outliers in time series. *Bureau of the Census, SRD Res. Rep. CENSUS/SRD/RR-88114*, 1988.
- [15] John N Campbell, Evan Z Macosko, Henning Fenselau, Tune H Pers, Anna Lyubetskaya, Danielle Tenen, Melissa Goldman, Anne MJ Verstegen, Jon M Resch, Steven A McCarroll, et al. A molecular census of arcuate hypothalamus and median eminence cell types. *Nature neuroscience*, 20(3):484, 2017.
- [16] Ricardo JGB Campello, Davoud Moulavi, Arthur Zimek, and Jörg Sander. Hierarchical density estimates for data clustering, visualization, and outlier detection. *ACM Transactions on Knowledge Discovery from Data (TKDD)*, 10(1):5, 2015.
- [17] Guilherme O Campos, Arthur Zimek, Jörg Sander, Ricardo JGB Campello, Barbora Mícenková, Erich Schubert, Ira Assent, and Michael E Houle. On the evaluation of unsupervised outlier detection: measures, datasets, and an empirical study. *Data Mining and Knowledge Discovery*, 30(4):891–927, 2016.
- [18] José M Carmona-Cejudo, Manuel Baena-García, José del Campo-Avila, Rafael Morales-Bueno, and Albert Bifet. GnuMail: Open framework for on-line email classification. 2011.
- [19] Rich Caruana, Thorsten Joachims, and Lars Backstrom. Kdd-cup 2004: results and analysis. *ACM SIGKDD Explorations Newsletter*, 6(2):95–108, 2004.
- [20] Robert Cattral, Franz Oppacher, and Dwight Deugo. Evolutionary data mining with automatic rule generalization. *Recent Advances in Computers, Computing and Communications*, 1(1):296–300, 2002.
- [21] Varun Chandola, Arindam Banerjee, and Vipin Kumar. Anomaly detection: A survey. *ACM computing surveys (CSUR)*, 41(3):15, 2009.
- [22] Moses S Charikar. Similarity estimation techniques from rounding algorithms. In *Proceedings of the thirty-fourth annual ACM symposium on Theory of computing*, pages 380–388, 2002.
- [23] Nitesh V Chawla, Kevin W Bowyer, Lawrence O Hall, and W Philip Kegelmeyer. Smote: synthetic minority over-sampling technique. *Journal of artificial intelligence research*, 16:321–357, 2002.
- [24] Igor Cima, Say Li Kong, Debarka Sengupta, Iain B Tan, Wai Min Phyoo, Daniel Lee, Min Hu, Ciprian Iliescu, Irina Alexander, Wei Lin Goh, et al. Tumor-derived circulating endothelial cell clusters in colorectal cancer. *Science translational medicine*, 8(345):345ra89–345ra89, 2016.
- [25] Jérôme Coffinet and Jean-Noël Kien. Detection of rare events: A machine learning toolkit with an application to banking crises. *The Journal of Finance and Data Science*, 5(4):183–207, 2019.
- [26] Yuwei Cui, Subutai Ahmad, and Jeff Hawkins. Continuous online sequence learning with an unsupervised neural network model. *Neural computation*, 28(11):2474–2504, 2016.

- [27] Mayur Datar, Nicole Immorlica, Piotr Indyk, and Vahab S Mirrokni. Locality-sensitive hashing scheme based on p-stable distributions. In *Proceedings of the twentieth annual symposium on Computational geometry*, pages 253–262, 2004.
- [28] Jesse Davis and Mark Goadrich. The relationship between precision-recall and roc curves. In *Proceedings of the 23rd international conference on Machine learning*, pages 233–240. ACM, 2006.
- [29] Roberto Souto Maior de Barros and Silas Garrido T de Carvalho Santos. An overview and comprehensive comparison of ensembles for concept drift. *Information Fusion*, 52:213–244, 2019.
- [30] Thomas G Dietterich. An experimental comparison of three methods for constructing ensembles of decision trees: Bagging, boosting, and randomization. *Machine learning*, 40(2):139–157, 2000.
- [31] Dheeru Dua and Casey Graff. UCI machine learning repository, 2017.
- [32] James Durbin and Siem Jan Koopman. *Time series analysis by state space methods*. Oxford university press, 2012.
- [33] Ryan Elwell and Robi Polikar. Incremental learning of concept drift in nonstationary environments. *IEEE Transactions on Neural Networks*, 22(10):1517–1531, 2011.
- [34] G Enderlein. Hawkins, dm: Identification of outliers. chapman and hall, london–new york 1980, 188 s., £ 14, 50. *Biometrical Journal*, 29(2):198–198, 1987.
- [35] Mani Malek Esmaeili, Mehrdad Fatourehchi, and Rabab Kreidieh Ward. A robust and fast video copy detection system using content-based fingerprinting. *IEEE Transactions on information forensics and security*, 6(1):213–226, 2010.
- [36] Martin Ester, Hans-Peter Kriegel, Jörg Sander, Xiaowei Xu, et al. A density-based algorithm for discovering clusters in large spatial databases with noise. In *Kdd*, volume 96, pages 226–231, 1996.
- [37] DB Fearnley, LF Whyte, SA Carnoutsos, AH Cook, and DNJ Hart. Monitoring human blood dendritic cell numbers in normal individuals and in stem cell transplantation. *Blood*, 93(2):728–736, 1999.
- [38] Shai Fine, Yoram Singer, and Naftali Tishby. The hierarchical hidden markov model: Analysis and applications. *Machine learning*, 32(1):41–62, 1998.
- [39] Anthony J Fox. Outliers in time series. *Journal of the Royal Statistical Society: Series B (Methodological)*, 34(3):350–363, 1972.
- [40] Yoav Freund and Robert E Schapire. A decision-theoretic generalization of on-line learning and an application to boosting. *Journal of computer and system sciences*, 55(1):119–139, 1997.
- [41] João Gama, Indrė Žliobaitė, Albert Bifet, Mykola Pechenizkiy, and Abdelhamid Bouchachia. A survey on concept drift adaptation. *ACM computing surveys (CSUR)*, 46(4):44, 2014.
- [42] Alexander Gerniers, Orian Bricard, and Pierre Dupont. MicroCellClust: mining

- rare and highly specific subpopulations from single-cell expression data. *Bioinformatics*, 37(19):3220–3227, 04 2021.
- [43] Corrado Gini. *Variabilità e mutabilità: contributo allo studio delle distribuzioni e delle relazioni statistiche.[Fasc. I.]*. Tipogr. di P. Cuppini, 1912.
 - [44] Aristides Gionis, Piotr Indyk, Rajeev Motwani, et al. Similarity search in high dimensions via hashing. In *Vldb*, volume 99, pages 518–529, 1999.
 - [45] Markus Goldstein and Andreas Dengel. Histogram-based outlier score (hbos): A fast unsupervised anomaly detection algorithm. *KI-2012: Poster and Demo Track*, pages 59–63, 2012.
 - [46] Markus Goldstein and Seiichi Uchida. A comparative evaluation of unsupervised anomaly detection algorithms for multivariate data. *PloS one*, 11(4):e0152173, 2016.
 - [47] Markus Goldstein and Seiichi Uchida. A comparative evaluation of unsupervised anomaly detection algorithms for multivariate data. *PloS one*, 11(4):e0152173, 2016.
 - [48] Heitor M Gomes, Albert Bifet, Jesse Read, Jean Paul Barddal, Fabrício Enembreck, Bernhard Pfahringer, Geoff Holmes, and Talel Abdesslem. Adaptive random forests for evolving data stream classification. *Machine Learning*, 106(9-10):1469–1495, 2017.
 - [49] Nico Görnitz, Marius Kloft, Konrad Rieck, and Ulf Brefeld. Toward supervised anomaly detection. *Journal of Artificial Intelligence Research*, 46:235–262, 2013.
 - [50] Frank E Grubbs. Procedures for detecting outlying observations in samples. *Technometrics*, 11(1):1–21, 1969.
 - [51] D. Grün, A. Lyubimova, L. Kester, K. Wiebrands, O. Basak, N. Sasaki, H. Clevers, and A. Van Oudenaarden. Single-cell messenger rna sequencing reveals rare intestinal cell types. *Nature*, 525(7568):251–255, 2015.
 - [52] Manish Gupta, Jing Gao, Charu C Aggarwal, and Jiawei Han. Outlier detection for temporal data: A survey. *IEEE Transactions on Knowledge and data Engineering*, 26(9):2250–2267, 2013.
 - [53] Prashant Gupta, Aashi Jindal, Debarka Sengupta, et al. Linear time identification of local and global outliers. *Neurocomputing*, 429:141–150, 2021.
 - [54] Ville Hautamaki, Ismo Karkkainen, and Pasi Franti. Outlier detection using k-nearest neighbour graph. In *Proceedings of the 17th International Conference on Pattern Recognition, 2004. ICPR 2004.*, volume 3, pages 430–433. IEEE, 2004.
 - [55] Douglas M Hawkins. *Identification of outliers*, volume 11. Springer, 1980.
 - [56] Jae-Pil Heo, Youngwoon Lee, Junfeng He, Shih-Fu Chang, and Sung-Eui Yoon. Spherical hashing. In *2012 IEEE Conference on Computer Vision and Pattern Recognition*, pages 2957–2964. IEEE, 2012.
 - [57] Sepp Hochreiter and Jürgen Schmidhuber. Long short-term memory. *Neural computation*, 9(8):1735–1780, 1997.

- [58] Victoria Hodge and Jim Austin. A survey of outlier detection methodologies. *Artificial intelligence review*, 22(2):85–126, 2004.
- [59] Hao Huang and Shiva Prasad Kasiviswanathan. Streaming anomaly detection using randomized matrix sketching. *Proceedings of the VLDB Endowment*, 9(3):192–203, 2015.
- [60] Piotr Indyk and Rajeev Motwani. Approximate nearest neighbors: towards removing the curse of dimensionality. In *Proceedings of the thirtieth annual ACM symposium on Theory of computing*, pages 604–613. ACM, 1998.
- [61] Y.-Y. Jang and S.J. Sharkis. Stem cell plasticity: A rare cell, not a rare event. *Stem Cell Reviews*, 1(1):45–51, 2005.
- [62] Nathalie Japkowicz and Shaju Stephen. The class imbalance problem: A systematic study. *Intelligent data analysis*, 6(5):429–449, 2002.
- [63] L. Jiang, H. Chen, L. Pinello, and G. . Yuan. Giniclust: Detecting rare cell types from single-cell gene expression data with gini index. *Genome biology*, 17(1), 2016.
- [64] Wen Jin, Anthony KH Tung, Jiawei Han, and Wei Wang. Ranking outliers using symmetric neighborhood relationship. In *Pacific-Asia Conference on Knowledge Discovery and Data Mining*, pages 577–593. Springer, 2006.
- [65] Wen Jin, Anthony KH Tung, Jiawei Han, and Wei Wang. Ranking outliers using symmetric neighborhood relationship. In *Pacific-Asia Conference on Knowledge Discovery and Data Mining*, pages 577–593. Springer, 2006.
- [66] Aashi Jindal, Prashant Gupta, Debarka Sengupta, et al. Enhash: A fast streaming algorithm for concept drift detection.
- [67] Aashi Jindal, Prashant Gupta, Debarka Sengupta, et al. Discovery of rare cells from voluminous single cell expression data. *Nature communications*, 9(1):4719, 2018.
- [68] Jeffrey Johnson. The future of the social sciences and humanities in the science of complex systems. *Innovation—The European Journal of Social Science Research*, 23(2):115–134, 2010.
- [69] Eric Jones, Travis Oliphant, Pearu Peterson, et al. SciPy: Open source scientific tools for Python, 2001–.
- [70] AllonM. Klein, Linas Mazutis, Ilke Akartuna, Naren Tallapragada, Adrian Veres, Victor Li, Leonid Peshkin, DavidA. Weitz, and MarcW. Kirschner. Droplet barcoding for single-cell transcriptomics applied to embryonic stem cells. *Cell*, 161(5):1187 – 1201, 2015.
- [71] Ralf Klinkenberg. Learning drifting concepts: Example selection vs. example weighting. *Intelligent data analysis*, 8(3):281–300, 2004.
- [72] Edwin M Knorr and Raymond T Ng. A unified notion of outliers: Properties and computation. In *KDD*, volume 97, pages 219–222, 1997.
- [73] Edwin M Knox and Raymond T Ng. Algorithms for mining distancebased outliers in large datasets. In *Proceedings of the international conference on very large data*

- bases*, pages 392–403. Citeseer, 1998.
- [74] J Zico Kolter and Marcus A Maloof. Dynamic weighted majority: An ensemble method for drifting concepts. *Journal of Machine Learning Research*, 8(Dec):2755–2790, 2007.
 - [75] Jeremy Z Kolter and Marcus A Maloof. Using additive expert ensembles to cope with concept drift. In *Proceedings of the 22nd international conference on Machine learning*, pages 449–456. ACM, 2005.
 - [76] Stine-Kathrein Kraeft, Rebecca Sutherland, Laura Gravelin, Guan-Hong Hu, Louis H Ferland, Paul Richardson, Anthony Elias, and Lan Bo Chen. Detection and analysis of cancer cells in blood and bone marrow using a rare event imaging system. *Clinical cancer research*, 6(2):434–442, 2000.
 - [77] M.G. Krebs, J.M. Hou, T.H. Ward, F.H. Blackhall, and C. Dive. Circulating tumour cells: Their utility in cancer management and predicting outcomes. *Therapeutic Advances in Medical Oncology*, 2(6):351–365, 2010.
 - [78] Hans-Peter Kriegel, Peer Kröger, Erich Schubert, and Arthur Zimek. Loop: local outlier probabilities. In *Proceedings of the 18th ACM conference on Information and knowledge management*, pages 1649–1652. ACM, 2009.
 - [79] Hans-Peter Kriegel, Peer Kröger, Erich Schubert, and Arthur Zimek. Outlier detection in axis-parallel subspaces of high dimensional data. In *Pacific-Asia Conference on Knowledge Discovery and Data Mining*, pages 831–838. Springer, 2009.
 - [80] Hans-Peter Kriegel, Arthur Zimek, et al. Angle-based outlier detection in high-dimensional data. In *Proceedings of the 14th ACM SIGKDD international conference on Knowledge discovery and data mining*, pages 444–452. ACM, 2008.
 - [81] Yu-Hsuan Kuo, Ching-Hung Lin, Wen-Yi Shau, Te-Jung Chen, Shih-Hung Yang, Shu-Min Huang, Chun Hsu, Yen-Shen Lu, and Ann-Lii Cheng. Dynamics of circulating endothelial cells and endothelial progenitor cells in breast cancer patients receiving cytotoxic chemotherapy. *BMC cancer*, 12(1):620, 2012.
 - [82] Snehalika Lall, Debajyoti Sinha, Sanghamitra Bandyopadhyay, and Debarka Sen-gupta. Structure-aware principal component analysis for single-cell rna-seq data. *Journal of Computational Biology*, 2018. PMID: 30133312.
 - [83] Longin Jan Latecki, Aleksandar Lazarevic, and Dragoljub Pokrajac. Outlier detection with kernel density functions. In *International Workshop on Machine Learning and Data Mining in Pattern Recognition*, pages 61–75. Springer, 2007.
 - [84] David D Lewis, Yiming Yang, Tony G Rose, and Fan Li. Rcv1: A new benchmark collection for text categorization research. *Journal of machine learning research*, 5(Apr):361–397, 2004.
 - [85] Chee Peng Lim and Robert F. Harrison. Online pattern classification with multiple neural network systems: an experimental study. *IEEE Transactions on Systems, Man, and Cybernetics, Part C (Applications and Reviews)*, 33(2):235–247, 2003.
 - [86] W Johnson J Lindenstrauss. Extensions of lipschitz maps into a hilbert space.

Contemp. Math, 26:189–206, 1984.

- [87] Fei Tony Liu, Kai Ming Ting, and Zhi-Hua Zhou. Isolation forest. In *2008 Eighth IEEE International Conference on Data Mining*, pages 413–422. IEEE, 2008.
- [88] Viktor Losing, Barbara Hammer, and Heiko Wersing. Knn classifier with self adjusting memory for heterogeneous concept drift. In *2016 IEEE 16th international conference on data mining (ICDM)*, pages 291–300. IEEE, 2016.
- [89] Qin Lv, William Josephson, Zhe Wang, Moses Charikar, and Kai Li. Ferret: a toolkit for content-based similarity search of feature-rich data. *ACM SIGOPS Operating Systems Review*, 40(4):317–330, 2006.
- [90] E. Z. Macosko, A. Basu, R. Satija, J. Nemesh, K. Shekhar, M. Goldman, I. Tirosh, A. R. Bialas, N. Kamitaki, E. M. Martersteck, J. J. Trombetta, D. A. Weitz, J. R. Sanes, A. K. Shalek, A. Regev, and S. A. McCarroll. Highly parallel genome-wide expression profiling of individual cells using nanoliter droplets. *Cell*, 161(5):1202–1214, 2015.
- [91] Danilo Mandic and Jonathon Chambers. *Recurrent neural networks for prediction: learning algorithms, architectures and stability*. Wiley, 2001.
- [92] Teresa Manzo, Helen E Heslop, and Cliona M Rooney. Antigen-specific t cell therapies for cancer. *Human molecular genetics*, 24(R1):R67–R73, 2015.
- [93] Hualing Mao, Guorui Feng, Xinpeng Zhang, and Heng Yao. A robust and fast video fingerprinting based on 3d-dct and lsh. In *2011 International Conference on Multimedia Technology*, pages 108–111. IEEE, 2011.
- [94] RB Marimont and MB Shapiro. Nearest neighbour searches and the curse of dimensionality. *IMA Journal of Applied Mathematics*, 24(1):59–70, 1979.
- [95] Jacob Montiel, Jesse Read, Albert Bifet, and Talel Abdesslem. Scikit-multiflow: A multi-output streaming framework. *Journal of Machine Learning Research*, 19(72):1–5, 2018.
- [96] Nikunj C Oza. Online bagging and boosting. In *2005 IEEE international conference on systems, man and cybernetics*, volume 3, pages 2340–2345. Ieee, 2005.
- [97] Nikunj C Oza and Stuart Russell. Experimental comparisons of online and batch versions of bagging and boosting. In *Proceedings of the seventh ACM SIGKDD international conference on Knowledge discovery and data mining*, pages 359–364. ACM, 2001.
- [98] Marco AF Pimentel, David A Clifton, Lei Clifton, and Lionel Tarassenko. A review of novelty detection. *Signal Processing*, 99:215–249, 2014.
- [99] Robi Polikar, Lalita Upda, Satish S Upda, and Vasant Honavar. Learn++: An incremental learning algorithm for supervised neural networks. *IEEE transactions on systems, man, and cybernetics, part C (applications and reviews)*, 31(4):497–508, 2001.
- [100] Marcel Prastawa, Elizabeth Bullitt, Sean Ho, and Guido Gerig. A brain tumor segmentation framework based on outlier detection. *Medical image analysis*, 8(3):275–

283, 2004.

- [101] Sridhar Ramaswamy, Rajeev Rastogi, and Kyuseok Shim. Efficient algorithms for mining outliers from large data sets. In *ACM Sigmod Record*, volume 29, pages 427–438. ACM, 2000.
- [102] Gregory C Reinsel. Vector arma time series models and forecasting. In *Elements of Multivariate Time Series Analysis*, pages 21–51. Springer, 1993.
- [103] Peter J Rousseeuw and Annick M Leroy. *Robust regression and outlier detection*, volume 589. John wiley & sons, 2005.
- [104] Saket Sathe and Charu C Aggarwal. Subspace outlier detection in linear time with randomized hashing. In *2016 IEEE 16th International Conference on Data Mining (ICDM)*, pages 459–468. IEEE, 2016.
- [105] Rahul Satija, Jeffrey A Farrell, David Gennert, Alexander F Schier, and Aviv Regev. Spatial reconstruction of single-cell gene expression data. *Nature biotechnology*, 33(5):495–502, 2015.
- [106] Robert E Schapire. The strength of weak learnability. *Machine learning*, 5(2):197–227, 1990.
- [107] Robert E Schapire, Yoav Freund, Peter Bartlett, Wee Sun Lee, et al. Boosting the margin: A new explanation for the effectiveness of voting methods. *The annals of statistics*, 26(5):1651–1686, 1998.
- [108] Markus Schneider, Wolfgang Ertel, and Fabio Ramos. Expected similarity estimation for large-scale batch and streaming anomaly detection. *Machine Learning*, 105(3):305–333, 2016.
- [109] Erich Schubert, Alexander Koos, Tobias Emrich, Andreas Züfle, Klaus Arthur Schmid, and Arthur Zimek. A framework for clustering uncertain data. *PVLDB*, 8(12):1976–1979, 2015.
- [110] Erich Schubert, Arthur Zimek, and Hans-Peter Kriegel. Generalized outlier detection with flexible kernel density estimates. In *Proceedings of the 2014 SIAM International Conference on Data Mining*, pages 542–550. SIAM, 2014.
- [111] Erich Schubert, Arthur Zimek, and Hans-Peter Kriegel. Local outlier detection reconsidered: a generalized view on locality with applications to spatial, video, and network outlier detection. *Data Mining and Knowledge Discovery*, 28(1):190–237, 2014.
- [112] E. Shapiro, T. Biezuner, and S. Linnarsson. Single-cell sequencing-based technologies will revolutionize whole-organism science. *Nature Reviews Genetics*, 14(9):618–630, 2013.
- [113] Debajyoti Sinha, Akhilesh Kumar, Himanshu Kumar, Sanghamitra Bandyopadhyay, and Debarka Sengupta. dropclust: Efficient clustering of ultra-large scRNA-seq data. *Nucleic Acids Research*, 2018.
- [114] Debajyoti Sinha, Pradyumn Sinha, Ritwik Saha, Sanghamitra Bandyopadhyay, and Debarka Sengupta. Improved dropclust r package with integrative analysis

support for scrna-seq data, 2020.

- [115] Malcolm Slaney, Yury Lifshits, and Junfeng He. Optimal parameters for locality-sensitive hashing. *Proceedings of the IEEE*, 100(9):2604–2623, 2012.
- [116] J.E. Slansky. Antigen-specific t cells: Analyses of the needles in the haystack. *PLoS Biology*, 1(3), 2003.
- [117] Samaneh Sorournejad, Zahra Zojaaji, Reza Ebrahimi Atani, and Amir Hassan Monadjemi. A survey of credit card fraud detection techniques: data and technique oriented perspective. *CoRR abs/1611.06439*, 2016.
- [118] Divyanshu Srivastava, Arvind Iyer, Vibhor Kumar, and Debarka Sengupta. Cellatlassearch: a scalable search engine for single cells. *Nucleic acids research*, 2018.
- [119] Karthik Subbian, Charu Aggarwal, and Kshiteesh Hegde. Recommendations for streaming data. In *Proceedings of the 25th ACM International on Conference on Information and Knowledge Management*, pages 2185–2190. ACM, 2016.
- [120] Jian Tang, Zhixiang Chen, Ada Wai-Chee Fu, and David W Cheung. Enhancing effectiveness of outlier detections for low density patterns. In *Pacific-Asia Conference on Knowledge Discovery and Data Mining*, pages 535–548. Springer, 2002.
- [121] Lionel Tarassenko, Paul Hayton, Nicholas Cerneaz, and Michael Brady. Novelty detection for the identification of masses in mammograms. 1995.
- [122] Cole Trapnell, Davide Cacchiarelli, Jonna Grimsby, Prapti Pokharel, Shuqiang Li, Michael Morse, Niall J Lennon, Kenneth J Livak, Tarjei S Mikkelsen, and John L Rinn. The dynamics and regulators of cell fate decisions are revealed by pseudotemporal ordering of single cells. *Nature biotechnology*, 32(4):381, 2014.
- [123] Andrew V Uzilov, Joshua M Keegan, and David H Mathews. Detection of non-coding rnas on the basis of predicted secondary structure formation free energy change. *BMC bioinformatics*, 7(1):173, 2006.
- [124] Alexandra-Chloé Villani, Rahul Satija, Gary Reynolds, Siranush Sarkizova, Karthik Shekhar, James Fletcher, Morgane Griesbeck, Andrew Butler, Shiwei Zheng, Suzan Lazo, Laura Jardine, David Dixon, Emily Stephenson, Emil Nilsson, Ida Grundberg, David McDonald, Andrew Filby, Weibo Li, Philip L. De Jager, Orit Rozenblatt-Rosen, Andrew A. Lane, Muzlifah Haniffa, Aviv Regev, and Nir Hacohen. Single-cell rna-seq reveals new types of human blood dendritic cells, monocytes, and progenitors. *Science*, 356(6335), 2017.
- [125] A. Wagner, A. Regev, and N. Yosef. Revealing the vectors of cellular identity with single-cell genomics. *Nature Biotechnology*, 34(11):1145–1160, 2016.
- [126] Avery Wang et al. An industrial strength audio search algorithm. In *Ismir*, volume 2003, pages 7–13. Washington, DC, 2003.
- [127] Boyu Wang and Joelle Pineau. Online bagging and boosting for imbalanced data streams. *IEEE Transactions on Knowledge and Data Engineering*, 28(12):3353–3366, 2016.

- [128] Chengwei Wang, Krishnamurthy Viswanathan, Lakshminarayan Choudur, Vanish Talwar, Wade Satterfield, and Karsten Schwan. Statistical techniques for online anomaly detection in data centers. In *12th IFIP/IEEE International Symposium on Integrated Network Management (IM 2011) and Workshops*, pages 385–392. IEEE, 2011.
- [129] Haixun Wang, Wei Fan, Philip S Yu, and Jiawei Han. Mining concept-drifting data streams using ensemble classifiers. In *Proceedings of the ninth ACM SIGKDD international conference on Knowledge discovery and data mining*, pages 226–235. AcM, 2003.
- [130] Jingdong Wang, Heng Tao Shen, Jingkuan Song, and Jianqiu Ji. Hashing for similarity search: A survey. *arXiv preprint arXiv:1408.2927*, 2014.
- [131] Jun Wang, Sanjiv Kumar, and Shih-Fu Chang. Sequential projection learning for hashing with compact codes. 2010.
- [132] Jun Wang, Sanjiv Kumar, and Shih-Fu Chang. Semi-supervised hashing for large-scale search. *IEEE Transactions on Pattern Analysis and Machine Intelligence*, 34(12):2393–2406, 2012.
- [133] Z. Wang, W. Dong, W. Josephson, Q. Lv, M. Charikar, and K. Li. Sizing sketches: A rank-based analysis for similarity search. In *Performance Evaluation Review*, volume 35, pages 157–168, 2007.
- [134] Zhe Wang, Wei Dong, William Josephson, Qin Lv, Moses Charikar, and Kai Li. Sizing sketches: a rank-based analysis for similarity search. In *ACM SIGMET-RICS Performance Evaluation Review*, volume 35, pages 157–168. ACM, 2007.
- [135] Zhe Wang, Wei Dong, William Josephson, Qin Lv, Moses Charikar, and Kai Li. Sizing sketches: a rank-based analysis for similarity search. In *ACM SIGMET-RICS Performance Evaluation Review*, volume 35, pages 157–168. ACM, 2007.
- [136] Yair Weiss, Antonio Torralba, and Rob Fergus. Spectral hashing. In *Advances in neural information processing systems*, pages 1753–1760, 2009.
- [137] F Alexander Wolf, Philipp Angerer, and Fabian J Theis. Scanpy: large-scale single-cell gene expression data analysis. *Genome biology*, 19:1–5, 2018.
- [138] Kaikun Xie, Yu Huang, Feng Zeng, Zehua Liu, and Ting Chen. scAIDE: clustering of large-scale single-cell RNA-seq data reveals putative and rare cell types. *NAR Genomics and Bioinformatics*, 2(4), 10 2020. lqaa082.
- [139] Chen Xu and Zhengchang Su. Identification of cell types from single-cell transcriptomes using a novel clustering method. *Bioinformatics*, 31(12):1974–1980, 2015.
- [140] Zhenxia Xue, Youlin Shang, and Aifen Feng. Semi-supervised outlier detection based on fuzzy rough c-means clustering. *Mathematics and Computers in Simulation*, 80(9):1911–1921, 2010.
- [141] Bo Yu, Mingqiu Song, and Leilei Wang. Local isolation coefficient-based outlier mining algorithm. In *2009 International Conference on Information Technology and Computer Science*, volume 2, pages 448–451. IEEE, 2009.

- [142] Mohamad Zamini and Seyed Mohammad Hossein Hasheminejad. A comprehensive survey of anomaly detection in banking, wireless sensor networks, social networks, and healthcare. *Intelligent Decision Technologies*, 13(2):229–270, 2019.
- [143] Luke Zappia, Belinda Phipson, and Alicia Oshlack. Splatter: simulation of single-cell rna sequencing data. *Genome Biology*, 18(1):174, Sep 2017.
- [144] Ke Zhang, Marcus Hutter, and Huidong Jin. A new local distance-based outlier detection approach for scattered real-world data. In *Pacific-Asia Conference on Knowledge Discovery and Data Mining*, pages 813–822. Springer, 2009.
- [145] Yan-Xia Zhang, A-Li Luo, and Yong-Heng Zhao. Outlier detection in astronomical data. In *Optimizing scientific return for astronomy through information technologies*, volume 5493, pages 521–529. SPIE, 2004.
- [146] Ye Zhao, Brad Lehman, Roy Ball, Jerry Mosesian, and Jean-François de Palma. Outlier detection rules for fault detection in solar photovoltaic arrays. In *2013 Twenty-Eighth Annual IEEE Applied Power Electronics Conference and Exposition (APEC)*, pages 2913–2920. IEEE, 2013.
- [147] Yue Zhao, Zain Nasrullah, and Zheng Li. Pyod: A python toolbox for scalable outlier detection. *arXiv preprint arXiv:1901.01588*, 2019.
- [148] G. X. Y. Zheng, J. M. Terry, P. Belgrader, P. Ryvkin, Z. W. Bent, R. Wilson, S. B. Ziraldo, T. D. Wheeler, G. P. McDermott, J. Zhu, M. T. Gregory, J. Shuga, L. Montesclaros, J. G. Underwood, D. A. Masquelier, S. Y. Nishimura, M. Schnall-Levin, P. W. Wyatt, C. M. Hindson, R. Bharadwaj, A. Wong, K. D. Ness, L. W. Beppu, H. J. Deeg, C. McFarland, K. R. Loeb, W. J. Valente, N. G. Ericson, E. A. Stevens, J. P. Radich, T. S. Mikkelsen, B. J. Hindson, and J. H. Bielas. Massively parallel digital transcriptional profiling of single cells. *Nature Communications*, 8, 2017.
- [149] Arthur Zimek, Erich Schubert, and Hans-Peter Kriegel. A survey on unsupervised outlier detection in high-dimensional numerical data. *Statistical Analysis and Data Mining: The ASA Data Science Journal*, 5(5):363–387, 2012.

List of Publications

Publications related to thesis chapters

1. Jindal A, Gupta P, Jayadeva, Sengupta D. Discovery of rare cells from voluminous single cell expression data. Nature communications. 2018 Nov 9;9(1):1-9.
2. Gupta P, Jindal A, Jayadeva, Sengupta D. Linear time identification of local and global outliers. Neurocomputing. 2021 Mar 14;429:141-50.
3. Jindal A, Gupta P, Sengupta D., Jayadeva Enhash: A Fast Streaming Algorithm for Concept Drift Detection. ESANN 2021 proceedings. Online event, 6-8 October 2021, i6doc.com publ., ISBN 978287587082-7.

Co-Authored Publications

1. Gupta P, Jindal A, Jayadeva, Sengupta D. ComBI: Compressed Binary Search Tree for Approximate k-NN Searches in Hamming Space. Big Data Research. 2021 Jul 15;25:100223.
2. Gupta P, Jindal A, Ahuja G, Jayadeva, Sengupta D. A new deep learning technique reveals the exclusive functional contributions of individual cancer mutations. Journal of Biological Chemistry. 2022 Aug 1;298(8).

Preprints

1. Gupta P, Jindal A, Jayadeva, Sengupta D. Guided Random Forest and its application to data approximation. arXiv preprint arXiv:1909.00659. 2019 Sep 2.

Brief Biodata of Author

Name: Aashi Jindal

Educational Qualifications

Ph.D. (completed) 2023

Department of Electrical Engineering

Indian Institute of Technology Delhi, Delhi, India.

Bachelor of Technology (B.Tech.) 2013

Department of Information Technology

Bharati Vidyapeeth's College Of Engineering, New Delhi, India.

Industrial Experience

Applied Solar Technologies India Pvt. Ltd. Dec 2021- till now

Data Scientist

NableIT Consultancy Pvt. Ltd. Nov 2020 - Dec 2021

Software Engineer (Machine Learning)

Aricent Aug 2013 - July 2015

Software Engineer

Areas of Interest

Machine Learning, Deep Learning, Computational Biology, Computer Vision, Natural Language Processing